Experimental research on the stability of the armour and secondary layer in a single layered tetrapod breakwater

Wesley de Jong
CT9406132

MSc Committee
Prof.dr.ir. M.J.F. Stive
Dr.ir. H.L. Fontijn
Dr.ir. M.R.A. van Gent
Ir. J. Olthof
Ir. H.J. Verhagen

Preface

This thesis was submitted in conformity with the requirements for the degree of Master of Science (MSc) in Civil Engineering. The preparation and evaluation of the experiments were performed at Royal Boskalis Westminster nv. The experiments have been carried out at the Fluid Mechanics Laboratory of the Faculty of Civil Engineering and Geosciences at Delft University of Technology.

This research was performed under the supervision of Prof. Marcel Stive. I want to thank him for guiding me through the total process of this research.
During this graduation work, Jelle Olthof guided me most extensively. I want to thank him for his valuable comments on the experiments and their results and for his undiminishing enthusiasm. I thank Marcel van Gent for his knowledgable insights and many detailed comments on my report. I also thank Harry Fontijn and Henk-Jan Verhagen for their practical advice on the set-up of the experiments and their useful comments during this research.

Furthermore I thank Royal Boskalis Westminster nv for their financial support during this complete research. WL|Delft Hydraulics provided me the miniature tetrapod units.

Finally I thank all the members of the support staff of the Fluid Mechanics Laboratory for their help and advice and of course for giving me a good time during the experiments.

Wesley de Jong
(Delft, September 2003)

Summary

Previous research by Bhageloe (1998), Van Gent et al. (1999) and Van den Bosch (2001) on single armour layer breakwaters exposed to irregular waves, demonstrated a positive relationship between an increase in the packing density of the armour layer and the stability of the structure. This relation particularly held if the single armour layer consisted of tetrapod units. A higher packing density increased interlocking, resulting in lesser displaced units. Within a packing density range of $n_v = 0.25 - 0.4$ a fairly stable top layer was achieved.
However, the single top layer with its slenderly shaped units caused the secondary layer to be rather exposed to wave attack, which led to wash-out of the secondary layer rock material, thereby seriously undermining the stability of the structure. Bhageloe and Van den Bosch both used rules of thumb recommended by Van der Meer (1993) to determine the dimensions of the secondary material used in their scale models. Therefore, these recommendations seem to lead to underlayer rock material that is too small for use in a single layered tetrapod armour layer.

This research focused on both the stability of the single tetrapod armour layer and the secondary layer. By means of several wave flume experiments, testing various combinations of secondary material, wave steepness and armour packing density, an attempt was made to establish the influence of these governing parameters on the stability of the structure.

The physical model tests were performed in the Fluid Mechanics Laboratory of the Faculty of Civil Engineering and Geosciences at Delft University of Technology. The wave flume has a length of 40 meter, a width of 0.80 meter and a height of 0.85 meter. A foreshore with a 1:30 slope was constructed over a length of 6.60 meter and started at 24.80 meter from the wave board.
Each experiment in principle consisted of 7 runs with increasing wave height and period, keeping the wave steepness constant. The irregular waves were generated according to the JONSWAP spectrum, while all runs consisted of approximately 1000 waves.
A series was completed when failure of the structure occurred. The model was rebuilt after each experiment, but not after each test-run.

To determine the damage development of the armour layer, both the displacement of units (movements $> 2.0D_n$) and sliding (movement between $0.5D_n$ and $2.0D_n$) were taken into account. Several digital images of the armour layer were taken at each run from a fixed position perpendicular to the slope. Through comparison of the images, displacement plots were generated. The erosion of the secondary layer was measured using an automatic surface profiler on a controlled carriage. Measurements were carried out at the beginning and end of each experiment.

The damage development of the top layer agreed with results of Van den Bosch (2001). An increase in the armour packing density improved the overall stability of the top layer. The results also showed a general decrease in stability with increasing wave periods.

In all the wave flume experiments, it was the formation of one or more gaps in the upper part of the armour layer that led to the failure of the structure. Frequently, it was a combination of sliding

and displacement that caused the formation of these gaps. In the experiments with $n_v = 0.4$, however, it was the mechanism of sliding that was solely responsible for failure of the top layer. The experiments with $n_v = 0.4$ demonstrated a very sudden resettlement at relatively low incident waves. The results of these major resettlements were the formation of intolerable gaps in the upper part of the armour layer. From observations followed the conclusion that a single tetrapod armour layer with a packing density of $n_v \geq 0.4$ is unsuitable.

There is a clear interaction between the two failure mechanisms of displacement and sliding. The displacement of units caused units placed higher upon the slope to slide down, thereby filling the newly formed gaps to some extend. Contrarily, the resettlement of units caused an increase of packing density, which results in the displacement of lesser units. Furthermore, it was observed that the resettlement of the armour units was an ongoing process. Throughout the experiments, the packing density increased until a 'natural' density of $n_v = 0.23 - 0.27$ was reached.

Because of their interaction, both the displacement and sliding of armour units should be taken into account when the overall stability of the armour layer is regarded. However, displacement by itself can serve as a good indication of the stability of the structure. Analysis of the data showed that an increase in wave steepness caused a decrease in displacement. The tests further demonstrated that the amount of displacement in the experiments with $n_v = 0.3$ and 0.25 did not really differ. Displacement did decrease, however, if during the tests there was a rapid increase in packing density towards the 'natural' $n_v = 0.23 - 0.27$. Therefore, displacement is also influenced by the size of the secondary layer material. From the experimental data a stability formula was derived.

The behavior of the secondary layer material was not as anticipated. Wash-out of the secondary layer material did not occur at all series. Though the erosion increased with a decrease in secondary rock size, it was the damage development of the armour layer rather than excessive erosion of the underlayer that caused an overall failure of the structure. The core of the model was scaled according to Burcharth's method (Burcharth et al., 1999), ensuring a flow field in the model that more accurately represents prototype design. This method of scaling led to rather course core rubble mound material. The first series showed only minor local erosion, mainly a consequence of armour response, as opposite to the observations of Van den Bosch. He reported heavy wash-out of secondary material which consequently caused a progressive loss of stability of the armour layer. The size of the secondary material in both experiments were similar, though the core in his model was Froude scaled. A possible explanation in the different outcome was sought in the difference in permeability of both models. To verify this, an extra series was performed with a geotextile placed between core and secondary layer, thus decreasing the permeability to approximate the setup of Van den Bosch. Though the overall erosion of the secondary layer increased due to the decrease in permeability of the core, still it was within tolerable limits.

Sliding or displacement -i.e. an increase in the size of the voids between particular armour units- often initiated erosion in the form of scoured holes. In all experiments, the depth of the scoured holes never exceed $3 \times D_{n50_S}$.

Even with the smallest secondary material, with $W_a/W_s \approx 120$ far exceeding the limit of Van der Meer's recommendation, armour instability pre-exceeded secondary layer instability. Although the size of the secondary layer material did influence the armour response. Smaller underlayer material caused an increase in armour resettlement. This, however, did not automatically mend a more rapid failure of the structure, especially if the initial packing density of the armour layer was already high.

The experiments, furthermore, demonstrated that the erosion of the secondary layer is a function of the incident wave height rather than of the top layer packing density or the wave steepness. Analysis of the data led to the derivation of a predictive relation concerning secondary layer erosion.

Contents

List of Symbols

A_e = *Eroded volume per unit length* (m^2)

D_{15} = *Particle diameter exceeded by 15% of the particles*(m)

D_{n_A} = *Nominal diameter of the armour unit* (m)

D_{n50} = *Nominal diameter* (m)

D_{n50_S} = *Nominal diameter of the secondary layer material* (m)

D_{85} = *Particle diameter exceeded by 85% of the particles* (m)

$E(f)$ = *Frequency spectrum* (m^2s)

f = *Frequency* (Hz)

Fr = *Froude number* (-)

g = *Gravitational acceleration* (m/s^2)

h_0 = *Still water depth* (m)

h_{cr} = *Height of the crest* (m)

H_s = *Significant wave height* (m)

I = *Hydraulic gradient* (-)

k_t = *Layer thickness coefficient* (-)

K = *Scale factor* (-)

K = *Hydraulic conductivity* (m/s)

K_R = *Reflection coefficient* (-)

KC = *Keulegan-Carpenter number* (-)

L = *Wave length* (m)

n_v = *Packing density of the armour layer* (-)

N = *Number of waves* (-)

N_a = *Number of tetrapods per square meter* (m^{-2})

N_o = *Number of displaced units over a distance* $> 2.0D_n$ (-)

N_{sl} = *Number of units moved over a distance* $> 0.5D_n$ *and* $< 2.0D_n$ (-)

N_{od} = *Damage number* (-)

N_{omov} = *Damage number* (-)

N_{os} = *Damage number* (-)

p = *Pore pressure* ($\mathrm{N/m}^2$)

P = *Permeability coefficient* (-)

Re = *Reynolds number* (-)

s_{m0} = *Deep water steepness based on the mean wave period* (-)

S = *Damage* (-)

W_{50} = *Weight of a unit/rock with a diameter* D_{n50} (kg)

W_a = *Weight of the armour units* (kg)

W_c = *Weight of the rock material in the core* (kg)

W_s = *Weight of the secondary rock material* (kg)

T_m = *Mean wave period* (s)

T_{m0} = *Mean wave period in deep water* (s)

T_p = *Peak wave period* (s)

U = *Characteristic pore velocity* (m/s)

δ = *Damping coefficient* (-)

Δ = *Relative density* (-)

ρ_a = *Density of the tetrapod units* ($\mathrm{kg/m}^3$)

ρ_r = *Density of the rocks* ($\mathrm{kg/m}^3$)

ρ_w = *Density of water* ($\mathrm{kg/m}^3$)

ξ = *Surf similarity parameter* (-)

ν = *Kinematic viscosity* (m^2/s)

Chapter 1

Introduction

Previous research by Bhageloe (1998), Van Gent et al. (1999) and Van den Bosch (2001) on single armour layer breakwaters exposed to irregular waves, demonstrated a positive relationship between an increase in the packing density of the armour layer and the stability of the structure. This relation particularly held if the single armour layer consisted of tetrapod units. A higher packing density increased interlocking, resulting in lesser displaced units. Within a packing density range of $n_v = 0.25 - 0.4$ a fairly stable top layer was achieved.
However, the single top layer with its slenderly shaped units caused the secondary layer to be rather exposed to wave attack, which led to wash-out of the secondary layer rock material, thereby seriously undermining the stability of the structure. Bhageloe and Van den Bosch both used rules of thumb recommended by Van der Meer (1993) to determine the dimensions of the secondary material used in their scale models. Therefore, these recommendations seem to lead to underlayer rock material that is too small for use in a single layered tetrapod armour layer.

This research focused on both the stability of the single tetrapod armour layer and the secondary layer. By means of several wave flume experiments, testing various combinations of secondary material, wave steepness and armour packing density, an attempt was made to establish the influence of these governing parameters on the stability of the structure. Secondly, an attempt was made to determine the limits wherein the secondary layer is considered stable and applicable.

Chapter 2

The design of armour and secondary layers

2.1 Design process

The sheltering effect of a breakwater is established through a reduction or cut-off of the incident wave energy. This is done by both the reflection of waves and by turbulent dissipation of the wave energy. An important dissipation mechanism is wave breaking. Wind generated waves usually break on a sloping structure since the decrease in depth causes a reduction in wave celerity. This will continue up to a point where the velocities of the crest particles exceed that of the wave celerity. Consequently the wave breaks. Another effective dissipation mechanism is the turbulent flow in a porous structure. The combining of both mechanism lead to a rubble mound breakwater in its simplest form, namely made out of a homogenous mound of rocks.
The structure however must consist of stones large enough to withstand displacement by wave forces. This in return will lead to a very permeable breakwater and considerable wave penetration and transmission. Additionally, large stones are expensive because most quarries yield a lot of finer material and only relatively small amounts of large rock material. In practice therefore the structure consists of fine materials armoured by large stones. Though in case of an insufficient availability of the larger stones, the armour layer consists of concrete units. In order to prevent the wash-out of the core material, filter layers are often provided.
During the design process all failure modes of a structure must be identified and assessed. Figure (2.1) shows the most common failure mechanisms of a conventional breakwater. This thesis focused on the hydraulic stability of the single tetrapod armour layer and its underlayer. The other failure modes -though equally important to consider during the design process- were ignored.

2.2 Hydraulic stability of the armour and secondary layer

When exposed to wave attack five forces act upon a unit, namely a drag force F_D, a lift force F_L, an inertia force F_I (the vectorial sum of these can be interpreted as a resulting flow force F_F, see fig. (2.2)). Furthermore, the gravitational force F_G and the reaction forces acting at the contact points with neighboring units. Whereas the gravitational force is considered to be stabilizing, the forces in the contact points can be either stabilizing or destabilizing depending on the position of the contact point and the direction of the force. In the case of complex interlocking types of armour like tetrapods, the forces in the contact points between the units increase the overall stability. Price (1979) found by dry pull-out tests that the interlocking ability of complex slender units increase with the slope angle. This effect is schematized in figure (2.3).
The flow around the units is non-stationary in both direction and velocity, thus -with the exception

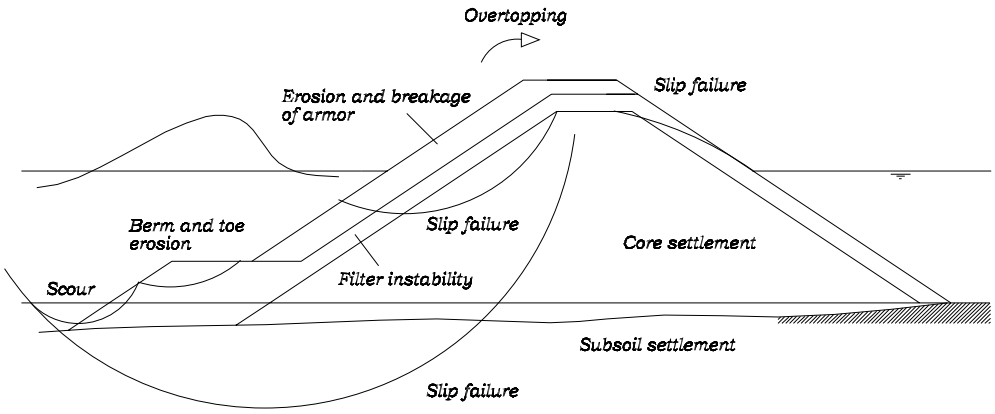

Figure 2.1: Failure modes of a conventional rubble mound breakwater

of the gravity force- all forces vary in size and direction with time. The velocity of the flow depends on the properties of the incoming waves and its action on the slope. Furthermore, it is affected by the permeability and surface roughness of the structure. A common way to express these flow forces on a unit is:

$$\begin{aligned} F_D &\approx C_D \rho_w A \overline{v}|v| \\ F_L &\approx C_L \rho_w A \overline{v}|v| \\ F_I &\approx C_I \rho_w V \frac{d\overline{v}}{dt} \end{aligned} \tag{2.1}$$

In which C_D, C_L and C_I are time dependent empirical coefficients. A is the cross sectional area of the units at right angles to $\overline{v}$ and V their volume. It becomes quite evident that when -beside the complexity of the flow field- also the unconventional shape of the tetrapod and its random placement on the underlayer is considered, deterministic calculation of the forces acting on the armour and secondary layer are impossible to perform. The latter statement results in a stochastic approach in which the response of the armour units and the secondary layer are related directly to the properties of the incident waves. The properties of the wave are captured in environmental parameters. Environmental parameters are boundary conditions which in most cases cannot be influenced by the designer. Because of this, a good insight in the effects of these parameters on the armour and secondary layer is paramount. Environmental variables are characterized by:

- the wave height;
- the wave period;
- the spectral shape of the waves;
- the number of waves;

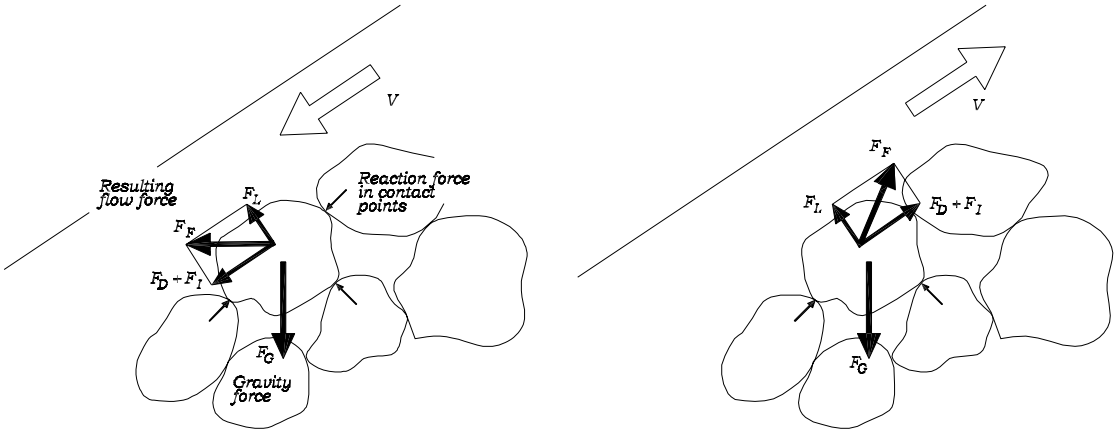

Figure 2.2: Forces on armour units

- the angle of wave attack;
- the water depth.

Structural parameters on the other hand, describe the resistance of the breakwater against the wave loads. The whole of these parameters represents the strength of the breakwater. The most significant structural parameters of the armour and secondary layer are given by:

- the weight of the units;
- the grading of the units;
- the packing density of the armour layer;
- the shape of the units;
- the structural integrity of the units;
- the ratio of diameter between armour, secondary and core material;
- the slope angle;
- the thickness of the layers;
- the height and width of the crest;
- the permeability of the structure.

When simple assumptions are made about the geometry of the units and the flow, it is possible to derive some expressions for the stability. The first simplification is the characterization of an equivalent cube length concerning the units geometry.

$$D_n = \left(\frac{W}{\rho}\right)^{1/3} \tag{2.2}$$

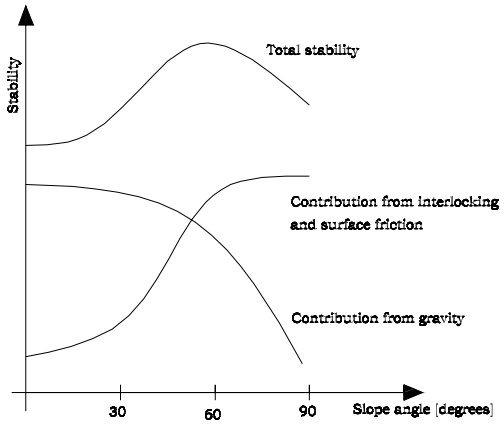

Figure 2.3: Illustration of the effect of interlocking and surface friction on the stability

Where W is the weight and ρ the density. A second assumption is to consider the flow quasi-stationary. The inertia forces can then be neglected. A qualitative stability ratio thus becomes.

$$\frac{\overline{F}_G}{\overline{F}_D + \overline{F}_L} \approx \frac{g(\rho - \rho_w)D_n}{\rho_w v^2} \cdot K \tag{2.3}$$

Or with v substituted by the velocity $v \approx \sqrt{gH}$ (where H represents the wave height) and $\Delta = \frac{\rho}{\rho_w} - 1$ the following expression is obtained:

$$\frac{H}{\Delta D_n} \leq K \tag{2.4}$$

Equation (2.4) can be regarded as a stability parameter. The dimensionless K is a function of the structural parameters, the Reynolds number [1] and the number of units that moved.

Iribarren (1954) considered the failure mode of sliding units and therefore entered a slope correction explicitly in expression (2.4). The dimensionless parameter becomes $K = (\tan\phi \cos\alpha \pm \sin\alpha) \cdot N^{-1}$. In which N is the so-called Iribarren-coefficient that depends, amongst others, on the shape of the unit. $tan\phi$ is the coefficient of friction between layers of armour units or between the armour layer and the underlayer.
Many experimental tests were performed by Hudson (1958). On the basis of model tests with regular waves on rock armour he derived:

$$\frac{H}{\Delta D_n} \leq K_D(\cot\alpha)^{1/3} \tag{2.5}$$

Van der Meer (1988a) presented an empirical formula for rock armour based on small and large scale model tests. It has the form of $\frac{H}{\Delta D_n} = f(S^{n_1}\xi^{n_2}N^{n_3}\alpha^{n_4}P^{n_5})$ where f stands for 'a function of', S signifies the damage level, ξ represents the wave kinematics, N is the number of waves, α is the slope angle and P is an empirical coefficient which signifies the permeability of the slope. For tetrapods on a 1 : 1.5 slope Van der Meer (1988b) presented the following formula:

$$\frac{H_s}{\Delta D_n} = \left(3.75\frac{N_{od}^{0.5}}{N^{0.25}} + 0.85\right) s_{m0}^{-0.2} \tag{2.6}$$

[1] A more detailed explanation of Reynolds number is found in paragraph (3.1)

Rubble mound breakwaters in coastal protection are normally constructed with an armour layer and one or more underlayers, sometimes called filters. Two types of filters can be distinguished, namely a geometrically closed and a geometrically open filter. In the first, the size of the stones of the underlayer are chosen such that they cannot move in and through the top layer. The classical filter rules of TERZAGHI state that -provided that the underlayer is internal stable ($D_{60}/D_{10} < 10$) and no pressure build-up will occur between the interface of the top and underlayer- a filter is considered geometrically closed if the ratio between the size of the armour unit and the underlayer unit is smaller then 6 to 10 ($D_{50_A}/D_{50_S} < 6 - 10$). VAN DER MEER (1993) however, recommends a weight range of the underlayer units of $\frac{1}{25}$ to $\frac{1}{15}$ times the armour unit weight, resulting in the more strict ratio of ($D_{50_A}/D_{50_S} < 2.3 - 3.0$).

In a geometrically open filter, the grains of the underlayer can erode through the top layer. When this type of filter is used, it is essential to keep the hydraulic loading forces on the underlayer smaller than the resisting forces.

Chapter 3

Wave flume experiments

This chapter deals with the set-up of the model tests. First the scaling of the model is discussed. The different environmental and structural parameters, as mentioned in the previous chapter, and their relevance to the model set-up will be treated in the following paragraphs. The method of damage assessment and the test programme conclude this chapter.

3.1 Scaling

A proper representation of reality by means of scale modelling is based on similarity between prototype and model. In fluid-mechanics, similarity generally includes three basic classifications:

- Geometric similarity
- Kinematic similarity
- Dynamic similarity

When all geometric dimensions of the model are related to the corresponding dimensions of the prototype by a constant scale factor, the model is geometrically similar:

$$K = \frac{x_M}{x_P} = \frac{y_M}{y_P} = \frac{z_M}{z_P} \tag{3.1}$$

The science of kinematics studies the space-time relationship. Kinematic similarity consequently signifies similarity of motion. If the velocities at corresponding points on the model and prototype are in the same direction and differ by a constant scale factor, the model is regarded as kinematic similar to the prototype.
In addition to the requirements for kinematic similarity the model and prototype forces must be in a constant ratio to be considered dynamic similar. Complete similarity is obtained if all relevant dimensionless parameters[1] have the same corresponding values for model and prototype:

$$\pi_P = \pi_M = f(\pi_1, \pi_2, ..., \pi_r) \tag{3.2}$$

In which the π's are a complete set of dimensionless products.
Two common dimensionless parameters in free-surface flow are the Reynolds number and the Froude number. The Reynolds number represents the inertia of the flow related to its viscosity. To obtain similarity the Reynolds number for both the model and prototype must be equal:

[1]Dimensionless groups are formally found through non-dimensionalizing conservation equations. An informal approach is the use of Buckingham Pi Theorem (e.g. Langhaar, 1951)

$$Re = \left(\frac{Vh}{\nu}\right)_P = \left(\frac{Vh}{\nu}\right)_M \tag{3.3}$$

With $K_V = V_M/V_P$, $K_h = h_M/h_P$ and $K_\nu = \nu_M/\nu_P = 1$ (modelling is done with water), equation (3.3) can be written as:

$$K_V = \frac{1}{K_h} \tag{3.4}$$

The Froude number represents the inertia of the flow related to the gravity. Again, to achieve similarity the Froude number must be equal in model and prototype:

$$Fr = \left(\frac{V^2}{gh}\right)_P = \left(\frac{V^2}{gh}\right)_M \tag{3.5}$$

With $K_V = V_M/V_P$, $K_h = h_M/h_P$ and $K_g = 1$ (gravity remains unscaled), equation (3.5) can be written as:

$$K_V = \sqrt{K_h} \tag{3.6}$$

The same principle can be applied on the celerity of waves. According to the linear wave theory, the celerity of a wave can be described as:

$$c = \sqrt{\frac{gL}{2\pi}\tanh\left(\frac{2\pi h}{L}\right)} \tag{3.7}$$

With $K_c = c_M/c_P$, $K_L = L_M/L_P$, $K_h = h_M/h_P$ and where the argument of the hyperbolic tangent in model and prototype are the same because of geometric similarity, equation (3.7) changes to:

$$K_c = \sqrt{K_L} = \sqrt{K_h} \tag{3.8}$$

With $c = L/T$, the Froude time scale between prototype and model becomes:

$$K_t = \sqrt{K_h} \tag{3.9}$$

Equation (3.4) shows that, if a small-scale model is tested in the same fluid as the prototype, the preservation of Reynolds number requires the stream velocity for the model to be greater than for the prototype. On the other hand, according to equation (3.6), the preservation of Froude's number requires the opposite condition. In free-surface flow, gravity is considered dominant over viscosity and therefore the wave flume experiments are Froude scaled. A deviation between Reynolds number in the model and prototype is consequently inevitable. This non-similitude of Reynolds number lead to scale effects.

In the model, the top and secondary layer were scaled with a constant length-scale factor between prototype and scale model to represent the stability of these layers correctly. According to Van Gent (1995), applying this scale factor to the top of the structure results in an acceptable representation of the non-linear friction for porous media flow.[2] However, this scale factor is not applicable to scale the linear friction. Since this friction term is usually dominant in the small-scale core of the model, the use of of the same scale factor would lead to a too high friction in the model. This discrepancy can be partly solved by scaling the core material by a different factor, which leads to more course core material. This can be achieved by scaling the core according to a method described by Burcharth et al. (1999).[3]

[2] see paragraph (3.2.2) for an explanation of the linear and non-linear friction as found in the Forchheimer equation.
[3] see paragraph (3.2.2) for a more detailed explanation of this core scaling procedure.

HUDSON (1959), claimed that viscous effects can be discounted in the model if the Reynolds numbers in the pores of a breakwater are above 3×10^4. More recent literature even suggest a value as low as 1×10^4 to discount for these effects (e.g. VAN DER MEER, 1988b).

3.2 Scope of the present study

Because of limitations in time and resources, not all involved parameters were examined. A selection in both environmental and structural parameters was made, mainly based on the relevance to engineering practice.

3.2.1 Environmental parameters

The wave height and period are obvious parameters to include. The wave period is often written as a wave length and when related to the wave height, results in the wave steepness:

$$s_{m0} = \frac{2\pi H_s}{gT_{m0}^2} \tag{3.10}$$

During each experiment the wave height was gradually increased till failure of the structure occurred or the maximum height that can be generated by the wave board was reached. Three different values of the dimensionless wave steepness were investigated, namely a (deep-water) steepness of $s_{m0} = 0.02$, 0.04 and 0.06. In general, the steepness of wind generated waves is between 0.02 and 0.06. By investigating these three steepnesses, this frequently occurring range is covered.
IRIBARREN (1950) related the slope angle of the structure to the wave steepness:

$$\xi = \frac{\tan\alpha}{\sqrt{2\pi H_s / gT_{m0}^2}} \tag{3.11}$$

BATTJES (1974) described possible breaker types as a function of this parameter and called it the *surf similarity parameter*. The parameter tells whether a wave will break and how the wave will break. For different values of ξ, waves brake in different ways. Battjes distinguished the following breaker types: surging, collapsing, plunging and spilling.
In engineering practice, when an armour layer is constructed of artificial concrete units, a slope angle more gentle than $\cot\alpha = 1.5$ is rare. Because of this fact, the influence of the slope angle on the stability of the structure will not be treated further. Therefore, the surf similarity is of lesser importance in this research and stability is related to the wave steepness instead.

Irregular waves

An irregular wave field is best described with a variance density spectrum. The spectrum provides a statistical description of the fluctuating wave height caused by wind. The surface elevation η as a function of time can be seen as the sum of an infinite number of periodic waves:

$$\eta(t) = \sum a_i \cos\left(2\pi f_i t + \varphi_i\right) \tag{3.12}$$

An analysis of a large data set of winds and waves led to the so-called Pierson-Moskowitz spectrum. The full expression, which PIERSON and MOSKOWITZ suggested on the basis of their observation, is:

$$E(f) = \alpha g^2 (2\pi)^{-4} f^{-5} exp\left\{-\frac{5}{4}\left(\frac{f}{f_{peak}}\right)^{-4}\right\} \tag{3.13}$$

In the early eighties a large field experiment in the North Sea led to the JONSWAP-spectrum (HASSELMAN et al., 1973). The spectra that were observed appeared to have a sharper peak

than the Pierson-Moskowitz spectrum. A solution was found in the enhancement of the Pierson-Moskowitz spectrum with a peak-enhancement function:

$$\Gamma(f) = \gamma^{exp\left\{-\frac{1}{2}\left(\frac{f-f_{peak}}{\sigma \cdot f_{peak}}\right)^2\right\}} \tag{3.14}$$

with $\sigma = \sigma_a$ for $f \leq f_{peak}$ and $\sigma = \sigma_b$ for $f > f_{peak}$ to account for a slightly different width on both sides of the spectral peak. The complete expression thus became:

$$E(f) = \alpha g^2 (2\pi)^{-4} f^{-5} exp\left\{-\frac{5}{4}\left(\frac{f}{f_{peak}}\right)^{-4}\right\} \cdot \gamma^{exp\left\{-\frac{1}{2}\left(\frac{f-f_{peak}}{\sigma \cdot f_{peak}}\right)^2\right\}} \tag{3.15}$$

In contrast to the Pierson-Moskowitz spectrum the energy scale parameter α, the shape parameters γ, σ_a and σ_b and the frequency scale parameter f_{peak} are free parameters. The peak frequency was found to be a function of the dimensionless fetch. The other parameters are equally functions of the dimensionless fetch but often are expressed in terms of the dimensionless peak frequency. The mean values of the shape parameters γ, σ_a and σ_b of the JONSWAP observations were $\gamma = 3.3$, $\sigma_a = 0.07$ and $\sigma_b = 0.09$. These values are often used in wave flume experiments. The JONSWAP spectra result in a good description of wind generated wave fields in the North Sea. This spectrum is also commonly used in wave flume experiments (e.g. Van den Bosch, 2001), making the laboratory data accessible for comparison. These two arguments are the most significant reasons to have the wave energy spectra prescribed by means of the JONSWAP spectral shape.
From the spectrum a wave height distribution can be derived. For wave conditions with a single-peaked spectrum in deep water, this distribution can be described with a Rayleigh distribution:

$$P(\underline{H} > H) = exp\left[-2\left(\frac{H}{H_s}\right)^2\right] \tag{3.16}$$

From equation (3.16) it directly follows that H_s is exceeded by 13.5% of the waves. The significant wave height can also be determined from the variance-density spectrum:

$$H_s = H_{13.5\%} \approx 4\sqrt{m_0} \tag{3.17}$$

with the total area of the spectrum being equal to the total variance:

$$m_0 = \int_0^\infty E(f)df \tag{3.18}$$

Storm duration

Van der Meer (1988a) reanalyzed results of Thompson and Shuttler (1975) to show the importance of the storm duration on the stability of a breakwater. He demonstrated that the relation between the number of waves (N) and the damage (S) can be described by:

$$f(S) = \frac{S(N)}{S(5000)} = 1.3\left[1 - e^{-3\times10^{-4}N}\right] \tag{3.19}$$

When only the most important region is considered ($N < 7000 - 10000$) a different relation can be established:

$$S = 0.014\sqrt{N} \tag{3.20}$$

Because of a limitation in time, the total number of generated waves in all tests was set at approximately 1000. This is consistent with the tests done by Van den Bosch (2001). The assumption is made that if no damage has developed after 1000 waves, more waves will also not lead to the development of damage. Secondly, the assumption is made that the JONSWAP-spectrum has been fully developed.

Water depth and angle of wave attack

Previous research (e.g. VAN DER MEER, 1988a) showed that damage will progress around the still water level (SWL). A change in water depth will only cause a variation in the location of the damage, but not of the amount. Therefore the water depth of the scale model was fixed at $h = 0.60m$.
The use of the wave flume did pose some limitations on the research since only perpendicular wave attack can be simulated. Perpendicular wave attack though is often regarded as the most severe condition for the stability of the structure, therefore other angles of incoming waves were not examined.

3.2.2 Structural parameters

Core material

VAN DER MEER (1988a) demonstrated that the permeability of the structure has significant influence on its stability. Froude scaling the material may lead to relatively large viscous forces corresponding with small Reynolds numbers. JENSEN and KLINTING (1983) pointed out that correct scaling requires similar flow fields in the prototype and the model. Similar flow fields are obtained if the hydraulic gradients I in geometric similar points are the same:

$$I_P = I_M \tag{3.21}$$

Furthermore they provided a method to calculate scale distortion for core and secondary material to achieve this requirement. The distortion is calculated from the Reynolds number at maximum pore velocity. However, because the flux in the core varies in time and space, BURCHARTH et al. (1999) proposed the usage of a time and space averaged pore velocity for the calculation of Reynolds number. An estimation of I in one-dimensional cases can be made by means of the extended Forchheimer equation:

$$I = aU + b|U|U + c\frac{\delta U}{\delta t} \tag{3.22}$$

In which U is a characteristic pore velocity and a, b and c are dimensional coefficients. The first term can be regarded as the laminar contribution and the second term as the contribution of turbulence. The last term represents the inertia. According to BURCHARTH (1995) the last term in equation (3.22) can be disregarded when scaling porous flow in breakwater cores. VAN GENT (1995) demonstrated the relative small importance of the inertia term in oscillatory flow tests, thereby validating Burcharth's assumption. The dimensional friction coefficients are denoted as (VAN GENT, 1995):

$$a = \alpha\frac{(1-n)^2}{n^3}\frac{\nu}{gD_{n50}^2} \tag{3.23}$$

$$b = \beta\frac{(1-n)}{n^3}\frac{1}{gD_{n50}} \tag{3.24}$$

$$\beta = \beta_c\left(1 + \frac{7.5}{KC}\right)$$

The non-dimensional α and β_c are empirical determined coefficients dependent on parameters like grading, shape, aspect ratio and orientation of the stones. VAN GENT (1995) states that values of 1000 and 1.1 can be used for α and β_c, respectively. KC stands for the Keulegan-Carpenter number and represents the ratio between the amplitude of the water particle oscillations and the diameter of the core rubble mound.

$$KC = \frac{\widehat{U}T}{nD_{n50}} \tag{3.25}$$

$\widehat{U}$ is the amplitude of the velocity and T the oscillation or wave period.

To determine the horizontal pressure gradient in the core, it can be seen as a function of harmonic oscillating pore pressure (BURCHARTH et al., 1999):

$$p(x,t) = (0.55\rho_w g H_s) e^{\delta(\frac{2\pi}{L'})x} cos\left(\frac{2\pi}{L'}x + \frac{2\pi}{T_p}t\right) \tag{3.26}$$

$$I_x = \frac{1}{\rho_w g}\frac{dp(x,t)}{dx} \tag{3.27}$$

Where L' represents the wave length in the core. The wave length in the core is found as the ratio between the length of the incident wave and a coefficient that accounts for seepage length as a result of the deviation of the flow path caused by the grains, $L' = L/\sqrt{D}$. LE MÉHAUTÉ (1957) gives the empirical coefficient a value of 1.4 for quarry rock material. δ is the dimensionless damping coefficient, characterized by:

$$\delta = 0.0141\frac{n^{1/2}L_p^2}{H_s b} \tag{3.28}$$

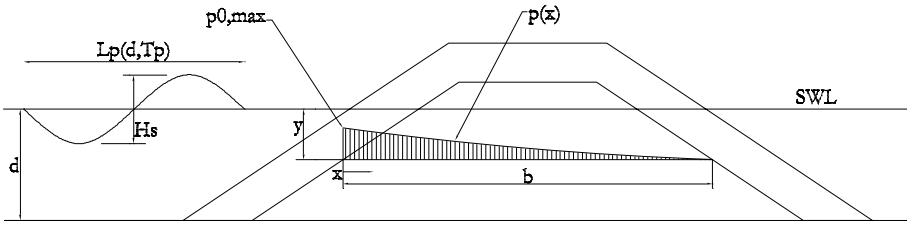

Figure 3.1: Horizontal distribution of the pore pressure amplitudes induced by irregular waves

BURCHARTH suggested that the diameter of the core material in models is chosen in such a way that the Froude scale law holds for a characteristic pore velocity. This method can be used in order to make a good approximation of the occurring Reynolds number in the core. The flux velocity is calculated by means of equations (3.22) and (3.27). These flux velocities are averaged with respect to time (one wave period) in 6 characteristic points (see table (3.4)). This is followed by space averaging these velocities in these points, and thus obtaining the characteristic pore velocity in the structure.

To apply the BURCHARTH method of scaling, first the model of VAN DEN BOSCH is re-scaled to prototype dimensions. These dimensions were used to determine the characteristic pore velocity in the core of this prototype design. Froude scaling this pore velocity by means of the above described method, resulted in the dimensions of the model core material as used in the wave flume experiments.
Re-scaling this model to prototype with $K = 1/25$ gives the characteristic dimensions as found in table (3.1).
The prototype with a W_s/W_a ratio of approximately 1/27 and a W_c/W_s ratio of 1/5 represents a fairly realistic design of a breakwater.
Relevant parameters were established to calculate the characteristic pore velocity in this prototype. The maximum velocity $\widehat{U}$ that occurred in the characteristic points was used to determine the

	Armour layer	Secondary layer	Core
W_{50}^M	206 g	7.3 g	1.6 g
D_{n50}^M	44 mm	14 mm	8.4 mm
W_{50}^P	3100 kg	115 kg	25 kg
D_{n50}^P	1075 mm	350 mm	210 mm

Table 3.1: Re-scaling of the model to prototype with $K = 1/25$

KC-number. Following VAN GENT's (1995) recommendation of $\alpha = 1000$ and $\beta_c = 1.1$ along with equations (3.23), (3.24), (3.25) and a usage of a (median) sea-state of $H_s^P = H_s^M/K = 4.0m$ (with corresponding $T_p = 8.01s$) led to the use of the following parameters:

	D_{n50} (mm)	n	$\widehat{U}$ (m/s)	KC	α	β	a (s/m)	b (s^2/m^2)
Prototype	210	0.4	0.115	10.96	1000	1.9	0.013	8.65

Table 3.2: Parameters used to calculate the characteristic pore velocity in the prototype

The above described parameters, along with equation (3.22) and (3.27) were used to calculate the time averaged pore velocity in all six characteristic points (see table (3.4)). The characteristic pore velocity in the prototype thus becomes $\overline{U}_P = 0.102m/s$. BURCHARTH suggested that the diameter of the core material in models is chosen in such a way that the Froude scale law holds for this characteristic pore velocity. Accordingly, the characteristic pore velocity in the model should be $\overline{U}_M = \overline{U}_P/\sqrt{K} = 0.020m/s$. This criterion is met by setting the diameter of the core material in the model at $D_{n50} = 18mm$ and using the parameters listed in table (3.3). The length scale for the core material now becomes $D_{n50}^M/D_{n50}^P = 1/12$ and $I_M = I_P = 0.084$, opposite to VAN DEN BOSCH's model with $D_{n50}^M/D_{n50}^P = 1/25$ and $I_M = 0.094 \neq I_P$.

	D_{n50} (mm)	n	$\widehat{U}$ (m/s)	KC	α	β	a (s/m)	b (s^2/m^2)
Model	18	0.4	0.032	7.12	1000	2.3	1.77	122

Table 3.3: Parameters used to calculate the characteristic pore velocity in the model

The characteristic pore velocity in the model leads to a Reynolds number $O(500)$. This Reynolds number is below the critical value of $Re = 1 \times 10^4$ and therefore viscous scale effects are inevitable. Although BURCHARTH's method of scaling leads to a better representation of reality, still it is far from perfect. A more suitable model is acquired if the size of the core material varied according to the local flow conditions. By averaging in time and space these local conditions are lost, leading to a model structure that is too permeable at the sides of the core and too impermeable in its center. A better solution lies in the stratification of the material along the complete width of the core, i.e. increase the size of the core material towards the center of the core.
Part of this solution was met by the introduction of an intermediate layer between the core and the secondary layer. This layer had a thickness of $5.0cm$ and a nominal diameter of $D_n = 15.2mm$. Using the same procedure as described earlier, an intermediate layer with a nominal diameter of $D_{n50} = 15.2mm$ (see table 3.5) calculates a time-averaged pore velocity in $x = 0$ of $0.054m/s$. Again, $\overline{U}_M \approx \overline{U}_P/\sqrt{K}$.

Secondary material

The dimensions of the secondary material are often determined by a rule of thumb recommended by VAN DER MEER (1993) that states:

$$W_s \approx \left(\frac{1}{25} - \frac{1}{15}\right) \times W_a \tag{3.29}$$

y (m)	0.0			4.0		
b (m)	20.25			32.25		
x (m)	0	$b/4$	$b/2$	0	$b/4$	$b/2$
U (m/s)	0.126	0.100	0.086	0.110	0.100	0.089

Table 3.4: Time-averaged pore velocity at six different locations

	D_{n50} (mm)	α	β	$\overline{U}$ (m/s)
Prototype	350	1000	4.0	0.28
Model	15.2	1000	4.2	0.054

Table 3.5: Parameters used to calculate the characteristic pore velocity in the transition layer at $x = 0$

With a tetrapod mass of $W_{50} = 206$ grams and a median mass of $W_{50} = 7.3$ grams for the secondary layer, VAN DEN BOSCH (2001) already chose relatively light material for the underlayer. He observed excessive wash-out of secondary layer material, which seriously undermined armour layer stability. The first tests, however, did not agree with his observations. An explanation was sought in the different core scaling procedures between the current scale model and the model used by VAN DEN BOSCH. This led to extra experiments with geotextile placed between secondary layer and core to approach the permeability of VAN DEN BOSCH's structure.[4] Nevertheless, the outcome resulted the initial test programme -in which the weight of rock material of the secondary layer gradually increased after each series- to be altered. Instead, the weight decreased after every series. Consequently, the material VAN DEN BOSCH used, formed a starting point of secondary layer rock weight that was examined. The following weight classes of secondary layer material formed the basis of this research.

Description	W_{50} (g)	D_{n50} (mm)	W_a/W_s
Large	6.5	13.6	31
Mid	4.3	11.3	47
Small	1.7	8.6	119

Table 3.6: Weight classes of the secondary layer as used in the wave flume experiments

Changing the grading of the material is time intensive. Therefore, the grading was not varied in the test series. VAN DER MEER et al. (1996) already conducted experiments to gain insight in the influence of rock shape and grading on stability of low-crested structures. From analysis of their laboratory data followed the conclusion that material properties of rock, such as shape and grading, appear to be of little influence on the stability of the armour layer. A careful assumption that this statement is also applicable for the secondary layer, justifies the choice of not varying the grading.

Literature (e.g. CUR, 1995; SPM, 1984) recommends a layer thickness of $2 \times D_{n50}$. However, the effect of the layer-thickness on the stability of the secondary layer was excluded by means of a fixed layer thickness for all three series. By excluding the effect of the layer-thickness the overall comparability of the different layers is improved. A secondary layer thickness of $4.0cm$ was chosen. When compared to CUR's guideline, this thickness of the secondary layer is considerable. Primarily, this substantial thickness was realized to minimize the effect of large additional friction forces between the rough texture of the core and the upper part ($2 \times D_{n50}$) of the secondary layer. BURCHARTH's method to determine the Reynolds number in the core also served to make an

[4] A more thorough discussion on the differences in outcome as well as the additional experiments can be found in paragraph (4.1)

estimation of this number in the secondary layer. With the nominal diameter ranging from $13.6mm$ to $8.6mm$, the Reynolds number showed $O(1000)$. With the Reynolds number in this range, the flow can be considered transitional between laminar and turbulent. As with the core, viscous scale effects are present and should be taken into consideration when model data is translated back to prototype.

The armour layer

In all tests, the armour layer consisted of concrete tetrapod units with a median weight of 206 grams. The units have a nominal diameter of $D_n = 44.3mm$, where $D_n = 0.65D$ (with D being the height of the unit). The variation in the density of placement of the units is an important variable in this research. According to CUR (1995) the number of units per square meter can be approximated by:

$$N_a = \frac{n_L k_t (1 - n_v)}{D_{n50}^2} \tag{3.30}$$

n_L represents the number of layers making up the total thickness of the armour layer. Because the tests focus on single armour layers, this expression consequently becomes one. For tetrapod units in a double layer the Shore Protection Manual (1984) gives a layer coefficient (k_t) value of 1.04. Although this value probably does not hold for a single layer, because of the absence of a more reliable value in literature, this layer coefficient was used in formula (3.30). The packing density of the tetrapods is characterized by a fictive porosity of the single top layer. Three packing densities were tested ($n_v = 0.25$, $n_v = 0.3$, $n_v = 0.4$). The necessity of investigating a larger porosity is absent. Bhageloe (1998) used a porosity of approximately 0.62. The use of such a wide packing density generates a highly unstable tetrapod armour layer. Wide packing densities characterize themselves by showing highly progressive development of damage, was a conclusion he derived out of his tests. On the other hand, by using a higher packing density ($n_v < 0.25$), the possible translation to practical engineering is as good as lost.
With the use of equation (3.30), the number of tetrapod units per square meter respectively becomes 403, 376 and 322. During the placement of the units in the single armour layer, the aim was to maintain the random character as found in prototype design. A deviation of approximately 3% from the total number of tetrapods per square meter was therefore accepted.

n_v	$N_a(m^{-2})$	deviation (m^{-2})
0.25	404	± 12
0.30	376	± 11
0.40	322	± 10

Table 3.7: Number of tetrapods per m^2

Rocking of artificial concrete units can lead to their breakage. This breakage can cause an early failure of the armour layer. The structural integrity of the tetrapods might be a problem in prototype design, but since this failure mode was not part of the model investigation, the effect is ignored.

3.3 Damage

The experiments focused on the stability of the secondary layer, the stability of the top layer and their interaction. The damage related to the hydraulic stability can be characterized either by measurement of the surface profile of the slope or by counting the numbers of moved units. The first method is used to characterize the damage of the secondary layer, the latter for the armour layer. The measurement of the damage of the armour layer will be progressive, meaning that the damage of the structure will be assessed after every sea-state of approximately 1000 waves. The

damage of the secondary layer was determined at the end of each experiment when failure of the structure had occurred or the maximum wave height that can be generated by the wave board was reached. A structure was classified as *failed* if armour unit movement caused secondary layer exposure of at least $D \times D$ at the end of a run. The structure also failed if erosion of the secondary layer caused exposure of the intermediate layer.

3.3.1 Damage assessment of the secondary layer

Broderick (1984) defined a dimensionless damage number.

$$S = \frac{A_e}{D_{n50}^2} \tag{3.31}$$

Where A_e is denoted as the eroded volume per unit length or cross-sectional eroded area. A physical description of the damage S is the number of cubic stones eroded within a width of one D_{n50}.

For the investigation an automatic surface profiler was used on a controlled carriage. The carriage moved from the top of the structure to the toe with a velocity of $v = 0.5cm/s$. The surface along the slope was measured every $0.2cm$. The cross-sectional spacing was set at $4.0cm$, counting up to a total of 19 measured profiles per experiment.
At the beginning of each experiment -before the placement of the tetrapods- the initial profile of the secondary layer was measured. At its end, the armour units were removed and the secondary layer profile was measured again.
The profiler followed the slope properly. The accuracy of the profile measurements was in the range of ± 0.1 to ± 0.3 cm. The profiler failed to accurately follow the profile of the slope only if a (long-shaped) rock actually 'stuck out' of the secondary layer. The profiler would consequently push the rock over. This occurred only a few times during the experiments, however.

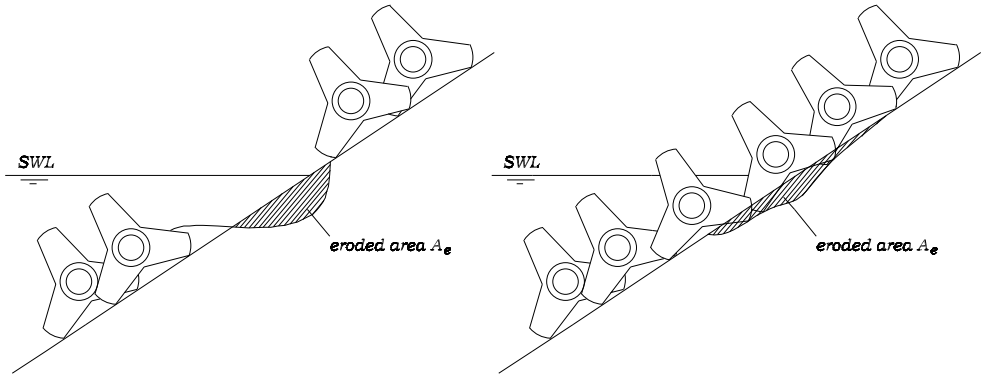

Figure 3.2: The two main mechanisms of failure of the secondary layer

The resulting area of erosion was used to determine the damage number. The use of the damage number must be done critically though. S includes the effect of settlement which are not parallel to the slope. To minimize the occurrence of settlement, before the actual start of the series, the structure was exposed to a small wave field for a duration of approximately 15 minutes. The

waves were low enough not to inflict any damage to the structure yet gave the secondary layer the possibility to settle. Furthermore the sliding of units is not indicated very well in the damage number. Though this failure mode is unlikely to occur on large scale because of the presence of the top layer and the course character of the intermediate layer. The two main failure modes are the wash-out of the rock material under a stable top layer and the erosion of the secondary layer as a result of damage at the top layer. The two failure modes are depicted in figure (3.2). The damage number also lacks a suitable representation of local damage, i.e. one eroded hole over a longer distance along the breakwater.

3.3.2 Damage assessment of the armour layer

A common method to characterize damage of an armour layer of artificial units is to count the number of moving units. This method does require some classification of the movements.

1. no movement
2. rocking of single units
3. movement of units from their initial position by a certain distance ($0.5D_n$ to $2.0D_n$)
4. units displaced from their initial positions (movement of more than $2.0D_n$)

The movement of the units is not uniformly distributed over the slope. In general, all movement takes place within the levels $SWL \pm H_s$. Therefore a reference area should be chosen that takes into account this non-uniformity of movement. In this research the complete slope ($SWL \pm 0.22$) was chosen as a reference value, mainly to facilitate the comparison of the various experimental results.
The rocking of the units is disclosed from the damage evaluation. This is because rocking is only relevant for the evaluation of breakage of the units, which in this thesis is not taken into account.

Through the use of digital imagery the movement of the tetrapod units were monitored. Several digital images of the armour layer were taken at each run from a fixed position perpendicular to the slope. Through comparison of the stills, displacement plots were generated.

To further improve the visualization of the displacement, the tetrapods were placed in colored bands, each having a width of approximately two times the length of a unit. A total of 8 color bands were placed upon the slope. Three different colors were available; at the toe of the structure a red band was placed, followed by a yellow and a green band. This color pattern was repeated twice, though at the eighth band, the crest of the structure was reached.

crest of the structure
yellow
red
green
yellow
red
green
yellow
red
toe of the structure

Table 3.8: Placement of the color bands

The number of stones displaced over a minimum of $2.0D_n$ (N_o) related to the width of the model and the nominal diameter generates the damage number:

$$N_{od} = \frac{N_o}{B/D_n} \tag{3.32}$$

To account for the sliding of the armour units the following definition is used.

$$N_{os} = \frac{N_{sl}}{B/D_n} \tag{3.33}$$

In which N_{sl} represents the number of units that moved a minimum of $0.5D_n$ and a maximum of $2.0D_n$. Furthermore, $N_{omov} = N_{od} + N_{os}$.
As with the damage evaluation of the secondary layer, critical notes can be made concerning this method. For instance, the self healing ability of a tetrapod layer is not included. Often, when a single unit is removed, the surrounding armour will resettle, resulting in an armour layer with a better stability than might be indicated by the counting of displaced units.

3.4 Model set-up

3.4.1 Model dimensions

The physical model tests were performed in the Fluid Mechanics Laboratory of the Faculty of Civil Engineering and Geosciences at Delft University of Technology. The wave flume has a length of 40 meter, a width of 0.80 meter and a height of 0.85 meter. A foreshore with a 1:30 slope was constructed over a length of 6.60 meter and started at 24.80 meter from the wave board. The distance between the toe of the structure and the wave board was 31.40 meter.

The stability of the toe of the structure was not part of the research and therefore the toe was reinforced to prevent development of damage. The influence of the crest height and width also fell outside the scope of this research. When the crest of the structure is low, overtopping will occur and wave energy will pass over the crest. A crest height of $h_{cr} = 0.86m$ insured that a minimum of waves would overtop the structure and almost all energy concentrated on the front slope.

To exclude wave set-up caused by excess pressures in the structure, the inner slope was constructed of homogenous rock material to insure sufficient permeability. The inner slope angle was $cot\alpha = 1.5$.

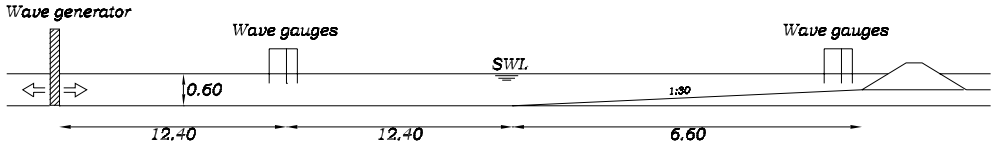

Figure 3.3: Set-up of the wave flume

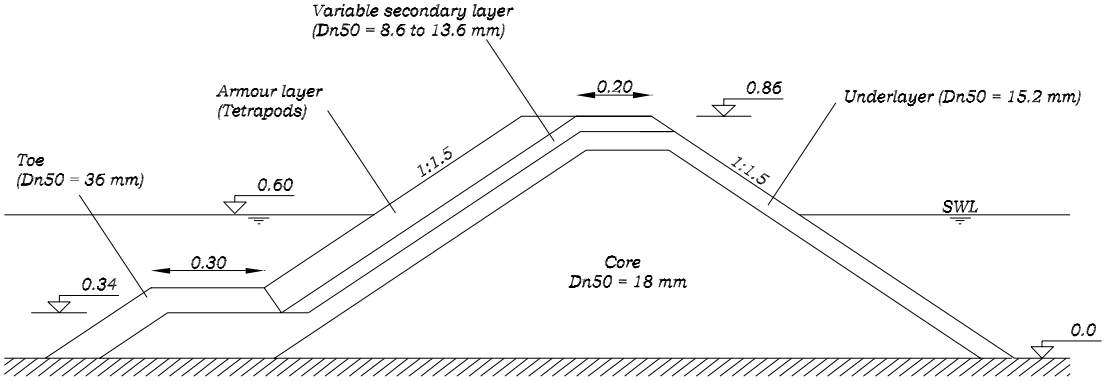

Figure 3.4: Cross-section of the breakwater

3.4.2 Test programme

In the test programme several combinations of secondary material, wave steepness and packing density of the armour layer were examined. The parameters variation in the test series were:

Description	Value
Length wave flume	$40.00m$
Width wave flume	$0.80m$
Height wave flume	$0.85m$
Length wave board to structure	$31.40m$
Length foreshore	$6.60m$
Slope angle foreshore	$1:30$

Table 3.9: Main dimensions of the model

Description	Value
Still water depth	$0.60m$
Height of the crest	$0.86m$
Width of the crest	$0.20m$
Slope angle structure	$1:1.5$

Table 3.10: Structural parameters

- *The secondary layer*; $D_{n50} = 8.6mm$, $11.3mm$ and $13.6mm$;
- *Packing density of the armour layer*; $n_v = 0.25, 0.3$ and 0.4;
- *Wave steepness* (on deep water); $s_{m0} = 0.02, 0.04$ and 0.06;

In this research three deep-water wave steepnesses were examined. Table (3.11) shows the wave steepness and wave height H_{s0}(m) (in italic), with resulting wave periods T_{m0}(s) as used in table (3.11).

s_{m0}	*0.10*	*0.12*	*0.14*	*0.16*	*0.18*	*0.20*	*0.22*
0.02	1.79	1.96	2.12	2.26	2.40	2.53	2.65
0.04	1.27	1.39	1.50	1.60	1.70	1.79	1.88
0.06	1.03	1.13	1.22	1.31	1.39	1.46	1.53

Table 3.11: Combinations of H_s and T_m as used in this research

Each test series in principle consisted of 7 sea-states with increasing wave height (and increasing wave period to maintain the same wave steepness at deep water). An experiment was completed if failure of the structure occurred, or if the wave board could not generate higher waves with sufficient accuracy. The structure was rebuilt after each experiment, but not after each sea-state.

Van den Bosch kept a constant deep water steepness of approximately $s_{m0} = 0.05$ based on argumentation of Van Gent (1998). In his research on single layer rubble mound breakwaters with concrete cubes, Van Gent concluded that there was no clear and consistent influence of the wave steepness. This statement is too bold to apply on the stability of the secondary layer, resulting in the investigation of three different wave steepnesses in each series.

During the variation in wave steepness, the packing density of the armour layer is kept constant at $n_v = 0.3$. This packing density is chosen as a reference value, because it is expected that the armour units have sufficient interlocking ability to show non-progressive development of damage. Thus handing the possibility of better examining the response of the secondary layer. It also stands closer to the reality of construction then $n_v = 0.25$, since the latter is very hard to establish in prototype design.

Series	Description	$D_{n50_S}(mm)$	$s_{m0}(-)$	$n_v(-)$
A0	Geotextile	13.6	0.04	0.3
A1	Large	13.6	0.04	0.25, 0.3, 0.4
A1	Large	13.6	0.02, 0.04, 0.06	0.3
A2	Mid	11.3	0.04	0.25, 0.3, 0.4
A2	Mid	11.3	0.02, 0.04, 0.06	0.3
A3	Small	8.6	0.04	0.25, 0.3, 0.4
A3	Small	8.6	0.02, 0.04, 0.06	0.3

Table 3.12: Test programme

The effect of the packing density of the armour layer will also be tested for all three series. By means of these tests possible trends in damage development for all three weight categories of secondary rock material must be recognized.

3.4.3 Instrumentation

At series A0 and A1 two arrays of two wave gauges were installed to split the recorded signals into incident and reflected components. To improve the accuracy, later series contained arrays of three wave gauges. The gauges were positioned at deep water (halfway between the wave board and the start of the foreshore) and in front of the toe of the structure. By positioning the wave gauges at these two locations, the wave propagating towards the structure could be separated from the reflected wave using WL|Delft Hydraulics' *Reflec*.

3.4.4 Test procedure

The following test procedure applied for all runs during the flume experiments. Every series started with the placement of a secondary layer (along with its settlement procedure) and the calibration of the automated profiler and the wave gauges.

1. measuring the initial profile of the secondary layer with the automated profiler
2. placement of the tetrapod layer
3. filling of the wave flume until SWL was set at $0.60m$
4. photographing the initial armour layer
5. start with first sea-state of $H_{m0} = 0.10m$
6. photographing the armour layer every 2 minutes
7. photographing the armour layer at the end of the sea-state after the water table became tranquil
8. repeat steps 4-7 for increasing wave height till failure occurred or the maximum of $H_{m0} = 0.22m$ was reached
9. removal of the armour layer units
10. measuring the profile of the secondary layer with the automated profiler

Chapter 4

Observations of the wave flume experiments

This chapter deals with the observations of the wave flume experiments. The hydraulic stability of the armour layer and secondary layer during the various experiments will be discussed. To put some results into perspective, parallels are made to observations and results of Van den Bosch (2001) throughout this chapter.

4.1 Observation of series A0

The model set-up closely followed the set-up of Van den Bosch. The main difference, as indicated earlier, is found in the core scaling procedure. While Van den Bosch followed the linear geometrical scaling of the core material, this model structure was scaled to maintain similarity of hydraulic gradients in model and prototype. This led to a more course material in the core and a more permeable structure. Because of the absence of expected wash-out of the secondary layer in the first series -expectations mainly founded on observations of Van den Bosch- a possible explanation was sought in the more permeable character of the structure. Van der Meer (1988a) already recognized the importance of the permeability by introducing a permeability parameter P in his stability formulae.
A decrease in the permeability of the core should lead to larger up-rush and down-rush velocities in the armour and secondary layer and consequently to a lower stability of both layers. Most probably even to the wash-out of the underlayer as observed by Van den Bosch. To accurately prove the latter statement, experiments with a structure identical to that of Van den Bosch should be conducted. Because of a limitation in time however, a compromise was found in the placement of a geotextile between the core and the intermediate layer.

Though it is emphasized that a thorough comparison of the permeability of the model with the geotextile and Van den Bosch' set-up should consist of permeability experiments, for reasons of practicality a qualitative analysis must suffice. One qualitative means of analysis is to compare the overall hydraulic conductivity of the core of both structures. The relation between the pore velocity and the pressure gradient can be written as:

$$U = \frac{K \cdot I^{(1/p)}}{n} \tag{4.1}$$

In which U is the pore velocity of the flow in the core, K the hydraulic conductivity, I the hydraulic gradient and n the porosity. p represents the character of the flow, with the outer limits of $p = 1$ for laminar flow and $p = 2$ for turbulent flow. Using equations (3.22) to (3.27) to determine the space

and time averaged pore velocity and hydraulic gradient of the core and calculating K for laminar and turbulent flow lead to:

	D_{n50} (mm)	n	$\overline{U}$ (m/s)	$\overline{I}$	$K_{p=1}$ (m/s)	$K_{p=2}$ (m/s)
Model	18	0.4	0.020	0.084	0.095	0.028
Bosch	8.4	0.4	0.009	0.094	0.038	0.012

Table 4.1: The hydraulic conductivity of the core

Adding the geotextile to the initial structure transforms the core in a two-layer system with different hydraulic conductivities for each layer. The effective hydraulic conductivity of the system as a whole can be described by $\frac{L}{K} = \frac{L_1}{K_1} + \frac{L_2}{K_2}$, in which L_1 represents the width of the core at SWL and L_2 stands for the thickness of the geotextile. Using the geotextile properties as listed in table (4.2), result in hydraulic conductivity values of $K_{p=1} = 0.048m/s$ and $K_{p=2} = 0.022m/s$.

properties	average	st. dev.
weight	179.7 g/m^2	1.7 g/m^2
thickness	2.2 mm	0.2 mm
K value	0.3 mm/s	0.08 mm/s
O_{90} value	252 μ	17 μ

Table 4.2: Properties of the geotextile

Figure (4.1) clearly demonstrates a decrease in the permeability of the structure because of the addition of the geotextile. In a transient flow regime the model approached the permeability of the model used by VAN DEN BOSCH.

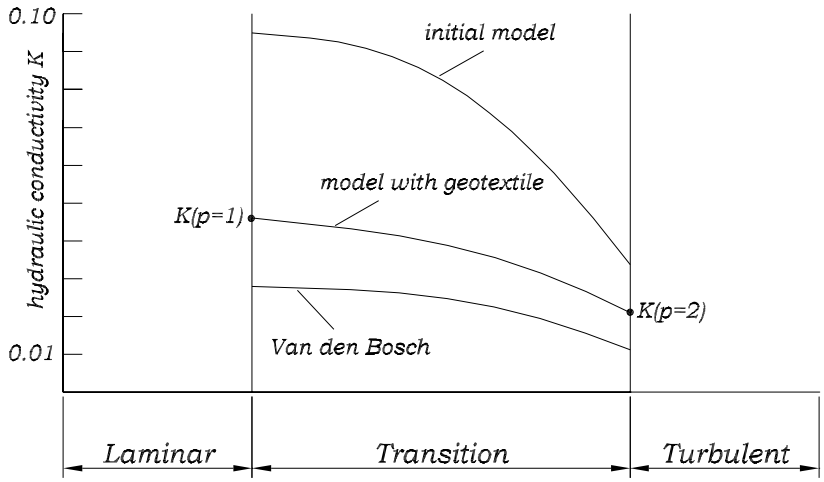

Figure 4.1: Illustration of the hydraulic conductivity of the different model set-ups

A second approach to determine wether the permeability of the various structures differ, is to compare the reflection of the incoming waves on the different model set-ups. POSTMA (1989) investigated the reflection of waves on an infinite high slope and recognized a clear influence of the slope angle, the wave-steepness and the permeability parameter P as defined by VAN DER MEER(1988). After curve-fitting the experimental results, in which different model structures with

various permeability parameters ($P = 0.1$, 0.5 and 0.6) were examined, POSTMA came up with the following relation.

$$K_R = 0.081 P^{-0.14} \cot\alpha^{-0.78} s_{m0}^{-0.44} \tag{4.2}$$

Applying the above described formula with the wave data obtained in series A1, lead to an average permeability parameter of $\overline{P} = 0.3$ and $\sigma_P = 0.1$, while series A0 shows $\overline{P} = 0.1$ and $\sigma_P = 0.02$. A decrease in the value of the permeability parameter means a decrease in permeability. Again, this demonstrates the effect of the geotextile. But how does the permeability of the structure with the geotextile relate to the model VAN DEN BOSCH used? From the wave data he collected, follows $\overline{P} = 0.1$ and $\sigma_P = 0.05$, which consequently verifies the statement that the permeability of the model with the geotextile approaches that of VAN DEN BOSCH' structure. A summary of the different permeability parameters is found in table (4.3). It should be noted that the results in table (4.3) only serves as a indication of the permeability of the different models. It can only be considered an indication because the reliability of the outcome is arguable, since some parameters that were used in POSTMA's formula, fall in the outer limits of the formula's validity range.

Model	$\overline{P}$	σ_P
without geotextile	0.3	0.1
with geotextile	0.1	0.02
VAN DEN BOSCH	0.1	0.05

Table 4.3: Permeability parameter of the different model set-ups

4.1.1 Armour layer stability

Two experiments were performed with the geotextile structure. Both experiments consisted of an armour layer with $n_v = 0.3$, while the wave steepness was kept constant at $s_{m0} = 0.04$.

The experiments are named, using the value of the test-parameters. For example A0N3S4(G)(R), in which A0 signifies the current series, N3 means $n_v = 0.3$ and S4 represents $s_{m0} = 0.04$. G indicates the use of a geotextile, while R stands for repeat.

Two failure mechanism occurred during the wave attack, namely the displacement of the tetrapod units out of the armour layer (movement of at least $2.0D_n$) and the sliding of units (movement between $0.5D_n$ and $2.0D_n$). The following test results are presented.

H_s (m)	$\frac{H_s}{\Delta D_{n_A}}$	T_m (s)	N_{od}	N_{os}	N_{omov}
0.083	1.38	1.12	0	0	0
0.102	1.70	1.21	0	0	0
0.127	2.11	1.33	0	0	0
0.147	2.44	1.46	0.17	0.28	0.45
0.164	2.72	1.58	0.39	2.86	3.25

Table 4.4: Test results for A0N3S4G

Figure (**??**) shows the damage curves of both experiments along with the damage curve VAN DEN BOSCH found at $n_v = 0.3$. The damage curves for all three experiments are rather similar. Initial damage (i.e. the start of displacement of units) started between $H_s/\Delta D_{n_A} = 2.2$ and 2.3.

VAN DEN BOSCH also did a visual observation on the relative small movement or sliding of the units. In his observation he describes that no sliding of the tetrapod units occurred throughout

H_s (m)	$\frac{H_s}{\Delta D_{n_A}}$	T_m (s)	N_{od}	N_{os}	N_{omov}
0.084	1.38	1.13	0	0	0
0.103	1.72	1.22	0	0	0
0.126	2.08	1.32	0	0	0
0.148	2.44	1.46	0.11	0.66	0.77
0.165	2.72	1.58	0.39	3.88	4.27

Table 4.5: Test results for A0N3S4GR

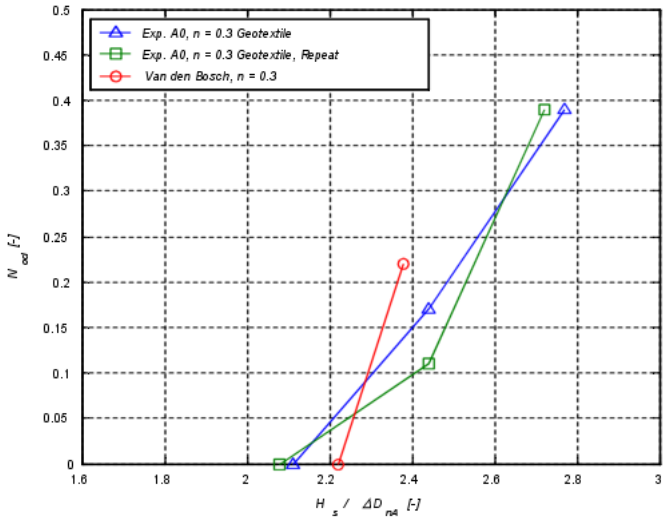

Figure 4.2: Damage curves (N_{od}) for A0N3S4G, A0N3S4GR and VAN DEN BOSCH

his experiments. Experiments A0N3S4G and A0N3S4GR on the other hand, showed considerable movement of units within the $0.5D_n$ to $2.0D_n$ range, namely a total number of 57 and 83 units respectively.

What could have caused such discrepancies between both results? All test conditions were very similar; the armour packing density set at $n_v = 0.3$ while the average deep-water wave steepness of both experiments was $s_{m0} = 0.044$ versus a steepness of $s_{m0} = 0.050$ by VAN DEN BOSCH. The only aspect of the model's set-up that could explain this difference is the core-scaling. Yet figure (4.2) demonstrates that the damage curves for all three runs were rather similar, i.e. the total number of displaced units out of the armour layer is comparable. If the difference in permeability between both models was so significant as to cause this substantial difference in the number of sliding units, most probably it would have also resulted in a considerable deviation of displaced units for both set-ups. Since this is not the case, the difference in permeability between the models can be excluded as the main cause of difference in the number of sliding units. The most likely explanation is found in the difference of observation methodology.
Displaced units fall outside their color band and are usually deposited at the toe of the structure. Visually observing this displacement is relatively easy. However, visually observing small movements of the tetrapod elements proved to be very inaccurate, mainly because movement occurs during the run-up en run-down of attacking waves. The turbulent flow around the tetrapods hinders a clear sight and therefore an accurate observation. The usage of digital imagery solves this problem completely. With the use of *Adobe Photoshop* and *Autodesk's AutoCAD* displacement plots were generated for all runs. These plots show which unit has moved and how much it has

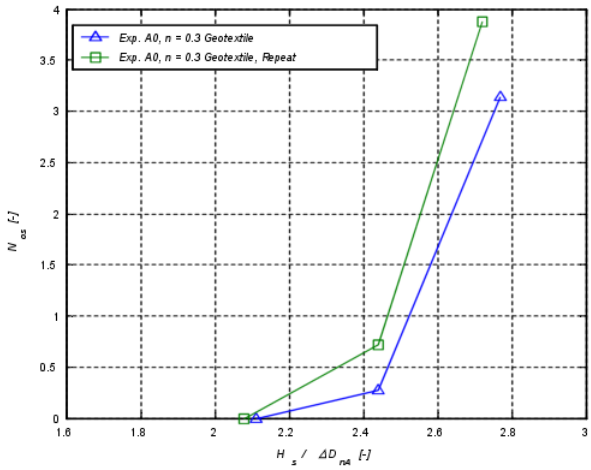

Figure 4.3: Damage curves (N_{os}) for A0N3S4G and A0N3S4GR

moved. Cross-checking these plots with visual observations during several experiments always led to a serious underestimation of the total of units that moved by the latter method. An improvement in observation technique therefore explains the difference in outcome of minor armour unit movement between the two reference models and the model as used by VAN DEN BOSCH.

For both geotextile models initial displacement and sliding of the units occurred simultaneously during the same sea-state. Displacement caused an increase of sliding units, because the surrounding units filled the newly founded gaps to some extend. Furthermore, at a packing density of $n_v = 0.3$ the units still had some margin of resettlement, resulting in a slightly more dense armour layer around and below SWL at the end of the experiment.

4.1.2 Secondary layer stability

Reference tests without the armour showed erosion of the secondary layer within an area of $SWL \pm H_s$. Since the erosion is calculated as the difference between the initial profile and the profile after an experiment, taking the complete slope as a reference area will lead to an overestimation of the eroded area. This is due to the considerable length of the slope compared to the diameter of the secondary material. Small errors in the measurement of the profile are inevitable. Errors that are largely contributed by small deviations from the grid line of the initially cross-sectional profile measurements and the measurements at the end of an experiment. However, these small errors add up significantly over a relatively long slope. To minimize these errors of measurement, a reference area of $SWL \pm H_s$ was chosen to calculate the erosion of the secondary layer. The significant wave height is the wave height at which failure of the structure occurred.

Table (4.6) and (4.7) show the damage of both series for all 19 measured cross-sectional profiles. The total damage of the secondary layer in experiment A0N3S4G was $\sum S = 181$, while A0N3S4GR showed a slightly higher overall damage of $\sum S = 224$. The average damage per cross-section is $S = 9.55$ and $S = 11.79$ respectively. Figure (4.4) and (4.5) show contour plots of the entire slope generated from the measured profile data. The x-axis is perpendicular to the incident waves. The lines in the plot ($x = 4cm$, $8cm$,..., $76cm$) indicate the locations of the measured cross-sectional profiles. The y-axis is projected on the slope. $y = 2cm$ is at the toe of the structure, while $y = 78cm$ is at the crest. The erosion of the slope is indicated in centimeters.
The decrease in permeability of the structure illustrates itself by a higher overall erosion of the

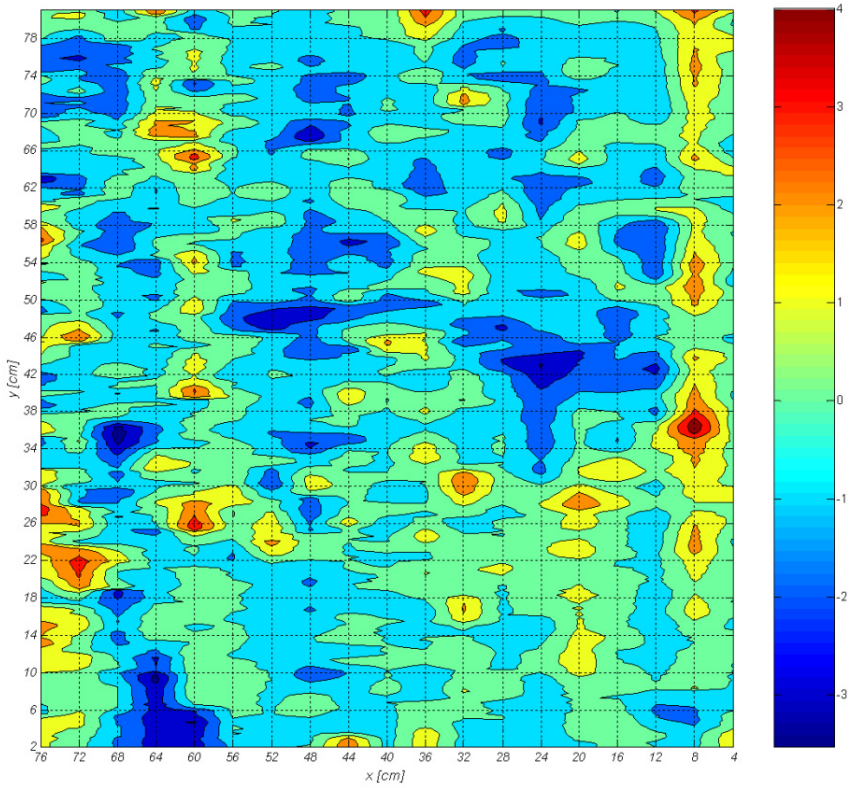

Figure 4.4: Erosion of the secondary layer (A0N3S4G)

secondary layer at series A0 than the experiments in series A1, held under similar conditions (see paragraph 4.2). Nevertheless, the secondary rock material did not show excessive wash-out as with the experiments of VAN DEN BOSCH and erosion was limited to local spots. The size of these local eroded areas were relatively small and none were deeper then $3.0cm$. If the secondary layer thickness was $2 \times D_{n50}$, however, these local erosions could become the critical failure mode of the structure.

Series A0 demonstrates the influence of the permeability of the structure on the hydraulic stability of the armour and secondary layer. But even more so, it demonstrates the importance of an accurate scaling technique.

To determine if there was a causal relation between the location of the eroded spots and the damage development of the armour layer, a $4cm \times 4cm$ grid was placed over both the digital images of the top layer -taken at the end of every sea-state- and the erosion plots of the secondary layer. The comparisons of these plots provide information on the location of the eroded spots and the response of the top layer at this location. This established the mechanism of failure of the secondary layer within the reference area. As depicted in figure (3.2), erosion can occur due to the formation of gaps in the top layer caused either by the sliding or displacement of individual or groups of units or wash-out of the material under a stable top layer.

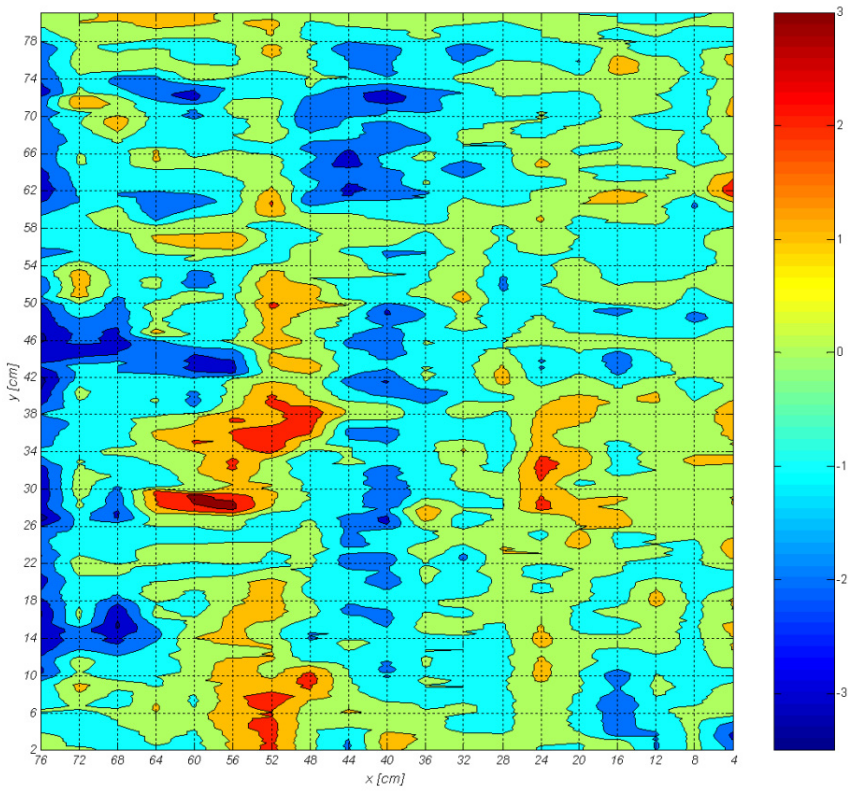

Figure 4.5: Erosion of the secondary layer (A0N3S4GR)

A summary of the comparison of the top and underlayer for A0N3S4G and A0N3S4GR is given in table (4.8) and (4.9). The coordinates define the locations of the eroded volumes with a minimal depth of 1.0*cm*, while *armour response* states the dominant damage mechanism of the armour layer on these locations during the experiment. Armour response is qualified by either *no movement*, *displacement* or *sliding*. A qualitative distinction is made between minor sliding -during which only very few units moved a little- and major sliding. *Mechanism* stands for the manner of erosion of the underlayer. *gap* represents the first above described mechanism; erosion of the secondary layer caused by an increase in void size between armour units, resulting from either sliding or displacement. *stable* stands for the mechanism of erosion of the secondary layer under a non-damaged armour layer. Sometimes a group of units slides down collectively. The armour response at that location is then classified as *sliding*. Nevertheless, it is possible that even with the occurrence of sliding, the void size between individual units does not increase. Therefore, despite the sliding of the armour units, if erosion of the secondary layer occurred at such a location, it was classified as wash-out under a *stable* armour layer.

The comparison of the top layer response with the underlayer erosion illustrates the significant effect of the -sometimes small- movement of units. The rearrangement of armour units -and thus the possible increase in void size between these units- could cause the wave to more directly penetrate the secondary layer. The test results further show that wash-out of secondary layer rock material under a *stable* armour layer happens only occasionally.

$x(cm)$	$S_x(-)$	$x(cm)$	$S_x(-)$	$x(cm)$	$S_x(-)$	$x(cm)$	$S_x(-)$
4	1.30	24	19.81	44	8.97	64	17.35
8	1.16	28	9.39	48	22.36	68	20.60
12	16.09	32	4.68	52	12.39	72	4.41
16	8.70	36	5.77	56	6.30	76	5.90
20	7.01	40	6.97	60	2.25		

Table 4.6: Damage of the secondary layer (A0N3S4G)

$x(cm)$	$S_x(-)$	$x(cm)$	$S_x(-)$	$x(cm)$	$S_x(-)$	$x(cm)$	$S_x(-)$
4	1.11	24	3.14	44	14.07	64	8.57
8	6.15	28	6.18	48	5.38	68	23.79
12	2.85	32	31.07	52	1.87	72	11.78
16	10.18	36	7.48	56	5.28	76	49.10
20	1.74	40	24.73	60	9.55		

Table 4.7: Damage of the secondary layer (A0N3S4GR)

$x(cm)$	$y(cm)$	Armour response	Mechanism
12 - 16	54 - 58	minor sliding	gap
20 - 28	38 - 46	displacement	gap
20 - 28	58 - 66	major sliding	gap
32 - 44	58 - 66	major sliding	gap
40 - 48	54 - 58	minor sliding	stable
44 - 56	46 - 50	minor sliding	stable
44 - 48	66 - 70	major sliding	gap
64 - 72	30 - 38	displacement	gap
64 - 72	54 - 58	major sliding	gap

Table 4.8: Failure mechanisms of the secondary layer (A0N3S4G)

$x(cm)$	$y(cm)$	Armour response	Mechanism
12 - 20	42 - 46	minor sliding	gap
36 - 44	22 - 30	minor sliding	gap
36 - 44	38 - 50	minor sliding	gap
36 - 40	62 - 70	major sliding	gap
56 - 68	42 - 46	minor sliding	stable
60 - 68	58 - 62	displacement	gap
60 - 68	70 - 74	displacement	gap
64 - 72	26 - 30	major sliding	gap

Table 4.9: Failure mechanisms of the secondary layer (A0N3S4GR)

4.2 Observation of series A1

Series A1 consisted of six experiments, all with a secondary layer of $D_{n50} = 13.6mm$. Two experiments were performed with an armour packing density of $n_v = 0.3$ and a wave-steepness of $s_{m0} = 0.04$. The influence of the armour packing density on the armour and secondary layer stability was investigated by conducting two experiments with respectively $n_v = 0.25$ and $n_v = 0.4$. Also the influence of the wave steepness was investigated by performing experiments with relative long wind waves ($s_{m0} = 0.02$) and short wind waves ($s_{m0} = 0.06$).

4.2.1 Armour layer stability

Two experiments were performed with $n_v = 0.3$ and $s_{m0} = 0.04$. An experiment with these parameters is a reference to both the experiments with different armour layer packing densities and wave steepnesses. By performing an experiment with this configuration twice, the reliability of the outcome can be somewhat validated. The first two experiments (A1N3S4 and A1N3S4R) showed the following outcome.

H_s (m)	$\frac{H_s}{\Delta D_{n_A}}$	T_m (s)	N_{od}	N_{os}	N_{omov}
0.084	1.38	1.12	0	0	0
0.104	1.71	1.24	0	0	0
0.124	2.04	1.35	0	0	0
0.144	2.38	1.48	0.11	0.55	0.66
0.164	2.73	1.58	0.28	2.64	2.92

Table 4.10: Test results for A1N3S4

H_s (m)	$\frac{H_s}{\Delta D_{n_A}}$	T_m (s)	N_{od}	N_{os}	N_{omov}
0.083	1.39	1.10	0	0	0
0.104	1.74	1.21	0	0	0
0.127	2.12	1.35	0	0	0
0.145	2.42	1.49	0.06	0.44	0.50
0.173	2.88	1.63	0.33	2.94	3.27

Table 4.11: Test results for A1N3S4R

The results of both experiments are quite similar. The armour layer showed neither displacement nor minor movement of units till a certain sea-state was reached. During this particular sea-state ($H_s = 0.144m$ for the first experiment and $H_s = 0.145m$ for the second experiment) the top layer slightly resettled around SWL to a more dense packing. Additionally, because of the random placement of the armour layer, the interlocking ability of several units was far from optimal. It are the unfavorable placed tetrapods that got displaced out of the armour layer during this sea-state. The following sea-state showed a progressive continuation of the described process. More units were displaced, followed by resettlement of surrounding units to fill the newly formed gaps. The two failure mechanisms combined, led to loss of armour stability and to failure of the structure, which in these experiments were intolerable gaps formed in the upper part of the structure's armour layer.

Influence of the packing density

The primary failure mode of the top layer at $n_v = 0.4$ was not the displacement of units out of the armour layer, but rather the significant resettlement of the units. This initial damage already occurred during the first sea-state at $H_s = 0.083m$. The resettlement caused an increase in packing

density around SWL, but left a considerable gap over the entire flume-width. The gap was formed around the level of the maximum run-up of incoming waves, between the top yellow band of units and the red band. The following sea-state did not show any development of damage. Also, the unprotected secondary layer -exposed because of the gap in the armour layer- did hardly erode. This led to a third run with $H_s = 0.126m$. The increase in wave run-up during this sea-state resulted in further -minor- resettlement and considerable downward movement of units in the unsupported yellow band and consequently in an unaccepted increase in gap size, i.e. failure of the structure. The results of this experiment are found in table (4.12).
The digital stills taken before and after the first sea-state showed an increase in packing density from $n_v = 0.4$ to approximately $n_v = 0.3$. The following sea-state did not show an increase in packing density. The final run did, however, leading to a packing density in the range of $n_v = 0.23 - 0.27$. Apparently a single layer of tetrapods has a natural packing density somewhere in this range.

H_s (m)	$\frac{H_s}{\Delta D_{n_A}}$	T_m (s)	N_{od}	N_{os}	N_{omov}
0.083	1.39	1.12	0	2.15	2.15
0.103	1.71	1.22	0	0	0
0.126	2.10	1.34	0	0.44	0.44

Table 4.12: Test results for A1N4S4

The experiment with $n_v = 0.25$ showed a different outcome. The initial stability of this configuration was considerable. During the first three increasing sea-states neither displacement nor resettlement of units occurred. At $H_s = 0.149m$ small movement of several units around the still water level took place in conjunction with the displacement of three units out of their original position at the lowest yellow band. The following sea-state led to the displacement of six units around SWL, which caused failure of the structure.

H_s (m)	$\frac{H_s}{\Delta D_{n_A}}$	T_m (s)	N_{od}	N_{os}	N_{omov}
0.082	1.36	1.12	0	0	0
0.104	1.72	1.22	0	0	0
0.126	2.10	1.35	0	0	0
0.146	2.42	1.47	0.17	1.16	1.32
0.161	2.67	1.60	0.39	2.42	2.75

Table 4.13: Test results for A1N25S4

The damage curves for $n_v = 0.3$ and $n_v = 0.25$ as shown in figure (4.6) are not very different. These curves are based on the displacement of the tetrapods out of the armour layer. The considerable resettlement occurring at $n_v = 0.4$ is made explicit in the damage curve (N_{os}), illustrated in figure (4.7). To compare the results of the experiments with different armour packing densities (and wave steepnesses), two criteria are formulated. Namely, a criterium of *no damage*, in which $N_{od} = 0$ and *severe damage*, in which $N_{od} = 0.28$. The latter value is chosen after comparing the development of damage for all experiments. Though the influence of sliding is not taken into account in these criteria, most experiments showed a rapid progression towards failure after $N_{od} = 0.28$. The stability numbers corresponding with the two damage numbers were determined assuming a linear relation between the measured test results, as illustrated in the damage curves. Assuming an exponential relation would approximate reality more exact (VAN DER MEER, 1988b), however because of the limited number of data points, plotting an exponential function through these points is inaccurate. The comparison of the stability at different packing densities of the armour layer is illustrated in figure (4.8). The upper points represent the *severe damage* criterium, while the lower points state the *no damage* criterium.

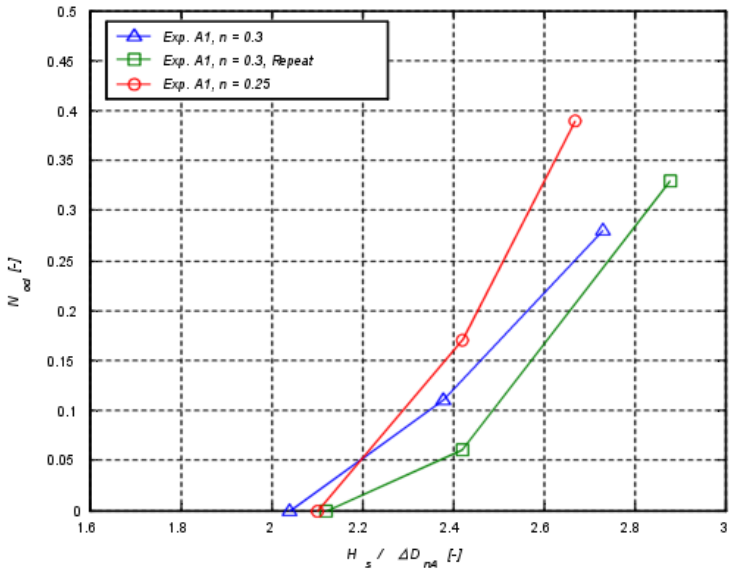

Figure 4.6: Damage curves (N_{od}) for A1N3S4, A1N3S4R and A1N25S4

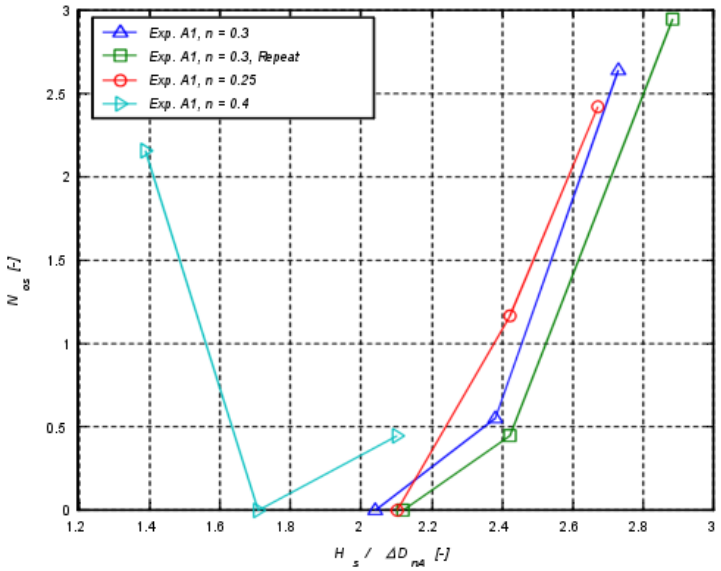

Figure 4.7: Damage curves (N_{os}) for A1N3S4, A1N3S4R,A1N4S4 and A1N25S4

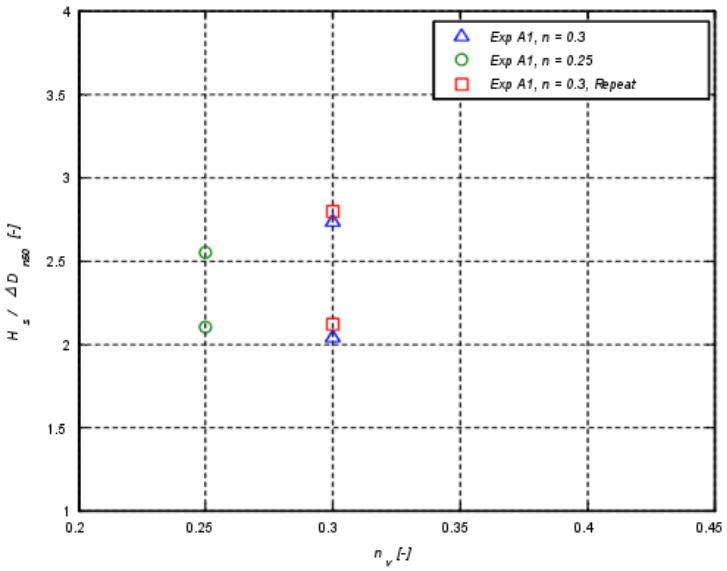

Figure 4.8: Comparison of stability

Influence of the wave steepness

The influence of the wave steepness on the stability of artificial armour units has been a subject of research over the years. Van der Meer (1988b) argued that longer wave periods increase the hydraulic stability of the top layer, made explicitly in his stability formula (2.6). Other studies however report a decrease in stability of the top layer with an increase in wave period. A common explanation for the latter tendency is the *reservoir effect* of the voids between the units. The voids are filled with water during run-up and filled with air during wave recession. The relative large porosity of the armour layer reduces not only the wave run-up considerably, but also the overflow velocities. Long waves carry more water per wave onto the slope which causes a reduction in the reservoir effect. This reduction leads to higher overflow velocities and consequently to a lower hydraulic stability. The above described trend is to some extend visible in the results of the experiments with $s_{m0} = 0.02$ (A1n3s2) and $s_{m0} = 0.06$ (A1n3s6).

H_s (m)	$\frac{H_s}{\Delta D_{n_A}}$	T_m (s)	N_{od}	N_{os}	N_{omov}
0.089	1.48	1.61	0	0	0
0.117	1.94	1.73	0	0.06	0.06
0.142	2.35	1.86	0	0.11	0.11
0.162	2.70	1.99	0.11	0.72	0.83
0.182	3.03	2.16	0.72	1.38	2.10

Table 4.14: Test results for A1n3s2

The experiment with the steepest waves revealed initial damage at a relatively high stability number. Progression of damage started at $H_s = 0.193m$. Displacement and sliding of the units occurred simultaneously while the displacement of several units increased the number of sliding units.
The experiment with longer waves showed a decrease in stability when compared to the short wave experiment. In this experiment, displacement and sliding of units did not occur at the same time. The resettlement of the armour layer started considerably sooner then the displacement of units. In this particular case, the early resettlement had a positive effect on the overall stability of the

H_s (m)	$\frac{H_s}{\Delta D_{n_A}}$	T_m (s)	N_{od}	N_{os}	N_{omov}
0.089	1.48	0.99	0	0	0
0.117	1.95	1.06	0	0	0
0.142	2.36	1.15	0	0	0
0.162	2.69	1.23	0	0	0
0.182	3.03	1.32	0	0	0
0.193	3.21	1.40	0.06	0.11	0.17
0.212	3.52	1.50	0.33	2.26	2.59

Table 4.15: Test results for A1N3S6

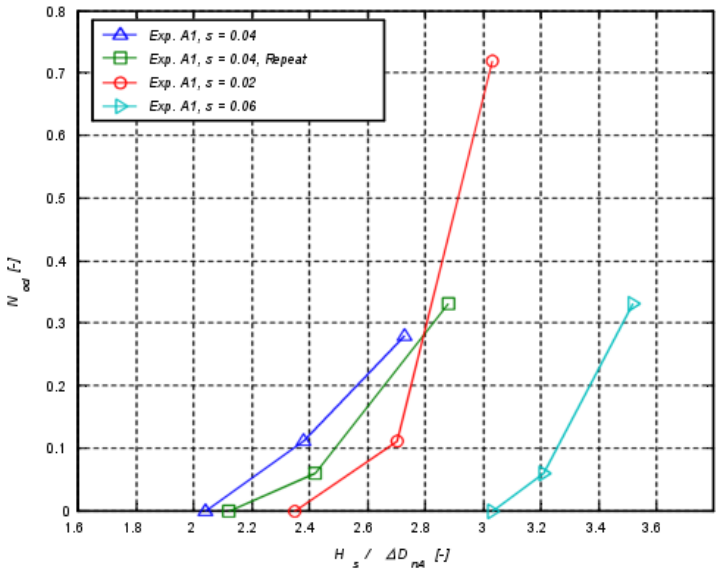

Figure 4.9: Damage curves (N_{od}) for A1N3S2, A1N3S4, A1N3S4R and A1N3S6

top layer. The armour layer could resist relative large up- and down-rush velocities -following from the longer wave periods- before displacement occurred. Therefore, the damage curves concerning the displacement of units (N_{od}) for $s_{m0} = 0.04$ and $s_{m0} = 0.02$ do not differ a lot, although the development of damage at $s_{m0} = 0.02$ does have a more progressive character.
A comparison on the stability at different wave steepnesses is found in figure (4.11). The same comparison criteria (*no damage* and *severe damage*) are used as in the previous paragraph.

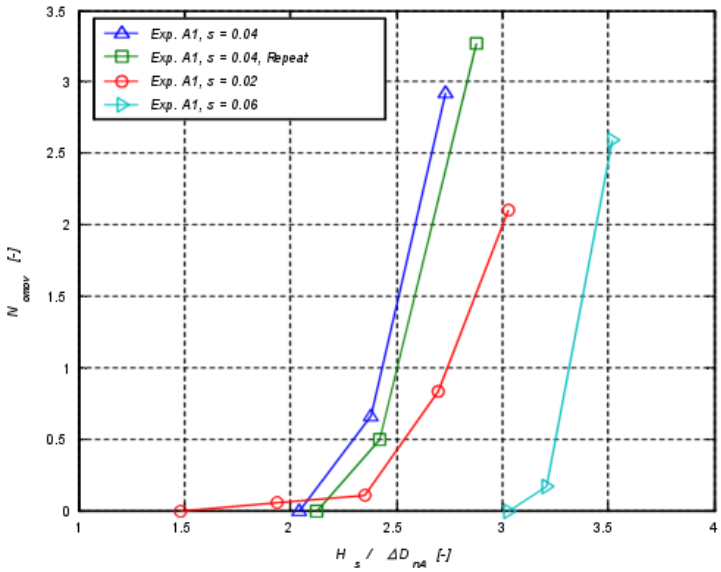

Figure 4.10: Damage curves (N_{os}) for A1N3S2, A1N3S4,A1N3S4R and A1N3S6

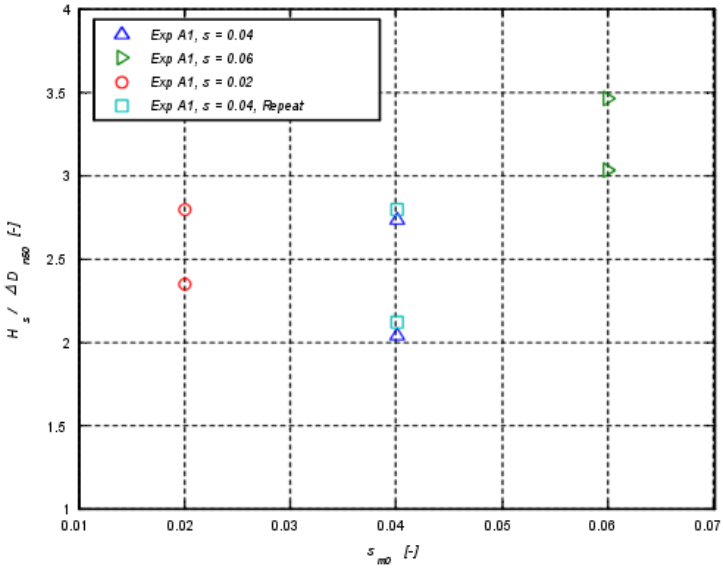

Figure 4.11: Comparison of stability

4.2.2 Secondary layer stability

The discussion on the stability of the secondary layer is conducted in the same manner as that of the armour layer stability. Distinction is made between the influence of the wave steepness and the packing density of the top layer. Firstly, however, the results of the reference tests (A1N3S4 and A1N3S4R) are discussed.

The damage of the two series is found in table (4.16) and (4.17). The overall damage of the secondary layer in experiment A1N3S4 was $\sum S = 122$, while the average damage per cross-section was $S = 6.42$. Experiment A1N3S4R showed a similar amount of damage of $\sum S = 142$ with an average damage of $S = 7.46$. Figure (4.12) and (4.13) illustrate the contour plots of both experiments. As with the experiments of series A0, the distribution of the erosion is rather random, showing local volumes of eroded material. The locations of these spots along with the armour layer response are found in table (4.18) and (4.19)

$x(cm)$	$S_x(-)$	$x(cm)$	$S_x(-)$	$x(cm)$	$S_x(-)$	$x(cm)$	$S_x(-)$
4	13.10	24	10.31	44	3.23	64	10.07
8	1.70	28	24.47	48	2.14	68	3.66
12	1.91	32	5.90	52	4.47	72	3.35
16	7.06	36	10.89	56	3.78	76	1.84
20	5.48	40	5.07	60	3.57		

Table 4.16: Damage of the secondary layer (A1N3S4)

$x(cm)$	$S_x(-)$	$x(cm)$	$S_x(-)$	$x(cm)$	$S_x(-)$	$x(cm)$	$S_x(-)$
4	2.14	24	5.76	44	14.29	64	16.06
8	7.68	28	6.21	48	4.92	68	8.52
12	8.20	32	7.33	52	3.89	72	6.17
16	3.63	36	8.65	56	14.96	76	2.40
20	8.07	40	8.81	60	4.14		

Table 4.17: Damage of the secondary layer (A1N3S4R)

$x(cm)$	$y(cm)$	Armour response	Mechanism
24 - 32	22 - 26	no movement	stable
24 - 32	34 - 38	minor sliding	gap
24 - 32	42 - 46	displacement	gap
24 - 32	50 - 54	major sliding	gap
24 - 32	58 - 66	major sliding	gap
28 - 36	30 - 34	minor sliding	stable
32 - 40	22 - 26	displacement	gap
36 - 44	42 - 46	major sliding	gap
40 - 44	62 - 70	minor sliding	gap
60 - 68	42 - 46	major sliding	gap

Table 4.18: Failure mechanisms of the secondary layer (A1N3S4)

Table (4.18) and (4.19) clearly show that erosion of the underlayer is mostly a result of resettlement and displacement of the armour unit. Since the armour layer response is most significant around SWL level, this also holds true for the erosion of the secondary layer; most eroded volumes are located around the level of still water. However, the amount of eroded material for both series was

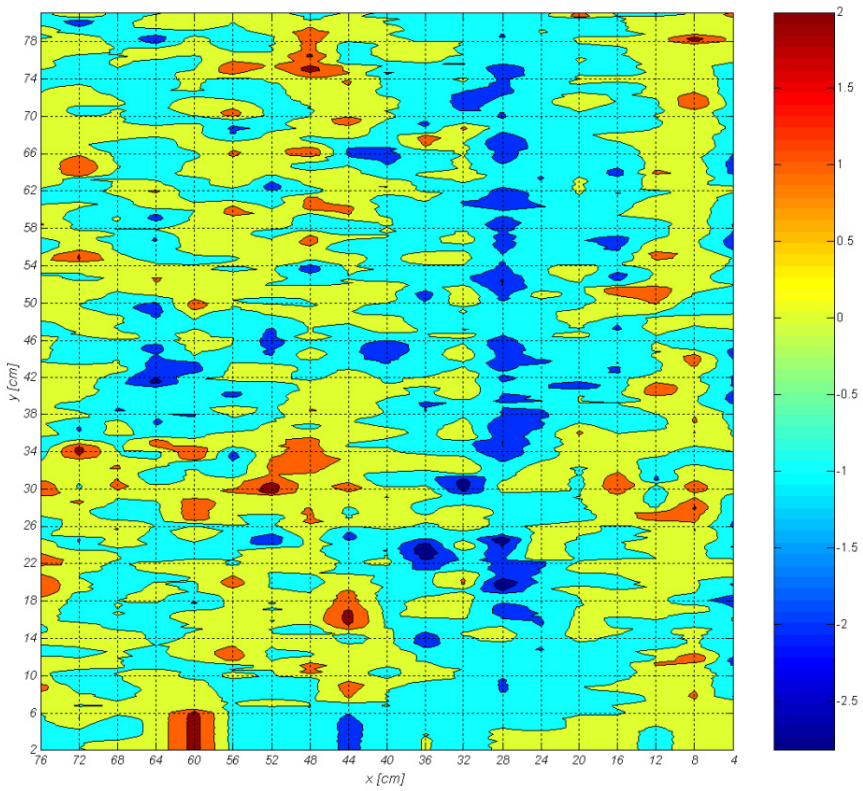

Figure 4.12: Erosion of the secondary layer (A1N3S4)

within tolerable limits. The covered area of the eroded volumes was limited -all well within an area of $8 \times 8cm^2$-, while the depth not ever exceeded $2.5cm$.

$x(cm)$	$y(cm)$	Armour response	Mechanism
8 - 16	18 - 22	minor sliding	stable
16 - 24	54 - 58	displacement	gap
20 - 28	26 - 34	minor sliding	gap
32 - 40	66 - 70	major sliding	gap
36 - 44	42 - 46	minor sliding	gap
36 - 44	46 - 54	displacement	gap
52 - 60	66 - 70	major sliding	gap
60 - 68	38 - 42	major sliding	gap

Table 4.19: Failure mechanisms of the secondary layer (A1N3S4R)

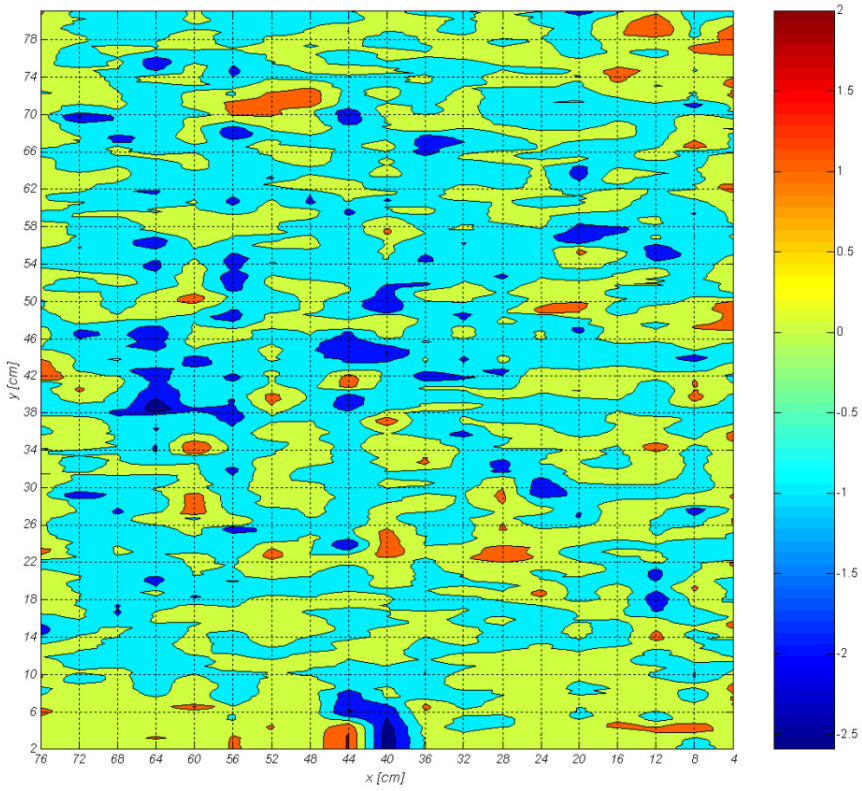

Figure 4.13: Erosion of the secondary layer (A1N3S4R)

Influence of the packing density

The outcome regarding the erosion of the secondary layer in experiments A1N4S4 and A1N25S4 is presented in the following tables and figures. The total erosion at the experiment with an armour packing density of $n_v = 0.4$ was $\sum S = 118$, while the armour packing density set at $n_v = 0.25$ gave an overall damage of $\sum S = 108$. The average damage of both experiments was $S = 6.21$ and $S = 5.67$, respectively.

$x(cm)$	$S_x(-)$	$x(cm)$	$S_x(-)$	$x(cm)$	$S_x(-)$	$x(cm)$	$S_x(-)$
4	6.74	24	2.14	44	12.07	64	0.04
8	4.49	28	5.76	48	25.90	68	2.22
12	9.86	32	2.53	52	6.83	72	13.42
16	10.71	36	2.20	56	8.01	76	7.21
20	3.50	40	4.18	60	3.05		

Table 4.20: Damage of the secondary layer (A1N4S4)

$x(cm)$	$S_x(-)$	$x(cm)$	$S_x(-)$	$x(cm)$	$S_x(-)$	$x(cm)$	$S_x(-)$
4	2.14	24	5.76	44	14.29	64	16.72
8	7.68	28	6.21	48	4.92	68	4.26
12	8.20	32	7.33	52	3.89	72	6.32
16	3.63	36	8.65	56	14.96	76	7.99
20	8.07	40	8.81	60	4.14		

Table 4.21: Damage of the secondary layer (A1N25S4)

$x(cm)$	$y(cm)$	Armour response	Mechanism
8 - 16	26 - 34	minor sliding	gap
12 - 20	54 - 58	major sliding	gap
24 - 32	42 - 46	major sliding	gap
44 - 56	38 - 42	major sliding	gap
52 - 56	18 - 22	minor sliding	gap
68 - 72	46 - 50	major sliding	gap
68 - 76	62 - 70	major sliding	gap

Table 4.22: Failure mechanisms of the secondary layer (A1N4S4)

Although the influence of the packing density on the erosion process of the secondary layer cannot be denied, it is however in this series not unambiguous. The tests with an armour packing density of $n_v = 0.25$ clearly showed less damage to the underlayer then the two reference tests with $n_v = 0.3$. It is expected that the experiment with an armour packing density of $n_v = 0.4$ would result in even more erosion of the secondary layer than these reference tests. Thus contributing to the notion that a decrease in armour packing density would lead to an increase of secondary layer erosion. This was not the case however. Although in general wider voids between the units mean more erosion, it was the response of the armour layer during the experiment that hindered significant erosion. As described in the paragraph on armour layer stability, the packing density of the top layer increased substantially during the first sea-state, going from $n_v = 0.4$ to approximately $n_v = 0.3$ and even to around $n_v = 0.25$ during the following sea-states. This increase in packing density clearly caused a decrease in the voids between individual units and hence less erosion of the underlayer. A second explanation for the relatively limited erosion occurring during the experiment with the initially widest packing density is its dependency on the incoming wave height. The significant

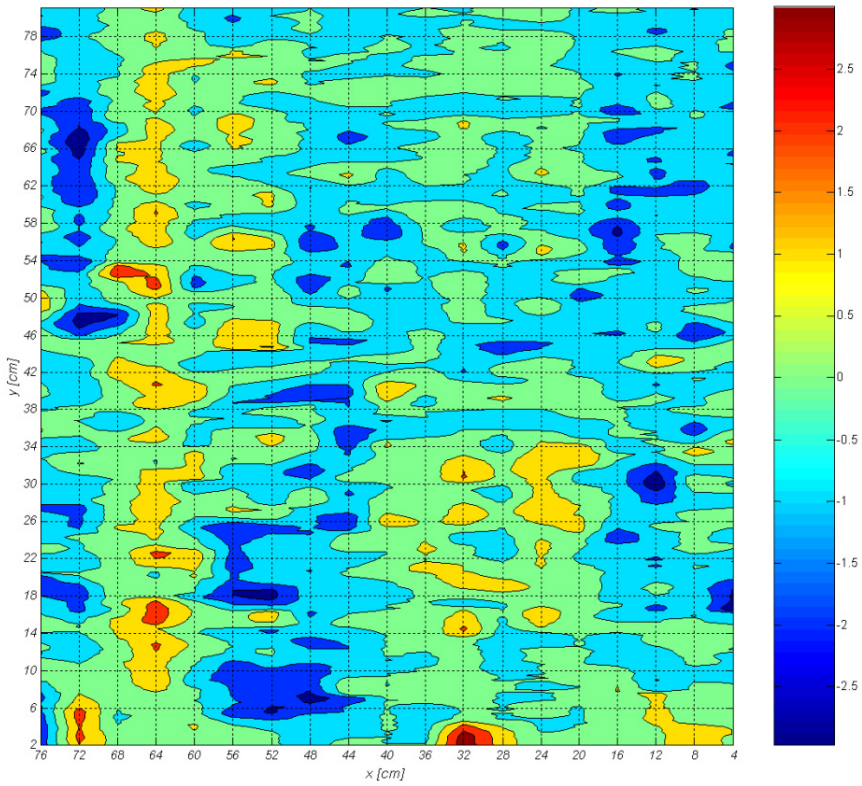

Figure 4.14: Erosion of the secondary layer (A1N4S4)

resettlement of the tetrapods caused failure at an early sea-state, resulting in a fairly small final incoming significant wave height. Since erosion occured mainly in an area of $SWL \pm H_s$, evidently smaller wave heights cause less damage.

The damage development of both experiments was comparable. Both showed locally eroded volumes, nowhere deeper than $2.5cm$. Most eroded volumes in the secondary layer were a consequence of armour unit sliding, i.e. an increase in the size of the voids between units. Particularly in series A1N25S4, displacement of units under SWL caused sliding of units surrounding the arisen gaps. Therefore, it was not so much the displacement of units that caused the erosion of the underlayer, but rather the following resettlment of units around SWL. The influence of the armour packing density on the secondary layer erosion is presented in figure (4.16).

$x(cm)$	$y(cm)$	Armour response	Mechanism
12 - 20	18 - 22	no movement	stable
12 - 20	42 - 46	major sliding	gap
12 - 20	50 - 58	minor sliding	stable
16 - 20	30 - 34	major sliding	gap
24 - 32	18 - 22	no movement	stable
44 - 56	30 - 38	major sliding	gap
44 - 52	50 - 54	major sliding	gap
44 - 52	58 - 62	major sliding	gap
60 - 68	18 - 22	no movement	stable
60 - 68	26 - 30	minor sliding	stable
60 - 68	46 - 50	major sliding	gap
60 - 68	58 - 62	major sliding	gap

Table 4.23: Failure mechanisms of the secondary layer (A1N25S4)

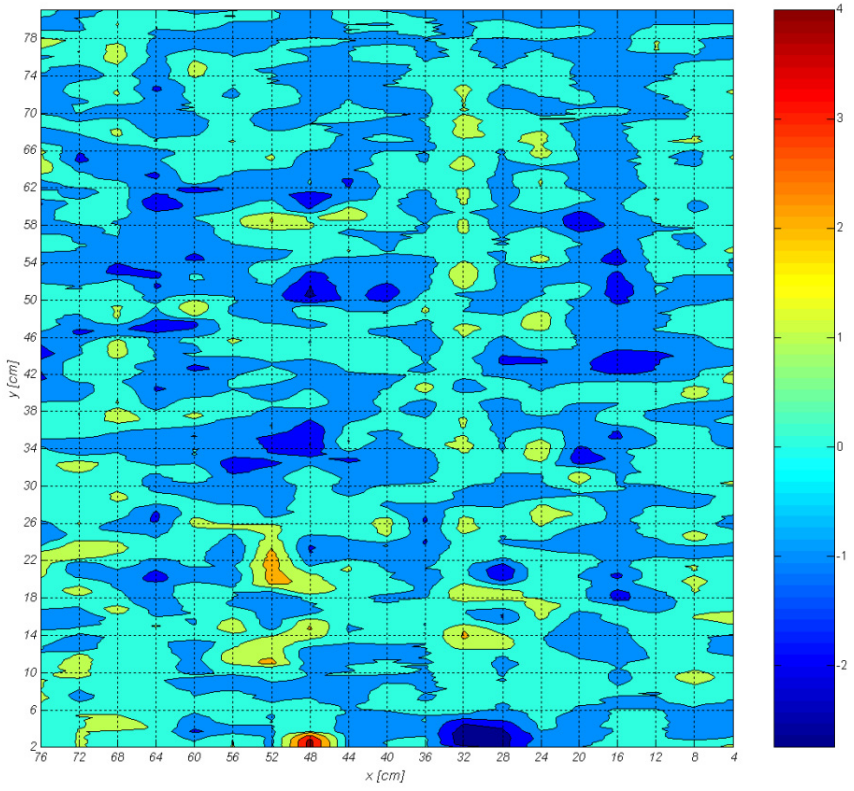

Figure 4.15: Erosion of the secondary layer (A1N25S4)

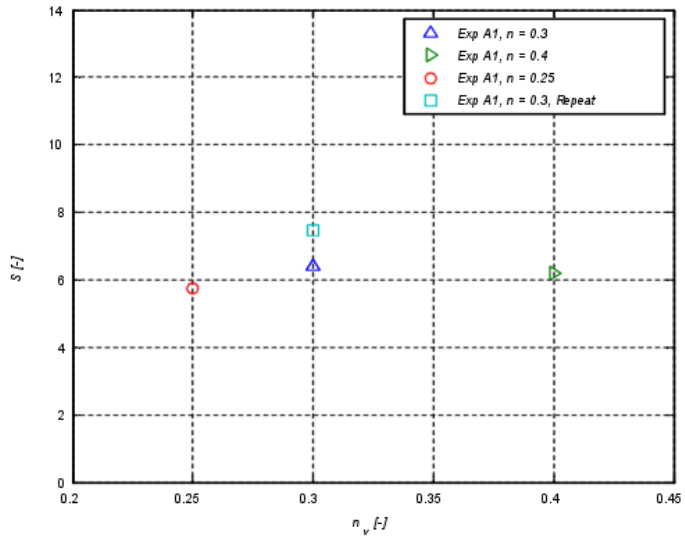

Figure 4.16: Comparison of stability

Influence of the wave steepness

The sum of all measured cross-sectional profiles of series A1N3S2 amounted to $\sum S = 172$, while the total damage of the secondary layer at series A1N3S6 was significantly higher, namely $\sum S = 252$. The average damage per cross section was $S = 9.04$ for the experiment with long waves and $S = 13.28$ for the short wave experiment. At both experiments the erosion of the underlayer proved more severe than tests with a wave steepness of $s_{m0} = 0.04$. An increase in the intensity of the erosion at $s_{m0} = 0.02$ could possibly be explained by the reservoir effect as mentioned in the section on armour layer stability. This experiment showed an early resettlement of the top layer, followed by a progressive development of damage during the consecutive sea-states. Displacement of several units on the lower left flank of the structure caused a considerable number of units, positioned higher on the slope, to slide downwards, explaining the concentration of erosion on the outer side of the profile.

$x(cm)$	$S_x(-)$	$x(cm)$	$S_x(-)$	$x(cm)$	$S_x(-)$	$x(cm)$	$S_x(-)$
4	6.07	24	15.09	44	7.04	64	22.88
8	6.52	28	4.26	48	4.64	68	11.86
12	18.08	32	4.17	52	6.73	72	7.32
16	10.16	36	8.56	56	10.94	76	4.63
20	6.78	40	11.66	60	4.46		

Table 4.24: Damage of the secondary layer (A1N4S2)

The *reservoir filling effect* -accounting for the results of experiment A1N3S2- forecasts lesser damage to the secondary layer for series A1N3S6. This is clearly not the case. Of all experiments in series A1, this configuration produced the most damage to the secondary layer. Thereby unmistakeably verifying the importance of the wave height as a parameter of influence concerning the damage of the secondary layer. A higher wave not only enlarges the area of possible erosion, the increase in energy causes the secondary layer to erode more extensively. Both effects are amplified by calculating the damage within a reference area that varies with the highest incoming significant wave height per experiment. But even when the complete slope is chosen as an area of reference,

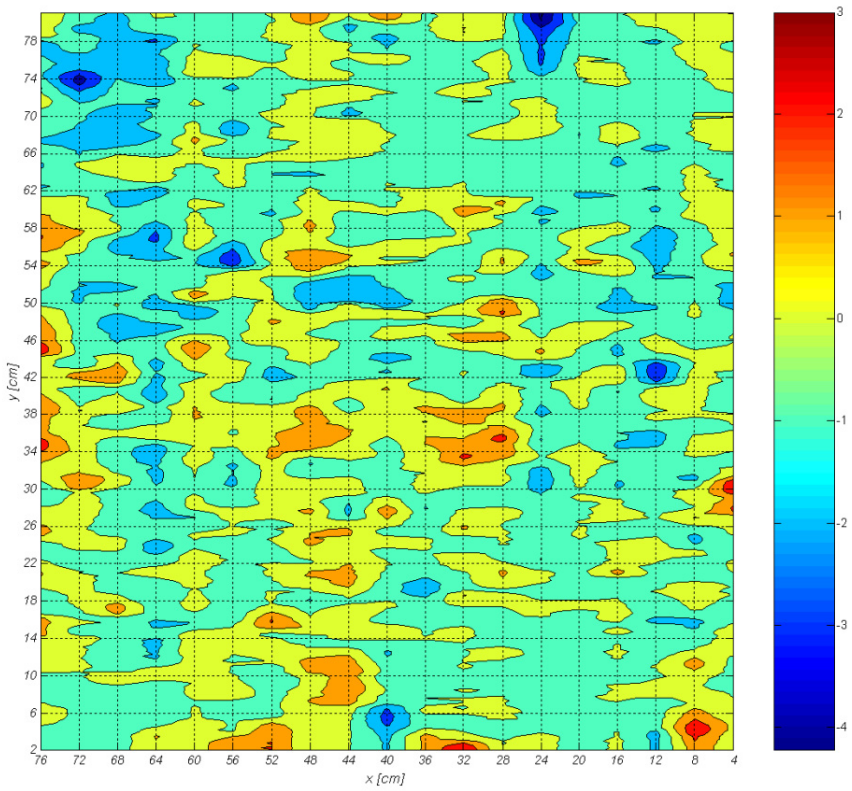

Figure 4.17: Erosion of the secondary layer (A1N3S2)

the influence of the wave height becomes evident ($S = 15.74$ for experiment A1N3S6, $S = 11.89$ for experiment A1N3S2, $S = 9.11$ and $S = 9.00$ for the experiments with $s_{m0} = 0.04$). The influence of the wave height is discussed more thoroughly in the comparison of all three series.

As with all the earlier described experiments, the mechanism mainly responsible for the erosion of the secondary layer was the increase in the size of the voids between specific units. Hardly any migration occurred under an armour layer still in its initial configuration. Sliding or displacement of units -i.e. armour response- was required to initiate erosion of the underlayer. A common failure mode was the displacement of a unit under SWL, which resulted in the sliding of units higher upon the slope. This sliding was the main cause for an increase in void sizes and thus erosion of the secondary layer.

Also, despite the increase in erosion compared to the reference tests, the eroded volumes never exceed a depth of $2.5cm$ The covered areas of scour do increase, but the erosion does not seriously endanger the stability of the structure.

$x(cm)$	$S_x(-)$	$x(cm)$	$S_x(-)$	$x(cm)$	$S_x(-)$	$x(cm)$	$S_x(-)$
4	7.97	24	13.03	44	10.63	64	22.26
8	20.59	28	16.93	48	16.39	68	12.33
12	10.80	32	18.17	52	8.32	72	4.78
16	14.44	36	26.46	56	13.31	76	9.28
20	15.58	40	2.58	60	8.55		

Table 4.25: Damage of the secondary layer (A1N4S6)

$x(cm)$	$y(cm)$	Armour response	Mechanism
8 - 16	18 - 22	no movement	stable
8 - 16	42 - 46	minor sliding	gap
8 - 16	54 - 58	minor sliding	gap
12 - 20	46 - 54	minor sliding	gap
20 - 28	30 - 34	minor sliding	stable
32 - 40	18 - 22	minor sliding	gap
36 - 44	6 - 10	no movement	stable
36 - 52	50 - 54	major sliding	gap
52 - 60	54 - 58	major sliding	gap
60 - 68	10 - 18	major sliding	gap
60 - 68	22 - 26	displacement	gap
60 - 68	26 - 30	major sliding	gap
60 - 68	30 - 34	major sliding	gap
60 - 72	46 - 54	major sliding	gap
60 - 68	54 - 58	displacement	gap
64 - 76	66 - 70	major sliding	gap
64 - 76	70 - 78	major sliding	gap

Table 4.26: Failure mechanisms of the secondary layer (A1N3S2)

$x(cm)$	$y(cm)$	Armour response	Mechanism
4 - 16	2 - 10	no movement	stable
4 - 12	38 - 42	minor sliding	gap
4 - 12	62 - 70	minor sliding	gap
8 - 24	42 - 46	major sliding	gap
12 - 36	30 - 38	major sliding	gap
12 - 20	66 - 74	minor sliding	stable
20 - 32	50 - 58	major sliding	gap
24 - 36	58 - 70	major sliding	gap
28 - 36	42 - 46	minor sliding	gap
28 - 36	66 - 78	minor sliding	gap
32 - 36	18 - 26	displacement	gap
44 - 52	22 - 26	minor sliding	stable
48 - 56	42 - 46	major sliding	gap
56 - 68	46 - 54	major sliding	gap
60 - 68	30 - 34	major sliding	gap
60 - 68	54 - 62	major sliding	gap

Table 4.27: Failure mechanisms of the secondary layer (A1N3S6)

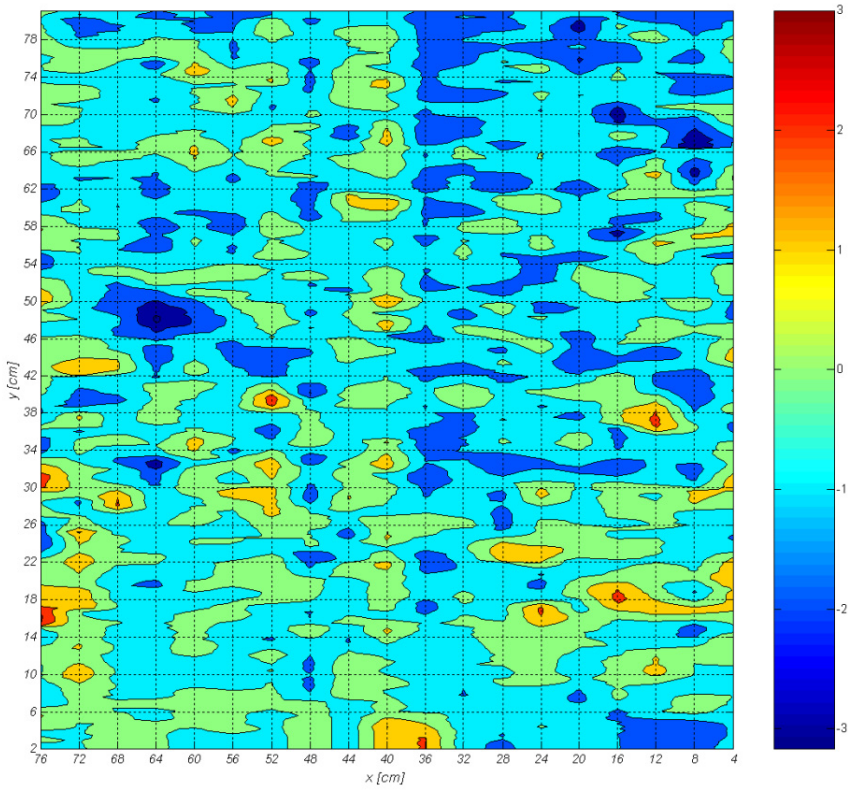

Figure 4.18: Erosion of the secondary layer (A1N3S6)

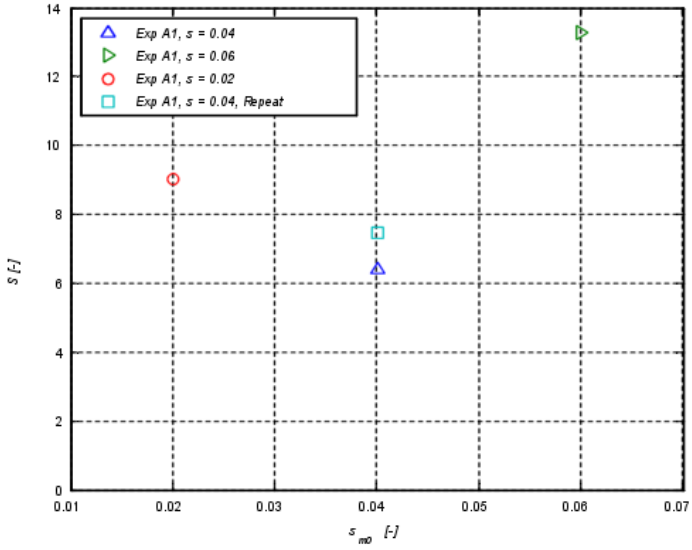

Figure 4.19: Comparison of stability

4.3 Observation of series A2

The same combinations of wave steepness and armour packing density were tested in series A2 as in the previous series. The secondary layer, however, was replaced by a new layer of smaller rock material with a nominal diameter $D_{n50} = 11.3mm$.

4.3.1 Armour layer stability

The armour layer response during the experiments with $n_v = 0.3$ and $s_{m0} = 0.04$ was anticipated. The test results of both experiments show much resemblance.

H_s (m)	$\frac{H_s}{\Delta D_{n_A}}$	T_m (s)	N_{od}	N_{os}	N_{omov}
0.082	1.37	1.16	0	0	0
0.103	1.71	1.26	0	0	0
0.144	2.39	1.49	0	0	0
0.161	2.67	1.58	0.11	1.65	1.76
0.168	2.80	1.63	0.39	3.74	4.13

Table 4.28: Test results for A2N3S4

H_s (m)	$\frac{H_s}{\Delta D_{n_A}}$	T_m (s)	N_{od}	N_{os}	N_{omov}
0.082	1.36	1.15	0	0	0
0.112	1.86	1.31	0	0	0
0.143	2.30	1.50	0	0	0
0.158	2.63	1.57	0.17	1.93	2.10
0.167	2.78	1.63	0.39	3.14	3.53

Table 4.29: Test results for A2N3S4R

Influence of the packing density

The experiment with the highest packing density ($n_v = 0.25$) characterized itself by a considerable initial stability. Damage did not occur untill the structure was exposed to a wave height of $H_s = 0.160m$. Both sliding and displacement of armour units took place during this run. The consecutive sea-state showed a progressive loss of hydraulic armour stability, eventually causing failure of the structure at $H_s = 0.183m$.

The structure at experiment A2N4S4 primarily failed due to the considerable resettlement of the units. During the first run major resettlement occurred -mainly- around SWL and left a sizable gap in the upper part of the armour layer. The following run showed a continuation of the resettlement, which caused the gap to increase to unacceptable proportions. As in series A1, the packing density of the armour layer around SWL increased to $n_v \approx 0.3$ in the first run up to $n_v \approx 0.25$ in the second.

The same criteria were used as in the previous series to compare the results of the various experiments; namely *no damage* ($N_{od} = 0$) and *severe damage* ($N_{od} = 0.28$). These damage numbers were plotted against corresponding stability numbers. The experimental outcome agrees with results of Van den Bosch (2001) and Van Gent et al. (1999) in the sense that the overall stability of the structure increased with a denser packing of the armour layer. However, figure (4.22) does not demonstrates this trend clearly regarding the displacement units. At $n_v = 0.4$ the structure already failed after the displacement of only one armour unit. Failure during this experiment was solemnly caused by the major resettlements, possible due to the wide initial packing density.

H_s (m)	$\frac{H_s}{\Delta D_{n_A}}$	T_m (s)	N_{od}	N_{os}	N_{omov}
0.082	1.37	1.16	0	0	0
0.102	1.70	1.24	0	0	0
0.124	2.07	1.36	0	0	0
0.144	2.39	1.47	0.06	0	0.06
0.160	2.66	1.58	0.33	1.38	1.71
0.183	3.05	1.70	0.77	3.14	3.91

Table 4.30: Test results for A2N25S4

H_s (m)	$\frac{H_s}{\Delta D_{n_A}}$	T_m (s)	N_{od}	N_{os}	N_{omov}
0.081	1.37	1.15	0	5.01	5.01
0.115	1.70	1.25	0.06	0.72	0.78

Table 4.31: Test results for A2N4S4

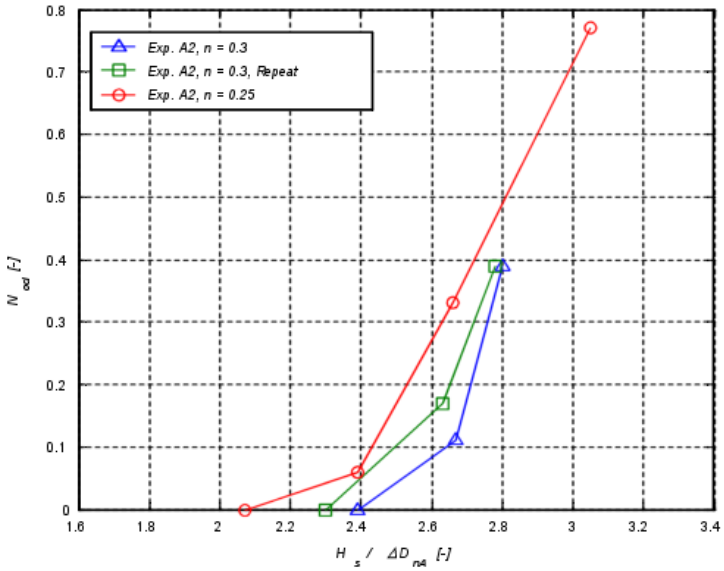

Figure 4.20: Damage curves (N_{od}) for A2N3S4, A2N3S4R and A2N25S4

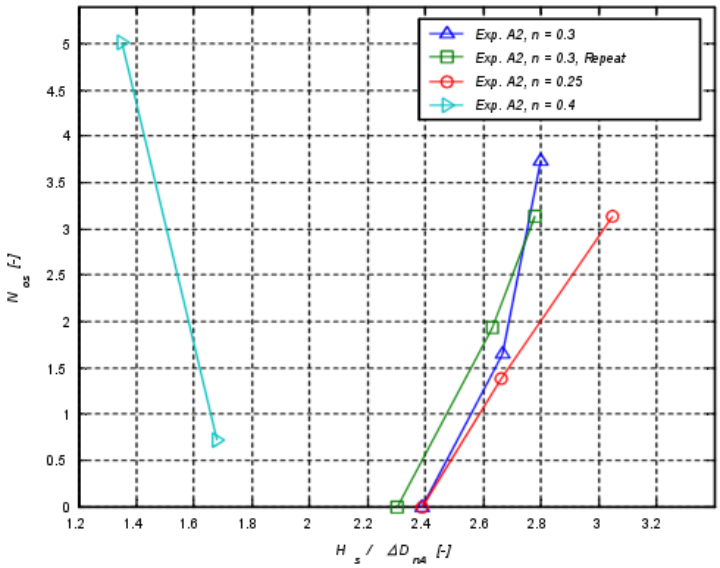

Figure 4.21: Damage curves (N_{os}) for A2N3S4, A2N3S4R and A2N25S4 and A2N4S4

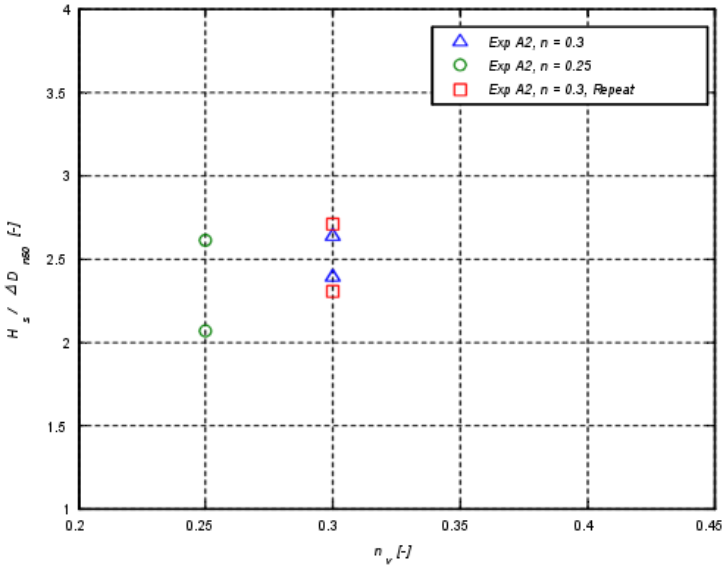

Figure 4.22: Comparison of stability

Influence of the wave steepness

The long waves in experiment A2N3S2 caused resettlement of the armour layer around SWL in an early stage of the experiment. This resulted in a slight improvement of the top layer stability. The following run therefore showed no movement of units, while only one unit was removed out of the armour layer. The development of damage in the final run, however, was substantial. At $H_s = 0.150m$ a total of 15 units was displaced. The displacement of these units caused neighboring units to fill the newly formed gaps, thereby significantly contributing to the number of sliding units.

The armour layer proved very stable during the first five runs of the short wave experiment. Only at the final run, with $H_s = 0.186m$, did the top layer lose its stability. The development of damage had a progressive character, resulting in the removal of 13 units from the top layer. As in experiment A2N3S2, the displacement of these units increased the number of sliding units.

The damage curves of the various experiments clearly demonstrate a decrease in stability with an increase in wave period. With the use of the previous defined criteria *no damage* and *severe damage*, this trend is made explicit in figure (4.36).

H_s (m)	$\frac{H_s}{\Delta D_{n_A}}$	T_m (s)	N_{od}	N_{os}	N_{omov}
0.092	1.53	1.61	0	0	0
0.116	1.92	1.75	0.06	0.55	0.61
0.139	2.32	1.89	0.06	0	0.06
0.150	2.49	2.02	0.72	6.05	6.77

Table 4.32: Test results for A2N3S2

H_s (m)	$\frac{H_s}{\Delta D_{n_A}}$	T_m (s)	N_{od}	N_{os}	N_{omov}
0.086	1.43	1.02	0	0	0
0.109	1.81	1.07	0	0	0
0.126	2.09	1.17	0	0	0
0.154	2.56	1.25	0	0	0
0.170	2.83	1.33	0.11	0	0.11
0.186	3.10	1.41	0.72	5.56	6.28

Table 4.33: Test results for A2N3S6

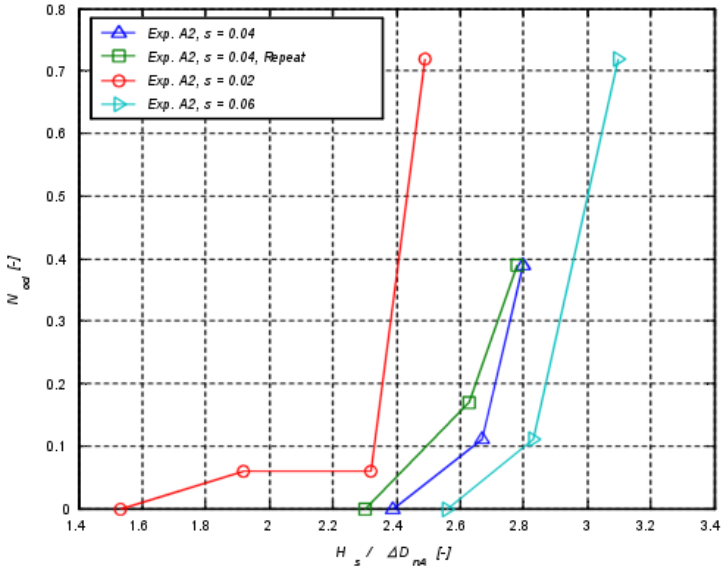

Figure 4.23: Damage curves (N_{od}) for A2N3S4, A2N3S4R, A2N3S2 and A2N3S6

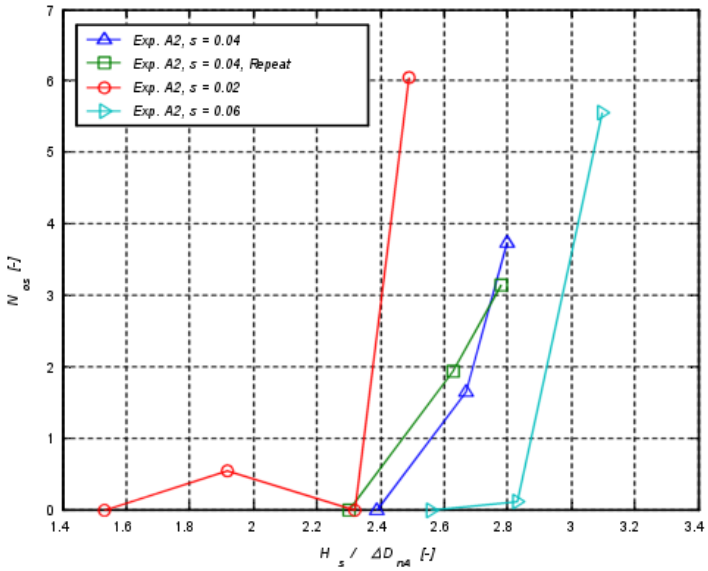

Figure 4.24: Damage curves (N_{os}) for A2N3S4, A2N3S4R, A2N3S2 and A2N3S6

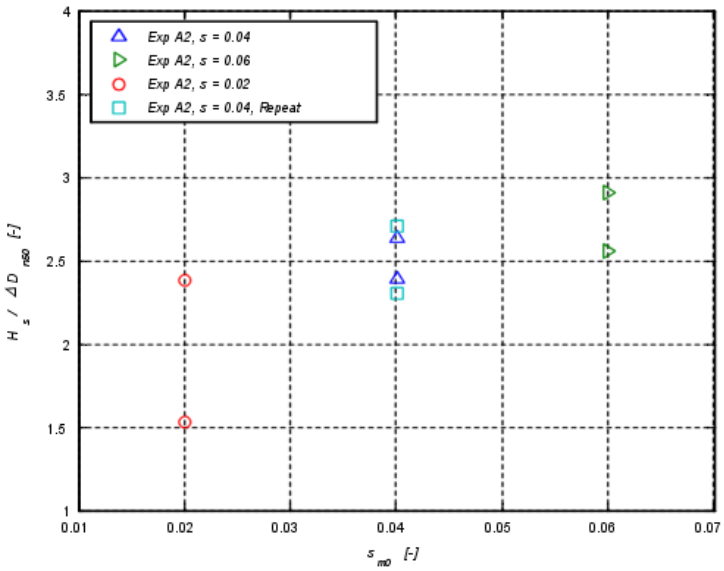

Figure 4.25: Comparison of stability

4.3.2 Secondary layer stability

The damage sustained to the secondary layer at the end of series A2N3S4 and A2N3S4R was quite similar. The damage number of the entire slope accumulated to $\sum S = 270$ for the first experiment and $\sum S = 258$ for the second. Averaged per cross-sectional profile, this was $S = 14.22$ and $S = 13.57$, respectively.

The displacements of the armour units during the first experiment were evenly distributed over several colored bands around SWL. The effect of an even distribution of these displaced units can be seen in the diversity of failure mechanisms which led to the erosion of the secondary layer (table (4.36)). The displacements in the second experiment, however, were rather unevenly distributed. Eight out of a total of ten units that were removed from the top layer, originated from the lowest green band. These displacements caused the armour units situated higher upon the slope to slide downwards. This significant sliding of units was the main cause of erosion of the underlayer, as becomes clear in table (4.37).

$x(cm)$	$S_x(-)$	$x(cm)$	$S_x(-)$	$x(cm)$	$S_x(-)$	$x(cm)$	$S_x(-)$
4	7.78	24	20.17	44	9.50	64	20.27
8	21.19	28	13.44	48	12.21	68	14.47
12	15.74	32	20.69	52	1.04	72	10.81
16	16.61	36	16.07	56	9.30	76	8.59
20	12.07	40	22.41	60	17.85		

Table 4.34: Damage of the secondary layer (A2N3S4)

$x(cm)$	$S_x(-)$	$x(cm)$	$S_x(-)$	$x(cm)$	$S_x(-)$	$x(cm)$	$S_x(-)$
4	13.75	24	4.10	44	7.62	64	14.72
8	10.48	28	23.12	48	33.95	68	14.84
12	13.59	32	5.81	52	29.13	72	5.93
16	1.79	36	9.05	56	19.44	76	11.00
20	11.91	40	15.50	60	12.13		

Table 4.35: Damage of the secondary layer (A2N3S4R)

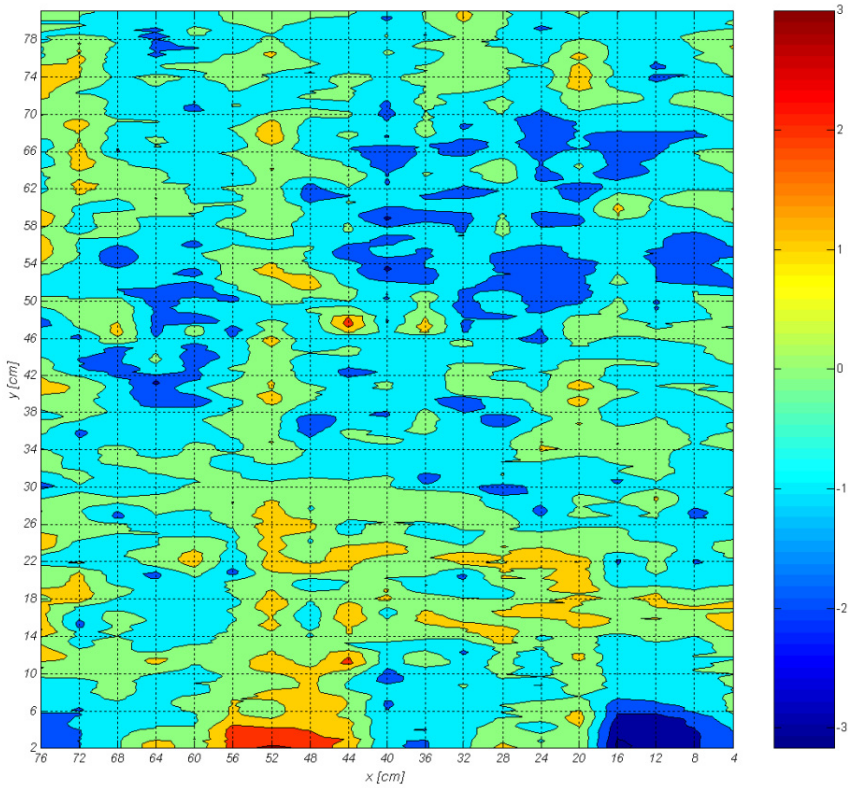

Figure 4.26: Erosion of the secondary layer (A2N3S4)

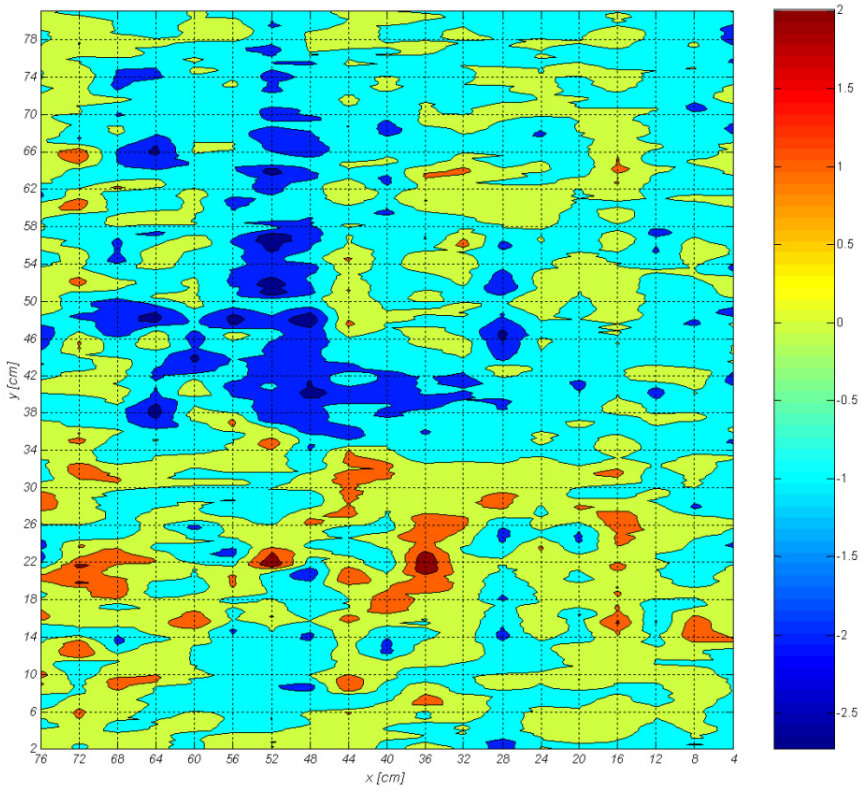

Figure 4.27: Erosion of the secondary layer (A2N3S4R)

$x(cm)$	$y(cm)$	Armour response	Mechanism
4 - 12	50 - 58	major sliding	gap
12 - 20	62 - 70	displacement	gap
20 - 28	50 - 54	major sliding	gap
20 - 28	62 - 70	major sliding	stable
28 - 36	34 - 42	displacement	gap
32 - 44	58 - 62	major sliding	gap
36 - 44	50 - 58	major sliding	stable
36 - 44	62 - 70	major sliding	stable
44 - 52	34 - 38	displacement	gap
60 - 68	38 - 46	major sliding	gap
60 - 68	46 - 54	major sliding	gap

Table 4.36: Failure mechanisms of the secondary layer (A2N3S4)

$x(cm)$	$y(cm)$	Armour response	Mechanism
24 - 32	42 - 50	major sliding	stable
24 - 32	50 - 54	major sliding	stable
32 - 44	38 - 42	major sliding	gap
44 - 56	34 - 50	major sliding	gap
48 - 56	50 - 58	major sliding	gap
48 - 56	62 - 70	major sliding	gap
56 - 64	42 - 46	major sliding	stable
60 - 68	34 - 42	major sliding	stable
60 - 72	46 - 50	minor sliding	stable
60 - 68	62 - 70	major sliding	gap

Table 4.37: Failure mechanisms of the secondary layer (A2N3S4R)

Influence of the packing density

Experiment A2N25S4 resulted in a total damage of $\sum S = 281$ and an average cross-sectional damage of $S = 14.78$. Experiment A2N4S4 resulted in an overall damage of $\sum S = 155$ and a cross-sectional damage of $S = 8.17$. The former damage number is considerably higher then the experiments with an armour packing density of $n_v = 0.3$, while the latter is considerably lower. It seems that wave height predominantly influences the erosion of the underlayer rather then the packing density of the armour layer, since the significant wave height during the final run of experiment A2N25S4 was $H_s = 0.161m$, while $H_s = 0.126m$ during experiment A2N4S4.

For both experiments, the scoured holes were mainly positioned around SWL, yet the number of holes in the experiment with $n_v = 0.25$ far exceed that of the experiment with $n_v = 0.4$. The top layer in experiment A2N4S4 was characterized by excessive resettlement of the armour units. The effect of this dominant failure mechanism is reflected in table (4.41). Erosion of the secondary layer was a result of waves penetrating through the voids between individual units, which were caused by the resettlement process.

The cause of the erosion of the secondary layer in experiment A2N25S4 is more diverse. The higher packing density of the armour layer does not tolerate significant gaps between units. The higher incoming waves during the final runs, however, damaged the underlayer despite the smaller gaps. Some eroded holes even occurred under a *stable* top layer.

$x(cm)$	$S_x(-)$	$x(cm)$	$S_x(-)$	$x(cm)$	$S_x(-)$	$x(cm)$	$S_x(-)$
4	6.14	24	10.33	44	22.67	64	37.16
8	1.67	28	20.39	48	13.86	68	16.86
12	10.30	32	11.92	52	16.33	72	8.13
16	2.63	36	22.25	56	7.33	76	11.49
20	10.46	40	22.46	60	28.48		

Table 4.38: Damage of the secondary layer (A2N25S4)

$x(cm)$	$S_x(-)$	$x(cm)$	$S_x(-)$	$x(cm)$	$S_x(-)$	$x(cm)$	$S_x(-)$
4	1.57	24	13.28	44	6.73	64	11.02
8	22.01	28	1.49	48	15.51	68	10.08
12	6.10	32	5.25	52	10.71	72	2.76
16	6.65	36	6.76	56	1.22	76	14.69
20	11.15	40	4.96	60	3.32		

Table 4.39: Damage of the secondary layer (A2N4S4)

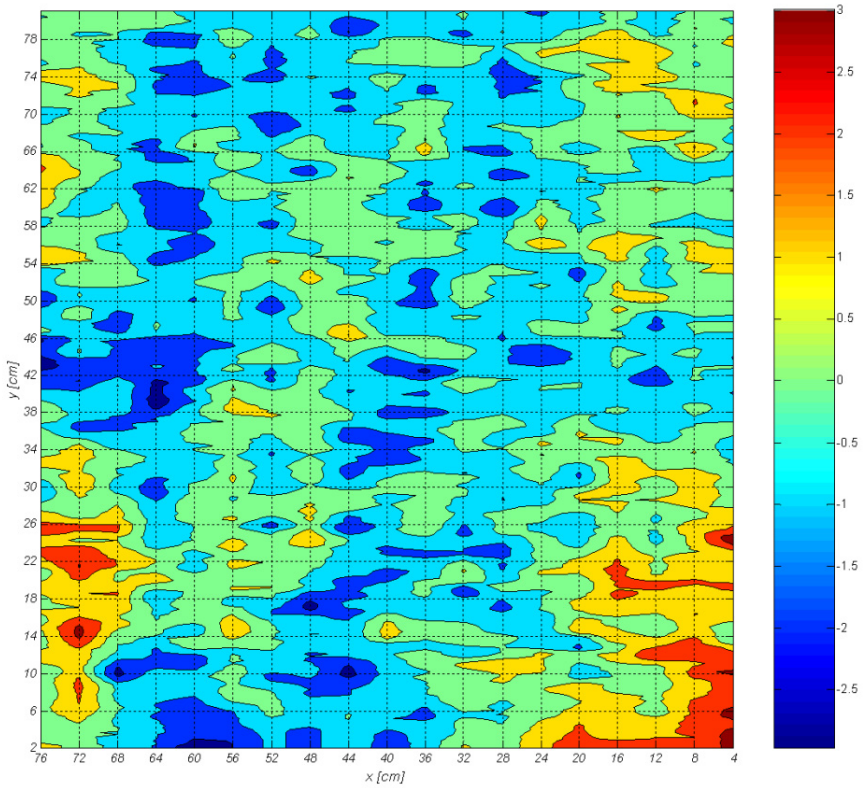

Figure 4.28: Erosion of the secondary layer (A2N25S4)

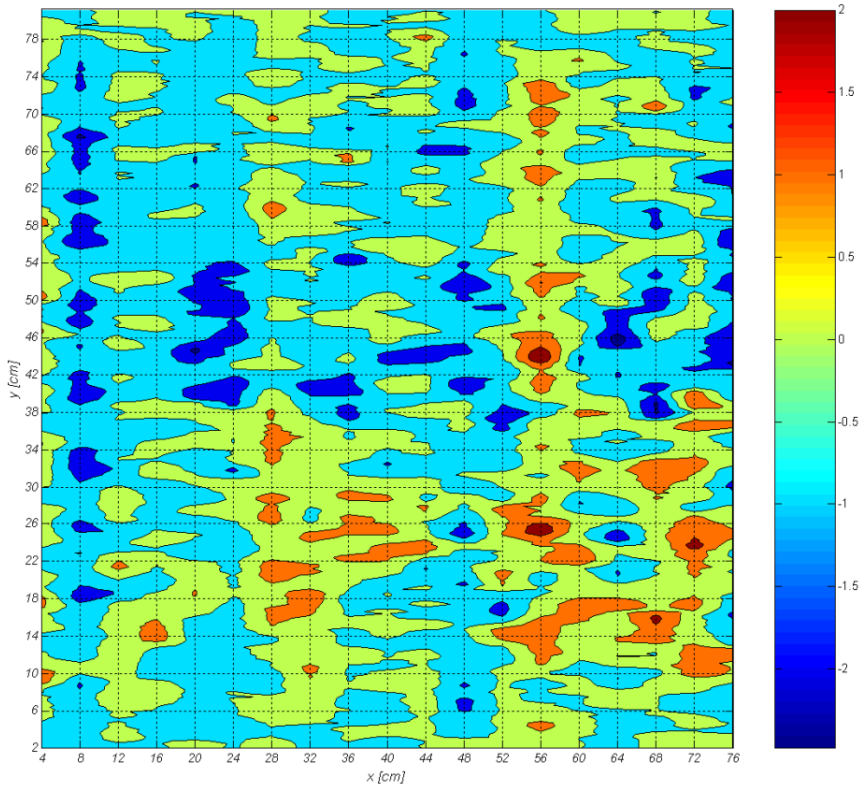

Figure 4.29: Erosion of the secondary layer (A2N4S4)

$x(cm)$	$y(cm)$	Armour response	Mechanism
8 - 16	38 - 46	major sliding	gap
20 - 28	42 - 46	minor sliding	stable
24 - 32	58 - 66	minor sliding	stable
28 - 40	22 - 26	displacement	gap
32 - 40	42 - 46	major sliding	gap
32 - 40	46 - 54	major sliding	stable
32 - 40	58 - 66	major sliding	stable
36 - 44	30 - 38	displacement	gap
44 - 52	14 - 22	no movement	stable
48 - 56	46 - 54	displacement	gap
60 - 68	26 - 34	major sliding	gap
60 - 68	38 - 46	major sliding	gap
60 - 68	54 - 63	major sliding	gap
60 - 68	62 - 70	major sliding	gap

Table 4.40: Failure mechanisms of the secondary layer (A2N25S4)

$x(cm)$	$y(cm)$	Armour response	Mechanism
20 - 28	38 - 42	major sliding	gap
20 - 28	46 - 54	major sliding	gap
32 - 36	40 - 48	major sliding	gap
44 - 52	22 - 30	major sliding	gap
44 - 52	50 - 54	major sliding	gap
60 - 68	42 - 50	major sliding	gap

Table 4.41: Failure mechanisms of the secondary layer (A2N4S4)

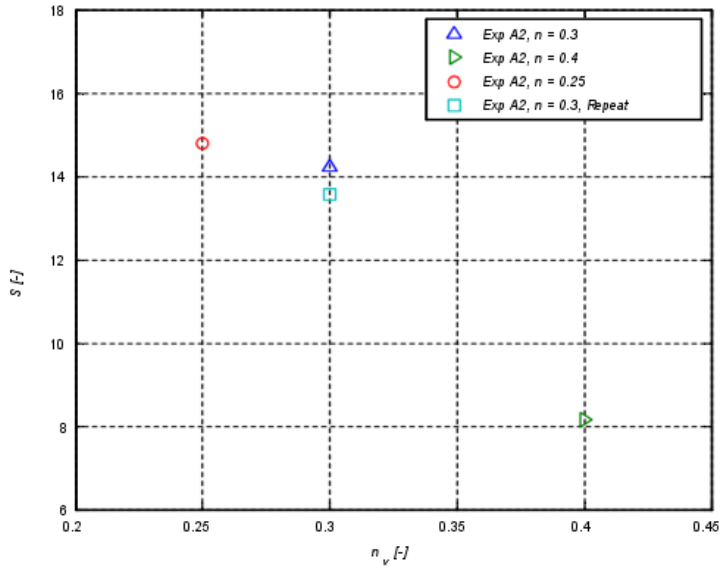

Figure 4.30: Comparison of stability

Influence of the wave steepness

Both wave steepness experiments showed the same tendency as the experiments in the first series, namely that the influence of the wave height overruled the effect of an increasing wave period. With a final wave height of $H_s = 0.186m$, the total damage of experiments A2N3S6 accumulated to $\sum S = 367$, while the averaged cross-sectional damage was $S = 19.30$. The final wave height during experiment A2N3S2 was considerably smaller ($H_s = 0.150m$), which led to an overall damage of $\sum S = 187$ and an average of $S = 9.87$.

The movement of armour units was the dominant failure mechanism to initiate erosion of the secondary layer. At both experiments, the displacement of units occurred mainly in the lower color bands. The resulting gaps caused units positioned higher on the slope to move downwards. Consequently, the resettlement sometimes caused an increase in void size between individual units and thereby an increase in the armour penetration of the incoming waves.

At both the long and short wave experiments, the eroded volumes of the secondary layer were mainly concentrated around SWL. The depth of the holes nowhere exceeded the $2.5cm$ and even though the covered areas of the spots were small, it could develop into a critical situation if CUR's guideline

concerning secondary layer thickness was followed. With a layer thickness of $4.0cm$, however, the armour layer instability pre-exceeded secondary layer instability considerably.

$x(cm)$	$S_x(-)$	$x(cm)$	$S_x(-)$	$x(cm)$	$S_x(-)$	$x(cm)$	$S_x(-)$
4	2.59	24	7.85	44	5.32	64	6.86
8	9.33	28	20.47	48	14.63	68	12.54
12	19.98	32	13.96	52	6.06	72	15.19
16	0	36	4.47	56	3.70	76	34.64
20	1.37	40	4.47	60	4.05		

Table 4.42: Damage of the secondary layer (A2N3S2)

$x(cm)$	$S_x(-)$	$x(cm)$	$S_x(-)$	$x(cm)$	$S_x(-)$	$x(cm)$	$S_x(-)$
4	17.30	24	18.29	44	13.40	64	40.56
8	11.91	28	35.53	48	40.70	68	1.99
12	12.59	32	16.39	52	17.36	72	17.21
16	8.30	36	13.96	56	21.22	76	10.51
20	10.95	40	42.72	60	15.75		

Table 4.43: Damage of the secondary layer (A2N3S6)

$x(cm)$	$y(cm)$	Armour response	Mechanism
8 - 16	34 - 38	major sliding	gap
8 - 16	46 - 50	major sliding	gap
24 - 32	38 - 46	major sliding	stable
24 - 32	46 - 54	major sliding	stable
44 - 52	22 - 26	displacement	gap
44 - 52	50 - 58	major sliding	gap
60 - 68	42 - 50	major sliding	gap
68 - 76	58 - 66	major sliding	gap

Table 4.44: Failure mechanisms of the secondary layer (A2N3S2)

$x(cm)$	$y(cm)$	Armour response	Mechanism
4 - 8	54 - 62	major sliding	gap
8 - 16	34 - 42	major sliding	gap
24 - 40	42 - 50	major sliding	gap
24 - 32	50 - 58	major sliding	gap
24 - 32	62 - 70	major sliding	gap
36 - 44	58 - 66	major sliding	gap
44 - 52	18 - 26	displacement	gap
44 - 52	50 - 58	major sliding	gap
44 - 52	58 - 62	major sliding	gap
52 - 60	42 - 50	major sliding	stable
60 - 64	30 - 34	major sliding	stable
60 - 64	42 - 50	major sliding	gap

Table 4.45: Failure mechanisms of the secondary layer (A2N3S6)

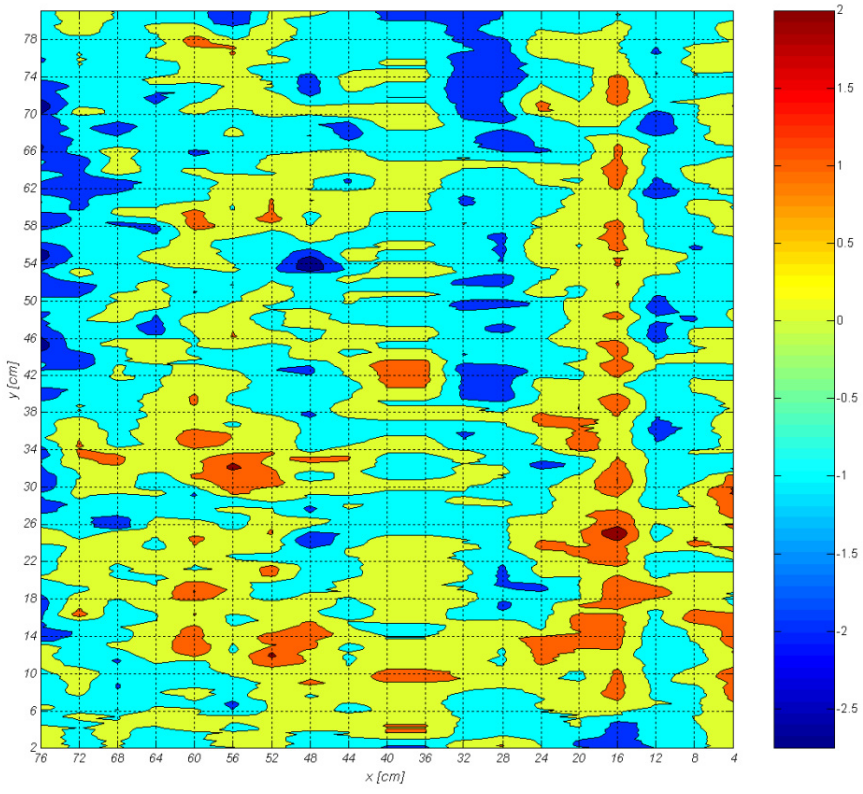

Figure 4.31: Erosion of the secondary layer (A2N3S2)

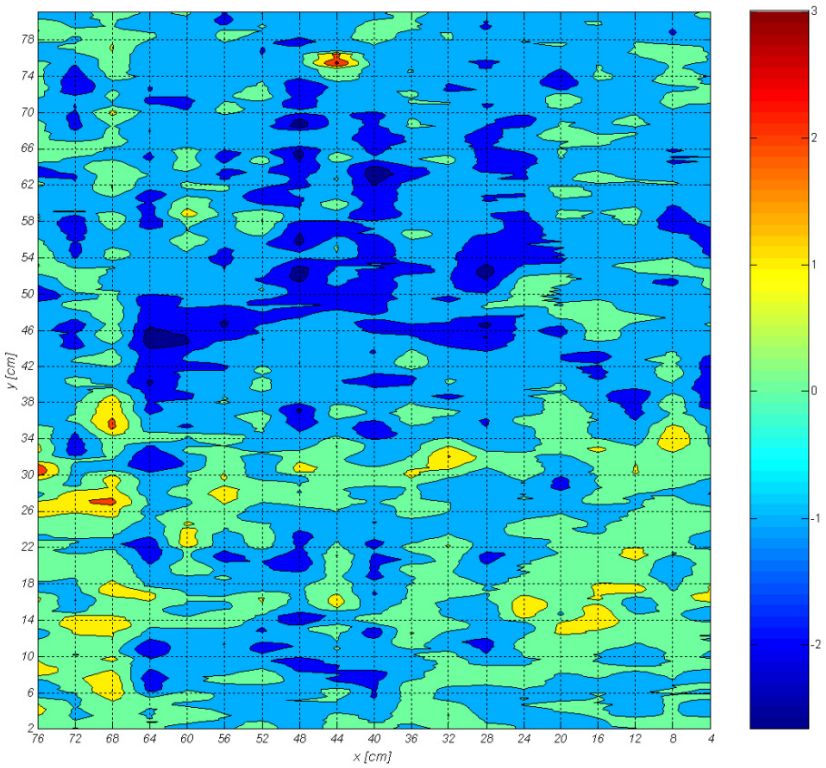

Figure 4.32: Erosion of the secondary layer (A2N3S6)

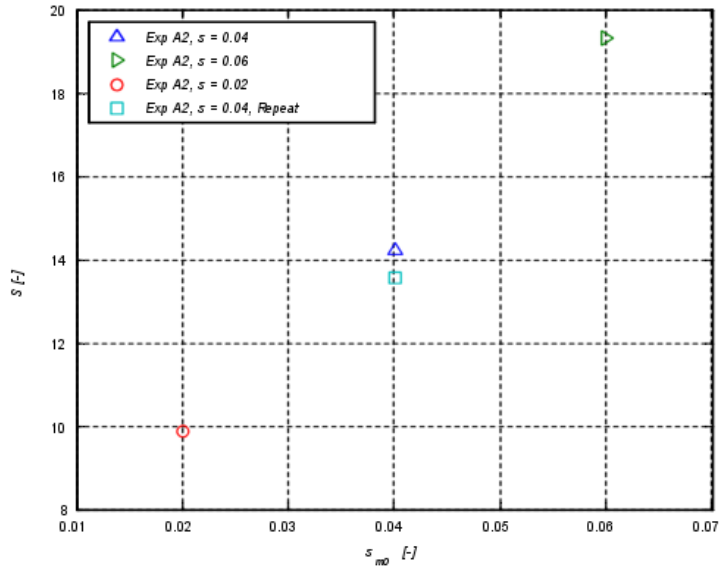

Figure 4.33: Comparison of stability

4.4 Observation of series A3

In the final test series the secondary layer consisted of rock material with a nominal diameter of $D_{n50} = 8.6mm$. The test programme, however, was similar to series A1 and A2. The results of the armour layer response will be treated first, followed by the discussion of the secondary layer response.

4.4.1 Armour layer stability

The damage development of the top layer differed considerably from the previous two series. The small underlayer material reduced friction such that many armour units already resettled in an early stage of the experiments. A total of 121 and 106 units moved more then half their nominal diameter during the third run of the first and second experiment and resettlement -though less extensive- continued in consecutive runs. The initial packing density of the armour layer was already relatively high ($n_v = 0.3$). Therefore, the major resettlement in the third run did not cause failure of the structure (i.e. intolerable gaps in the upper part of the top layer). In the latest run, wherein further resettlement simultaneously occurred with the displacement of several units, it did, however.

H_s (m)	$\frac{H_s}{\Delta D_{n_A}}$	T_m (s)	N_{od}	N_{os}	N_{omov}
0.082	1.37	1.15	0	0	0
0.102	1.70	1.25	0	0	0
0.124	2.07	1.37	0	6.66	6.66
0.144	2.40	1.48	0	2.86	2.86
0.162	2.69	1.58	0.11	0.83	0.94
0.179	2.98	1.68	0.28	0.28	0.56

Table 4.46: Test results for A3N3S4

H_s (m)	$\frac{H_s}{\Delta D_{n_A}}$	T_m (s)	N_{od}	N_{os}	N_{omov}
0.081	1.35	1.16	0	0	0
0.101	1.68	1.26	0	0	0
0.122	2.02	1.37	0	6.22	6.22
0.143	2.37	1.50	0	0.39	0.39
0.158	2.62	1.61	0.11	0.44	0.55
0.181	3.01	1.71	0.28	1.32	1.60

Table 4.47: Test results for A3N3S4R

Only a few units were displaced from the top layer; considerably less than in the previous series. This was due to the rapid increase in packing density that resulted from the resettlement of the units. Both experiments show a similar development of armour layer damage, as can be observed in table (4.46) and (4.47).

Influence of the packing density

The response of the armour layer units during the experiment with $n_v = 0.4$ was comparable to the response of the armour units in the previous series. In these earlier experiments the resettlement of tetrapods took place during the first few runs of the experiment. The process of resettlement also occurred in experiment A3N4S4. However, due to the decrease in friction between top and underlayer, resettlement occurred less gradually. The density increased from $n_v = 0.4$ to approximately 0.25 in the first run, consequently forming unacceptably large gaps in the upper part of the armour layer. A total of 117 units moved more than $0.5D_n$.

H_s (m)	$\frac{H_s}{\Delta D_{n_A}}$	T_m (s)	N_{od}	N_{os}	N_{omov}
0.082	1.16	1.16	0	6.44	6.44

Table 4.48: Test results for A3N4S4

Though resettlement was also observed in experiment A3N25S4, due to the high initial density, lesser units moved then in the previous experiments with $n_v = 0.3$ and 0.4. It was at $H_s = 0.142m$ that a first resettlement occurred. During the consecutive sea-state three units were displaced out of the top layer. Displacement continued during the following two runs along with further resettlement of units, which was to some extend initiated by the displacement of units. The overall stability of the structure was considerable, since the density of $n_v = 0.25$ increased a little around SWL at the fourth run. Therefore, it was not until $H_s = 0.195m$ that failure occurred.

The *no damage* as well as the *severe damage* ($N_{od} = 0.28$) criteria do not really differ in the experiments with $n_v = 0.3$ and $n_v = 0.25$. This can be seen in the $H_s/\Delta D_{n_A}$ - n_v plot. As with earlier experiments, there does not seems to be a clear trend in packing density and displacement of units.

H_s (m)	$\frac{H_s}{\Delta D_{n_A}}$	T_m (s)	N_{od}	N_{os}	N_{omov}
0.082	1.36	1.16	0	0	0
0.102	1.70	1.25	0	0	0
0.123	2.04	1.39	0	0	0
0.142	2.36	1.49	0	2.31	2.31
0.158	2.63	1.60	0.17	0.94	1.10
0.177	2.94	1.72	0.22	1.93	2.15
0.195	3.25	1.83	0.39	1.38	1.76

Table 4.49: Test results for A3N25S4

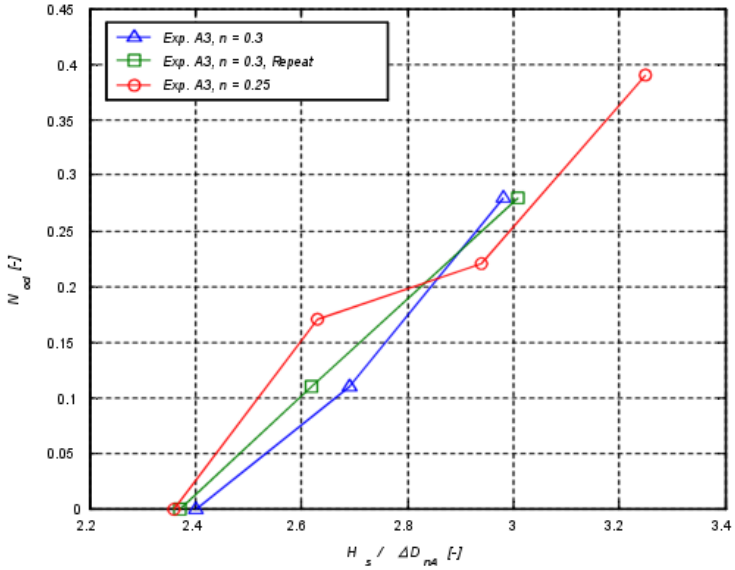

Figure 4.34: Damage curves (N_{od}) for A3N3S4, A3N3S4R and A3N25S4

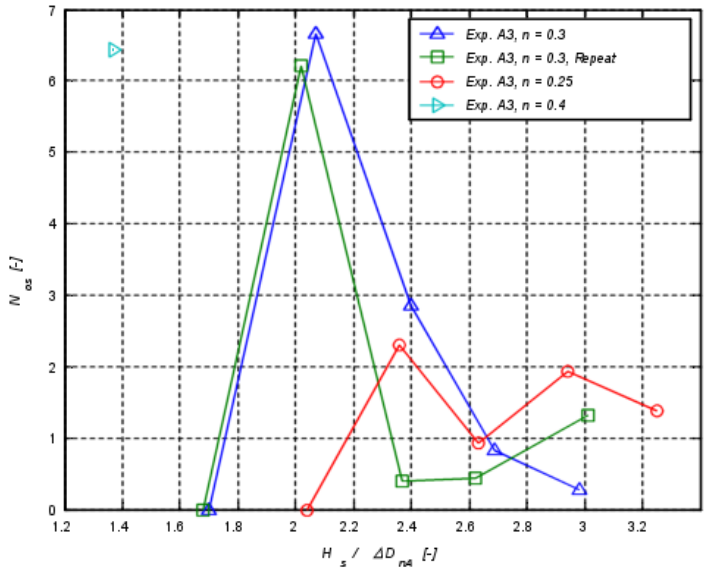

Figure 4.35: Damage curves (N_{os}) for A3N3S4, A3N3S4R, A3N4S4 and A3N25S4

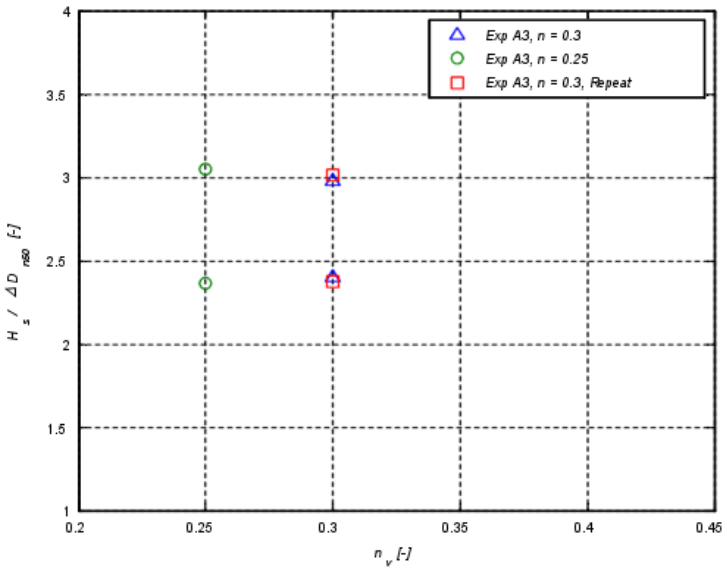

Figure 4.36: Comparison of stability

Influence of the wave steepness

At $H_s = 0.135m$, the long waves in experiment A3N3S2 caused the considerable amount of 113 units to move more than $0.5D_n$. Resettlement already started during the previous two runs, but movements stayed below $0.5D_n$. Small movements were observed during the sea-state following the major resettlement. In the final run, however, 7 units were displaced accompanied by the sliding of 85 units.

The development of damage during the short wave experiment was quite similar to the long wave experiment, though the initial resettlement occurred at a higher significant wave height ($H_s = 0.171m$). The next run was characterized by lesser movement, followed by a final run in which the displacement of 6 units was observed. Again, the displacement initiated further resettlement.

The influence of the wave steepness is depicted quite evidently in the comparison plot. This trend is also visible in the previous series; incoming waves with a relative high steepness cause less damage then waves with a smaller steepness.

H_s (m)	$\frac{H_s}{\Delta D_{n_A}}$	T_m (s)	N_{od}	N_{os}	N_{omov}
0.091	1.52	1.62	0	0	0
0.115	1.92	1.78	0	0	0
0.135	2.24	1.91	0	6.22	6.22
0.166	2.76	2.04	0	1.43	1.43
0.176	2.92	2.17	0.39	4.29	4.68

Table 4.50: Test results for A3N3S2

H_s (m)	$\frac{H_s}{\Delta D_{n\,A}}$	T_m (s)	N_{od}	N_{os}	N_{omov}
0.088	1.46	0.97	0	0	0
0.111	1.85	1.07	0	0	0
0.125	2.07	1.15	0	0	0
0.153	2.54	1.28	0	0	0
0.171	2.85	1.34	0	5.67	5.67
0.187	3.11	1.42	0.06	4.95	5.01
0.202	3.36	1.47	0.33	4.18	4.51

Table 4.51: Test results for A3N3S6

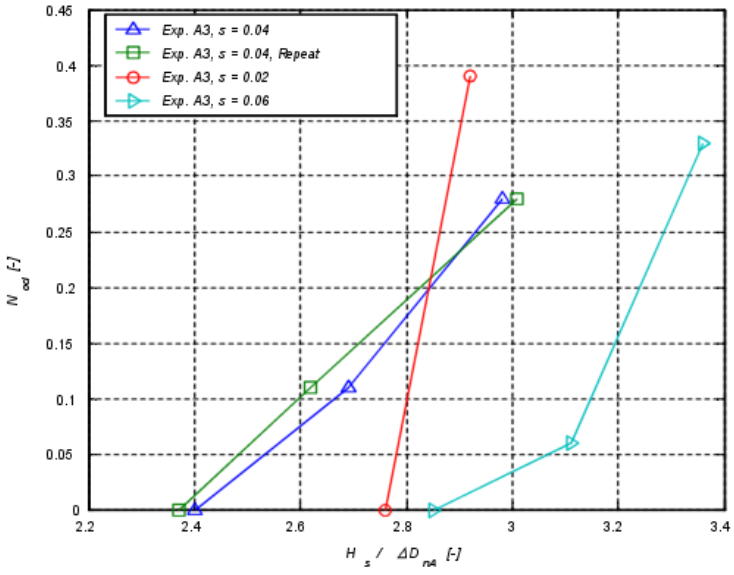

Figure 4.37: Damage curves (N_{od}) for A3N3S4, A3N3S4R, A3N3S2 and A3N3S6

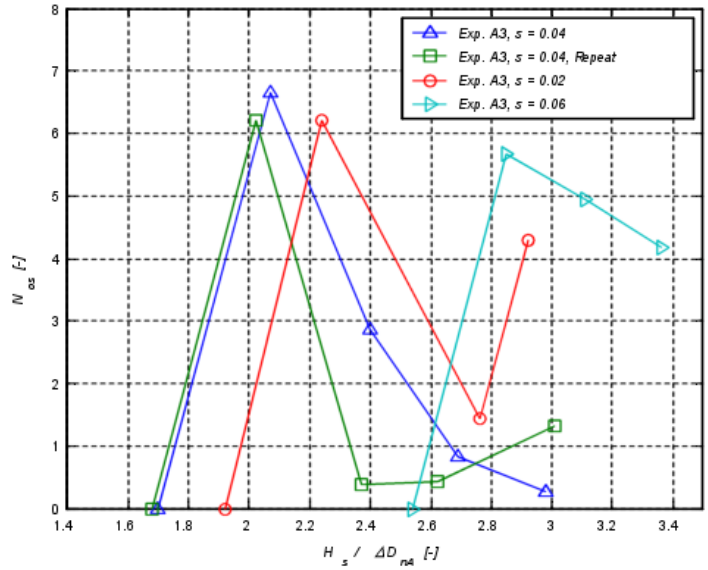

Figure 4.38: Damage curves (N_{os}) for A3N3S4, A3N3S4R, A3N3S2 and A3N3S6

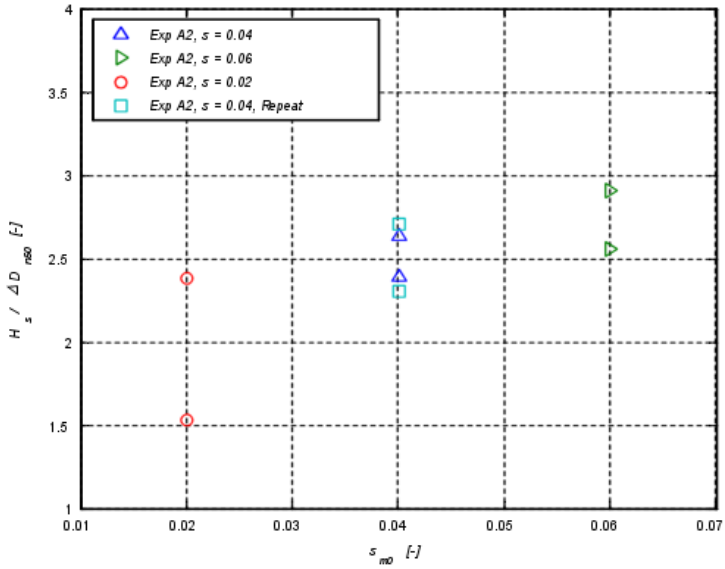

Figure 4.39: Comparison of stability

4.4.2 Secondary layer stability

The overall erosion of the secondary layer increased significantly when compared to similar experiments in the previous series. The total damage of experiment A3N3S4 accumulated to $\sum S = 690$, while the average damage per cross-section was $S = 36.29$. The second experiment yielded an overall damage of $\sum S = 599$ and an average damage of $S = 31.53$.

The resettlement of the armour units predominately initiated the erosion of the underlayer as can clearly be seen in table (4.54) and (4.55). While similarly the eroded holes mainly originated around SWL, their covered area is often larger then observed in the experiments with larger secondary layer material. Yet their depth nowhere exceeded $2.5cm$ or $3 \times D_{n50}$. It was not the excessive erosion of the secondary layer that caused failure of the structure, but rather armour instability that resulted from a deficiency of inter-layer friction between armour and underlayer.

Although some local wash-out occurred at the toe of the structure, it was not near as significant as in VAN DEN BOSCH's experiments. This is rather striking, since the weight of the secondary layer rocks was but a fourth of the material VAN DEN BOSCH used. Still, indirectly, the small size of the secondary layer rocks ($W_a/W_s \approx 120$) contributed to the failure of the entire structure.

$x(cm)$	$S_x(-)$	$x(cm)$	$S_x(-)$	$x(cm)$	$S_x(-)$	$x(cm)$	$S_x(-)$
4	6.46	24	24.48	44	44.09	64	72.32
8	15.44	28	32.85	48	40.80	68	34.03
12	3.57	32	31.35	52	39.81	72	42.80
16	20.80	36	48.22	56	57.46	76	48.38
20	32.82	40	48.43	60	45.49		

Table 4.52: Damage of the secondary layer (A3N3S4)

$x(cm)$	$S_x(-)$	$x(cm)$	$S_x(-)$	$x(cm)$	$S_x(-)$	$x(cm)$	$S_x(-)$
4	29.64	24	17.16	44	28.61	64	55.95
8	27.60	28	32.99	48	20.85	68	12.16
12	27.61	32	28.46	52	13.43	72	28.27
16	38.16	36	68.04	56	9.55	76	49.23
20	43.00	40	49.47	60	18.78		

Table 4.53: Damage of the secondary layer (A3N3S4R)

$x(cm)$	$y(cm)$	Armour response	Mechanism
12 - 24	34 - 42	major sliding	gap
24 - 32	14 - 18	minor sliding	stable
32 - 48	26 - 34	major sliding	gap
32 - 48	34 - 46	major sliding	gap
48 - 56	18 - 22	major sliding	gap
52 - 64	50 - 58	major sliding	gap
52 - 60	62 - 70	major sliding	gap
56 - 68	42 - 50	major sliding	gap
60 - 68	58 - 66	major sliding	gap

Table 4.54: Failure mechanisms of the secondary layer (A3N3S4)

$x(cm)$	$y(cm)$	Armour response	Mechanism
4 - 8	38 - 46	major sliding	gap
12 - 24	54 - 66	major sliding	gap
20 - 28	46 - 54	major sliding	gap
28 - 44	42 - 50	major sliding	gap
32 - 40	18 - 26	displacement	gap
32 - 48	26 - 34	major sliding	gap
32 - 44	34 - 42	major sliding	gap
60 - 68	38 - 50	major sliding	gap
60 - 68	54 - 62	major sliding	gap
68 - 72	38 - 50	displacement	gap

Table 4.55: Failure mechanisms of the secondary layer (A3N3S4R)

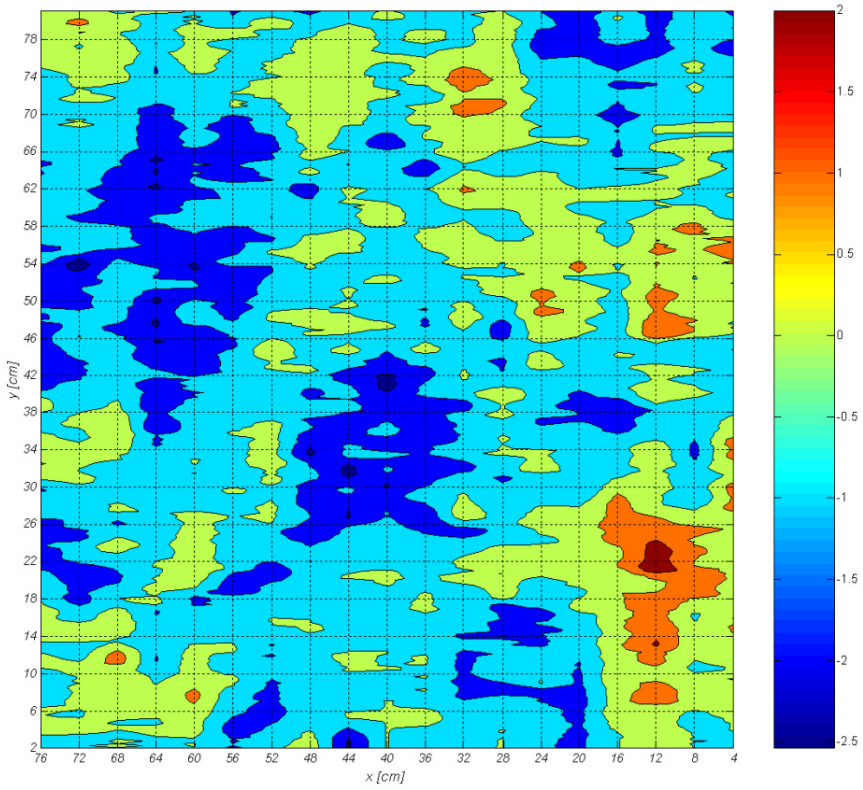

Figure 4.40: Erosion of the secondary layer (A3N3S4)

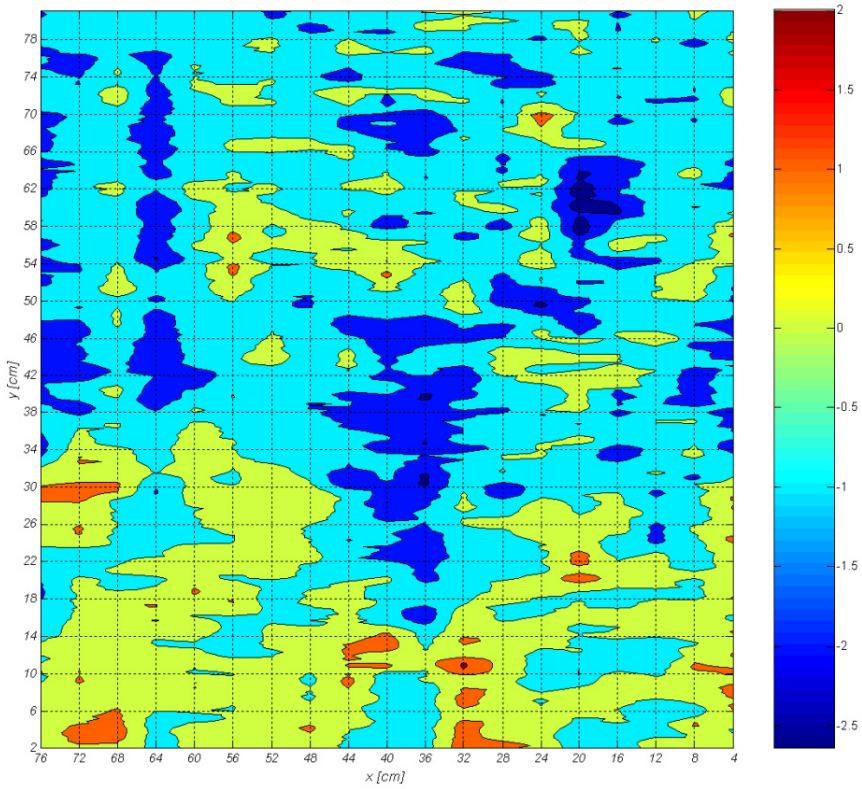

Figure 4.41: Erosion of the secondary layer (A3N3S4R)

Influence of the packing density

Due to the reduced friction between armour and underlayer caused by the limited dimensions of the secondary layer rocks, major resettlement of armour units occurred at the very first run of experiment A3N4S4 ($H_s = 0.082m$). The structure consequently was exposed to a relatively small incoming wave height for a short duration. Earlier experiments already demonstrated the importance of wave height in relation to secondary layer damage. The earlier observed causality applied to experiment A3N4S4 as well, since the overall damage was small, namely $\sum S = 126$ and $S = 6.62$.

The erosion took place because of waves penetrating through the voids between the armour units, caused by the resettlement process. The resettlement occurred over the entire width of the flume, which resulted in several increased voids, yet only two scoured holes were formed. This *randomness* of the secondary layer erosion is mostly due to the -ill-quantifiable- complexity of the flow field in the different layers of the structure and the unconventional shape of the tetrapod.

The overall damage of the underlayer at the end of experiment A3N25S4 was $\sum S = 705$ or averaged per cross section $S = 37.10$. The high packing density of the top layer did not prevent the development of considerable erosion of the underlayer. A few scoured holes were formed under a relative stable top layer (i.e. narrow voids between the individual units), though the secondary layer also eroded because of the displacement of armour units; displacement that left the underlayer

fairly unprotected against incoming waves.

Some wash-out of secondary layer rock occurred at the toe of the slope. This accumulation of material is clearly visible in figure (4.43).

$x(cm)$	$S_x(-)$	$x(cm)$	$S_x(-)$	$x(cm)$	$S_x(-)$	$x(cm)$	$S_x(-)$
4	1.32	24	1.87	44	4.33	64	3.76
8	3.97	28	6.99	48	3.22	68	9.33
12	4.48	32	17.89	52	4.72	72	1.29
16	11.96	36	23.71	56	7.73	76	1.33
20	1.54	40	6.86	60	9.48		

Table 4.56: Damage of the secondary layer (A3N4S4)

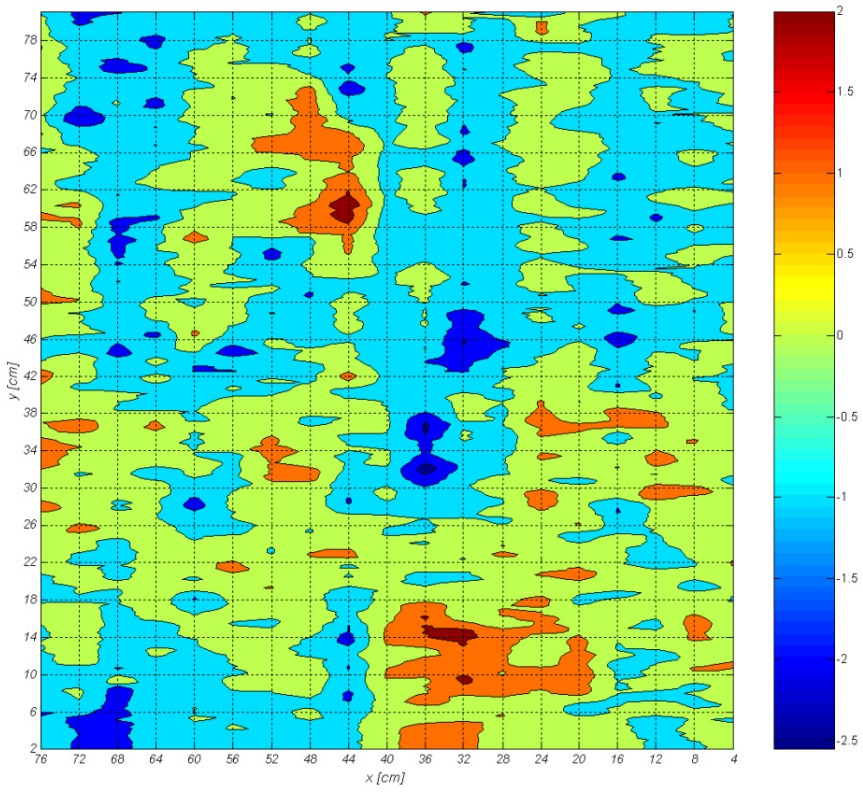

Figure 4.42: Erosion of the secondary layer (A4N4S4)

$x(cm)$	$S_x(-)$	$x(cm)$	$S_x(-)$	$x(cm)$	$S_x(-)$	$x(cm)$	$S_x(-)$
4	54.89	24	64.23	44	27.20	64	23.14
8	26.55	28	40.40	48	28.45	68	53.02
12	46.86	32	19.91	52	28.19	72	29.77
16	48.70	36	29.20	56	19.81	76	43.40
20	44.19	40	36.38	60	40.61		

Table 4.57: Damage of the secondary layer (A3N25S4)

$x(cm)$	$y(cm)$	Armour response	Mechanism
28 - 36	42 - 50	major sliding	gap
32 - 40	30 - 38	major sliding	gap

Table 4.58: Failure mechanisms of the secondary layer (A3N4S4)

$x(cm)$	$y(cm)$	Armour response	Mechanism
4 - 12	38 - 46	major sliding	stable
8 - 20	30 - 38	major sliding	stable
12 - 28	38 - 50	displacement	gap
12 - 24	58 - 66	major sliding	gap
20 - 32	26 - 34	displacement	gap
48 - 64	38 - 42	major sliding	stable
52 - 60	30 - 34	minor sliding	stable
64 - 72	38 - 46	major sliding	gap

Table 4.59: Failure mechanisms of the secondary layer (A3N25S4)

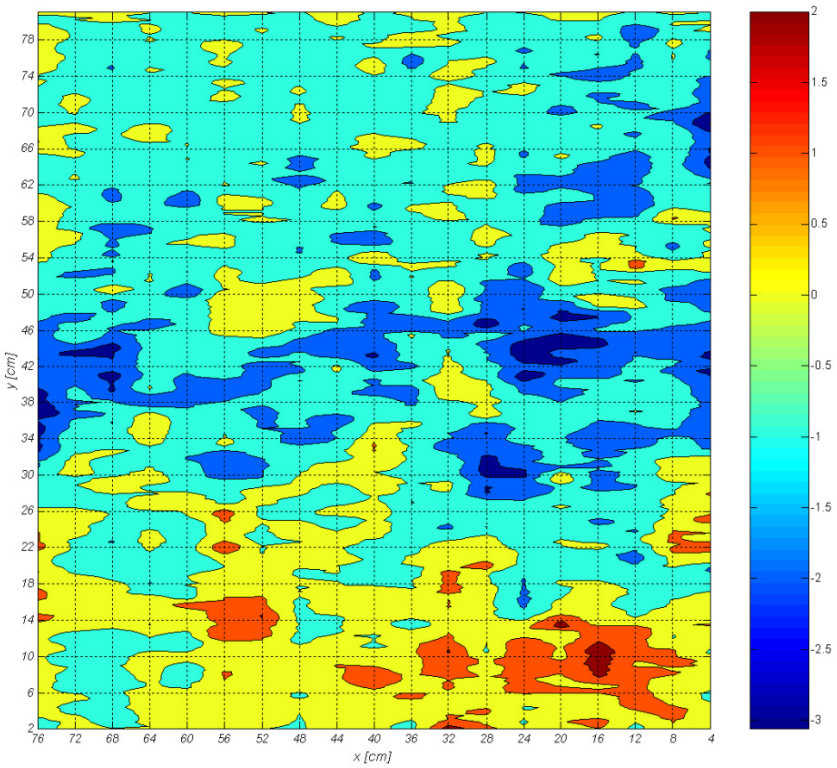

Figure 4.43: Erosion of the secondary layer (A3N25S4)

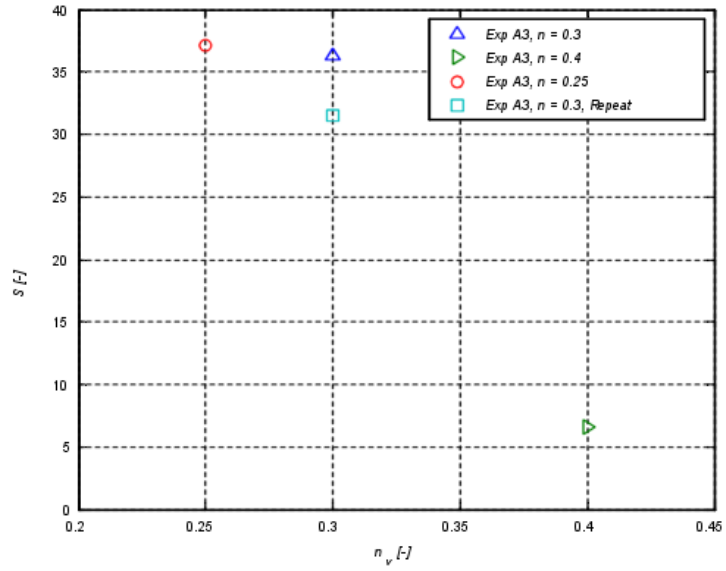

Figure 4.44: Comparison of stability

Influence of the wave steepness

The damage at the end of the long wave experiment amounted to $\sum S = 560$ and $S = 29.50$, whereas at the end of experiment A3n3s6 the secondary layer damage was $\sum S = 742$ and $S = 39.05$. The predominant cause of the erosion for both experiments was similar: resettlement leading to increased void sizes between units. In experiment A3N3S2, this resettlement is intensified by the displacement of several units in the lower yellow band. At both experiments did the depth of the scoured holes not surpass the $2.5cm$, yet the area they covered was sometimes substantial.

$x(cm)$	$S_x(-)$	$x(cm)$	$S_x(-)$	$x(cm)$	$S_x(-)$	$x(cm)$	$S_x(-)$
4	28.98	24	17.08	44	28.32	64	54.38
8	26.80	28	32.14	48	20.85	68	11.26
12	27.20	32	28.32	52	13.43	72	27.74
16	37.55	36	66.46	56	9.55	76	47.91
20	42.33	40	22.14	60	17.99		

Table 4.60: Damage of the secondary layer (A3N3S2)

$x(cm)$	$S_x(-)$	$x(cm)$	$S_x(-)$	$x(cm)$	$S_x(-)$	$x(cm)$	$S_x(-)$
4	39.09	24	44.19	44	10.01	64	42.60
8	42.82	28	34.50	48	11.87	68	47.23
12	33.80	32	23.81	52	45.51	72	73.08
16	43.51	36	21.34	56	21.09	76	42.30
20	46.80	40	50.63	60	67.84		

Table 4.61: Damage of the secondary layer (A3N3S6)

$x(cm)$	$y(cm)$	Armour response	Mechanism
12 - 24	54 - 66	major sliding	gap
16 - 28	46 - 54	major sliding	gap
28 - 40	34 - 42	major sliding	stable
28 - 40	46 - 50	major sliding	stable
32 - 48	26 - 34	major sliding	gap
60 - 68	38 - 50	major sliding	gap
60 - 68	54 - 62	major sliding	gap
68 - 72	38 - 46	major sliding	gap

Table 4.62: Failure mechanisms of the secondary layer (A3N3S2)

$x(cm)$	$y(cm)$	Armour response	Mechanism
4 - 12	34 - 42	major sliding	gap
4 - 12	42 - 50	major sliding	stable
12 - 24	58 - 66	major sliding	gap
16 - 28	34 - 42	major sliding	gap
32 - 44	42 - 54	major sliding	gap
48 - 60	38 - 50	major sliding	gap
60 - 76	38 - 54	major sliding	gap
68 - 76	18 - 26	displacement	gap

Table 4.63: Failure mechanisms of the secondary layer (A3N3S6)

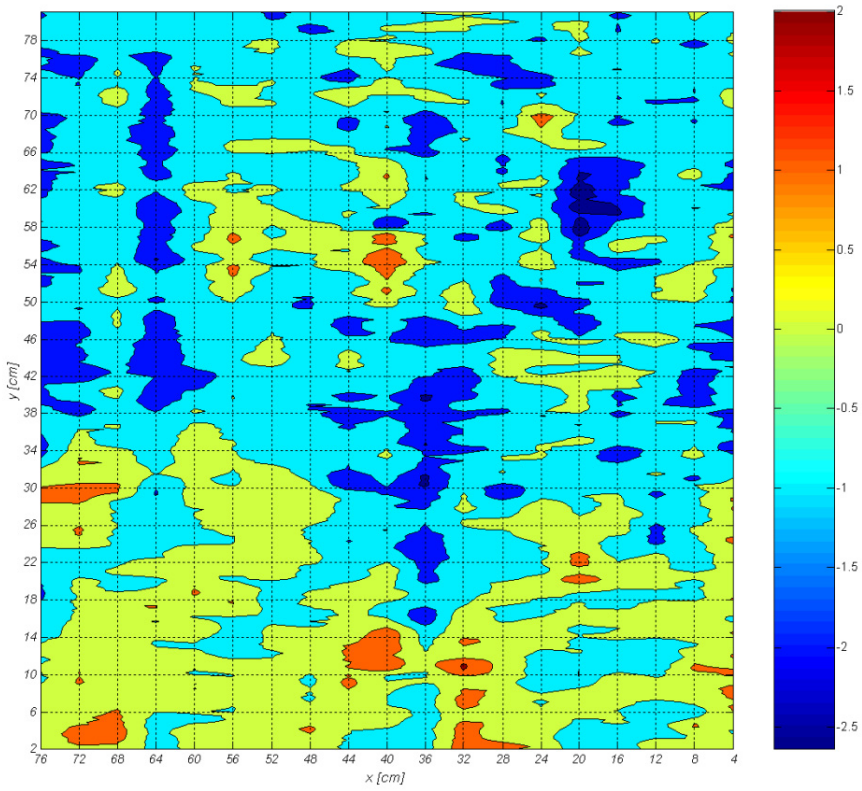

Figure 4.45: Erosion of the secondary layer (A4N3S2)

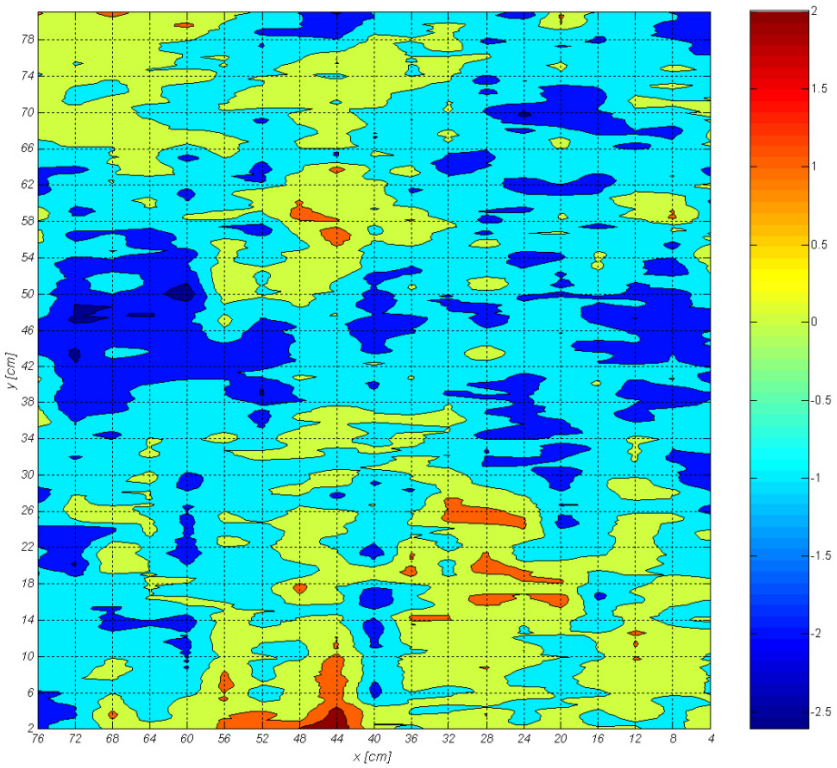

Figure 4.46: Erosion of the secondary layer (A3N3S6)

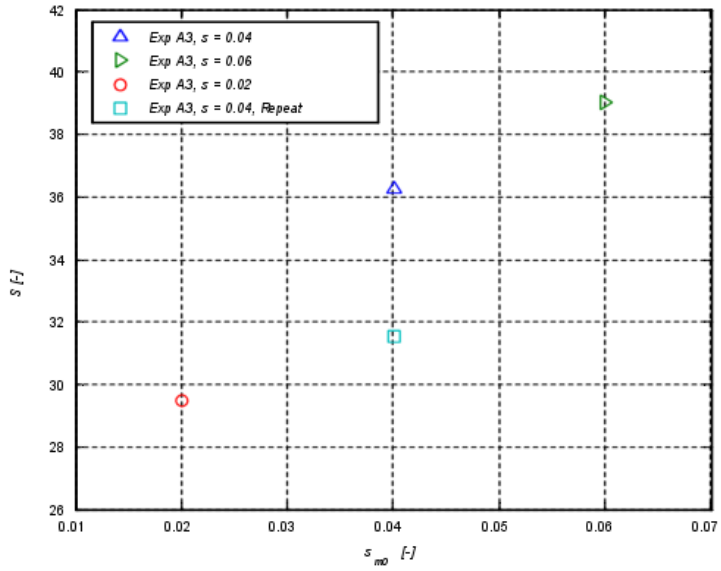

Figure 4.47: Comparison of stability

Chapter 5

Analysis of the wave flume experiments

An overall comparison of all the experimental results is the focal point of this chapter. The influence of the test parameters on the stability of both the top and secondary layer will be discussed and analyzed. The data-analysis will lead to the derivation of a stability formula for single armour layered tetrapod breakwaters. Furthermore, the influence of the parameters concerning the secondary layer will be discussed and quantified.

5.1 Failure mechanism of the armour layer

Without exception, it was the formation of one or more gaps -exceeding the failure criterium of $D \times D$- in the upper part of the armour layer that led to failure of the structure. Primarily this was brought about by a combination of sliding and displacement of armour units, although in the experiments with $n_v = 0.4$, the mechanism of sliding was solely responsible. There is a distinct mutual influence between the two failure mechanisms. In the experiments, the sliding of units reduced the occurrence of displacements to some extent. Yet the occurrence of displacement promoted sliding of individual units.

The decrease in displacement resulting from the resettlement of units is eminently visible in the last series. The reduction in secondary rock size caused a reduction in friction between top and underlayer. This directly resulted in a considerable resettlement of units, which in return caused lesser units to displace compared to the previous series. The underlying principles of this mutual influence is evident. The process of resettlement generally caused an increase in packing density around and below SWL -precisely the area that is most severely exposed to wave attack. This increase in armour density resulted in the improvement of interlocking ability between the units, which consequently led to lesser units being able to complete the required rotation necessary for displacement. Contrarily, if a unit was displaced out of the top layer it created additional room, which often caused units placed higher upon the slope to slide downwards, thereby filling the gap left by the displaced unit to some extend.

As far as failure mechanisms are concerned almost all research on artificial armour units (e.g. Van der Meer, 1988b; Bhageloe, 1998; Van den Bosch, 2001) describes stability only by means of the number of displaced units. Rocking and sliding of units are ignored as is evident from Van der Meer's (1988b) widely used stability formula. Especially in single tetrapod layers this is a too incomplete representation of the stability. For example, all experiments with $n_v = 0.4$ showed a rapid failure of the top layer, though not a single unit was displaced.

Furthermore, if only displacement was related to stability, the improper notion would arise that within the armour packing density range of $n_v = 0.25-0.3$, small underlayer material -or insufficient friction between top and underlayer- would lead to a more stable armour layer. The reduced friction in series A3 initiated a rapid increase of an already relatively packed top layer. Although gaps in the upper part of the armour did arise, the high numbers of tetrapods per square meter prevented the formation of sudden inadmissible gaps -as was the case in the experiment with $n_v = 0.4$. Though for the initially higher packed armour layers the damage process had a more moderate character, the end result was the same; failure of the structure due to the formation of unacceptable gaps. The rapid resettlement hindered displacement, but to conclude from these observations that the top layer in the final series is more stable than in the previous series would be untrue.

Ideally, a stability formula would incorporate both failure mechanisms, while also respecting their interdependency. The derivation of such a relation, however, falls outside the scope of this analysis. A predictive formula will be derived for a single armour layer of tetrapods. This formula will predict only the damage suffered by displaced units, which in itself is a good indication of the overall stability.

5.1.1 Influence of the wave steepness

The various $H_s/\Delta D_{n_A}$ - s_{m0} plots in the chapter on the observation of the experiments as well as previous research (Van der Meer, 1988; De Jong, 1996) ascertain a trend that can be expressed as:

$$\frac{H_s}{\Delta D_{n_A}} = a_1 \left(s_{m0}\right)^{b_1} \tag{5.1}$$

In which a_1 is a function of amongst others, the permeability, the storm duration, damage level and the underlayer material. The coefficient b_1 was established at various fixed damage levels ($N_{od} = 0$, 0.1, 0.2 and 0.3) for all three series, which led to an average (rounded) value of $b_1 = 0.2$ and a standard deviation of $\sigma_{b_1} = 0.09$. This is identical to the value De Jong (1996) obtained while deriving his stability formula. The majority of b_1 values are relatively consistent as can be seen in table (5.1).

damage level N_{od}	b_1 for $N = 1000$
0.0	0.16
0.1	0.15
0.2	0.14
0.3	0.18

Table 5.1: b_1 values for series A1

5.1.2 Influence of the packing density

A similar approach was used to determine the influence of the packing density on the stability of the top layer. The experiments with $n_v = 0.4$ showed failure of the armour layer without the displacement of units. Therefor, at $n_v \geq 0.4$, N_{od} does not give any indication as to the stability of the top layer. Consequently, only the experiments with $n_v = 0.3$ and 0.25 were analyzed to determine the influence of the packing density.

$$\frac{H_s}{\Delta D_{n_A}} \left(s_{m0}\right)^{-0.2} = a_2 \left(n_v\right)^{b_2} \tag{5.2}$$

b_2 was also calculated at fixed damage levels. From the calculated values no clear trend could be established. The scatter of b_2 was significant, though the average value amounted to $b_2 = 0$. On the basis of the observations of the experiments, as well as of the calculated values of b_2, the influence of the initial packing density on the damage development concerning the displacement of units in the range of $n_v = 0.25 - 0.3$ is negligible. More important than the initial packing density is the *rate of increase* of the packing density. The process of sliding continuously causes an increase in the packing density -especially around and below SWL. Observations indicate that the rate of increase (towards an equilibrium of $n_v = 0.23 - 0.27$) is mainly dependent upon the the size of the underlayer material. It seems therefore, more logic to include the dimension of the secondary layer material in the stability formula, thereby incorporating this effect of increase in density occurring during the experiments (see paragraph (5.1.5)).

Summarizing, the packing density (n_v) shall be discarded from the stability formula. Again, it is emphasized that, even though the initial packing density has no direct influence on the number of displaced units, it is indeed very important in relation to the total stability of the structure. Observations show that for a single layer of tetrapods, packing densities equal or larger then $n_v = 0.4$ are unsuitable.

5.1.3 Influence of the permeability

There certainly seems to be an influence of the core permeability regarding the top layer stability. The tests with a geotextile placed between the intermediate layer and the core show more damage than similar tests without the additional geotextile. In the final run ($H_s/\Delta D_{n_A} \approx 2.7 - 2.8$) the damage level without the geotextile amounted to 0.28 and 0.33, while $N_{od} = 0.39$ for the two similar experiments with the geotextile.
Despite this apparent influence, not enough tests were performed to take the permeability of the structure into account in the derivation of a stability formula.

5.1.4 Influence of the storm duration

All tests were performed with a storm duration of approximately $N = 1000$. From the obtained data, therefore, no conclusion can be drawn regarding the impact of storm duration. However, previous research (e.g. Van der Meer, 1988a,b) indicates that the relationship between the damage and the storm duration for the area $N < 7000 - 10000$ can be described by:

$$\frac{N_{od}}{\sqrt{N}} = constant \tag{5.3}$$

De Jong (1996) checked this relation for various large data sets. His findings further supported the validity of equation (5.3). Based upon previous research therefore, the influence of storm duration will be acknowledged, leading to the incorporation of this relation in the stability formula. The formula thus becomes;

$$\frac{H_s}{\Delta D_{n_A}} \left(s_{m0}\right)^{-0.2} = a_5 \left[a_3 + a_4 \left(\frac{N_{od}}{\sqrt{N}} \right)^{b_3} \right] \tag{5.4}$$

A regression analysis of the data led to a parametric value of $a_3 = 3.7$, $a_4 = 8.0$ and $b_3 = 0.5$; resulting in

$$\frac{H_s}{\Delta D_{n_A}} = a_5 \left[3.7 + 8.0 \left(\frac{N_{od}}{\sqrt{N}} \right)^{0.5} \right] s_{m0}^{0.2} \tag{5.5}$$

5.1.5 Influence of the nominal diameter of the secondary layer

As described earlier, the size of the underlayer rock material mostly influenced the rate of resettlement of the armour units. Smaller material led to lesser friction between armour and underlayer. Consequently, the reduction in friction led to an increase in the collective sliding of units. This resettlement created gaps in the upper part of the armour layer. Yet a positive effect of this substantial resettlement process was an increase in packing density.

The predicative reliability of formula (5.5) increases by introducing a factor $(D_{n_A}/D_{n50_S})^{b_4}$ in the formula. This term signifies the ratio between armour layer and secondary layer diameter. Regression analysis shows that the highest reliability is acquired if b_4 is set at 0.05. The final formula now becomes:

$$\frac{H_s}{\Delta D_{n_A}} = \left(\frac{D_{n_A}}{D_{n50_S}}\right)^{0.05} \left[3.7 + 8.0\left(\frac{N_{od}}{\sqrt{N}}\right)^{0.5}\right] s_{m0}^{0.2} \tag{5.6}$$

5.1.6 Validity of the formula

The 90% confidence bands are acquired after the regression of $N_{od}^{0.5}$ against $\frac{H_s}{\Delta D_{n_A}}\left(\frac{D_{n_A}}{D_{n50_S}}\right)^{-0.05} N^{-0.25} s_{m0}^{-0.2}$. From the analysis followed an a_3 and a_4 value of 3.5 and 6.0 for the lower 90% band and $a_3 = 3.8$ and $a_4 = 10.0$ for the upper 90%. Furthermore, considering a_3 and a_4 to be stochastic variables, the analysis led to a standard deviation (assuming a normal distribution) of $\sigma = 0.40$.

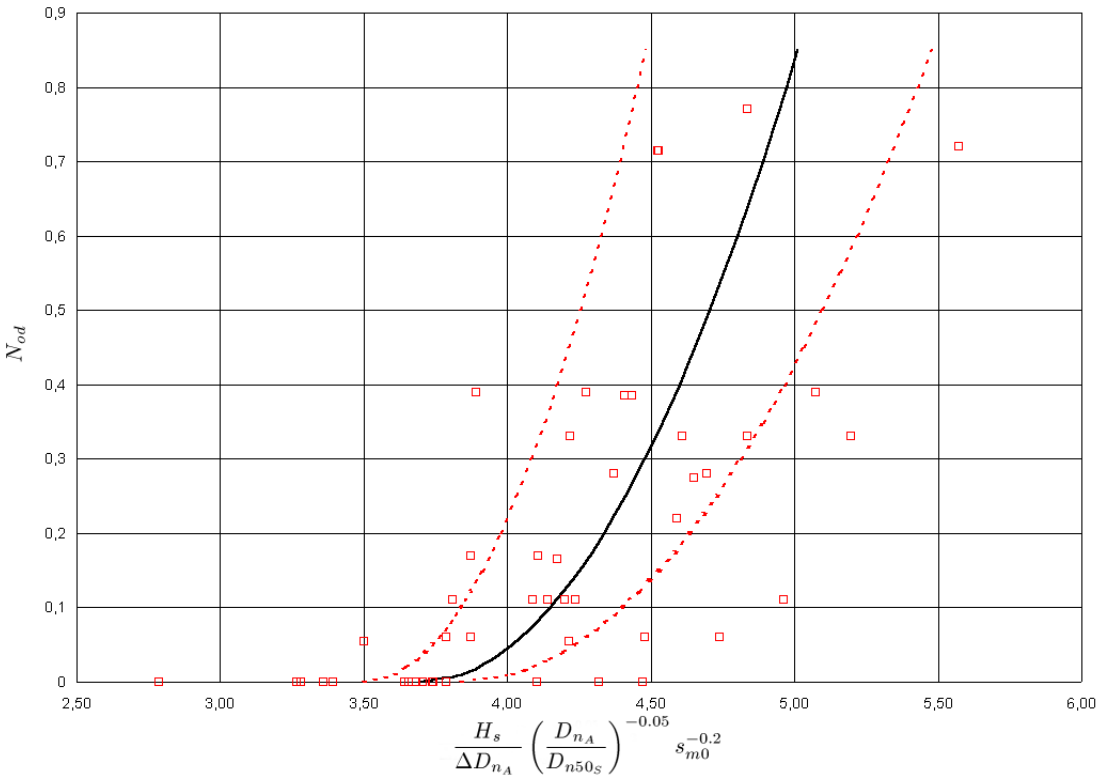

Figure 5.1: Stability formula with 90 % confidence bands

Scatter is still present in the figure. The scatter of the stability results can be due to:

- differences due to the random behaviour of the armour units;
- accuracy of measuring the wave height and period;
- curve fitting.

It should be noted that the derived formula is only applicable in the range of the minimum and maximum values of the tested parameters.

Double layer versus single layer tetrapod stability formula

The most noticeable difference between VAN DER MEER's stability formula (1988b) for a double armour layer of tetrapods and the derived stability formula for a single layer is the influence of the wave steepness. Longer wave periods increase the stability, VAN DER MEER observed in his experiments. However, from the single layer experiments, the opposite conclusion followed; shorter wave periods increase the stability. The latter trend was also established by DE JONG (1996) while investigating wave flume data for double layered tetrapod breakwaters.

Though the addition of the term $(D_{n_A}/D_{n50_S})^{0.05}$ in the derived stability formula improves the overall predictability of the outcome, its influence compared to the wave steepness is limited. To improve the usability of the formula, it can be reduced to the more general form;

$$\frac{H_s}{\Delta D_{n_A}} = \left[3.7 + 8.0\left(\frac{N_{od}}{\sqrt{N}}\right)^{0.5}\right] s_{m0}^{0.2} \tag{5.7}$$

The results of both formulae can now easily be compared, since only the wave steepness, the damage level and the storm duration determine the stability. Plotting the damage number against the stability number for (a frequently in nature occurring) $s_{m0} = 0.04$ and taking a storm duration of $N = 1000$, leads to figure (5.2).
The plot clearly demonstrates that the initial stability for a single layer is higher then for a double layer. Because of the fact that in a double layer more tetapods are placed per square meter -or in other words; the single layer consist of fewer units, while the packing density is lower ($n_v \leq 0.4$ in the experiments versus $n_v \approx 0.5$ for a double layer)-, chances are that the start of damage occurs sooner in a double than in a single layer.

The damage development for a single layer, however, has a more progressive character. Because of the numerous units in a double layer, it has a more self-healing ability. Additionally, a tetrapod has more neighboring units, which generally improves its interlocking properties.

The formulae start to deviate if a different wave steepness (e.g. $s_{m0} = 0.06$) is used. This is due to the difference in the observed effect of the wave steepness between VAN DER MEER's experiments and the current tests. More test should be conducted to determine the effect of the wave steepness on the armour stability.

5.2 Failure mechanism of the secondary layer

The erosion of the secondary layer is an overall result of complex factors (e.g. the turbulent motion of the water in the top and underlayer, the unusual shape of the armour units, the form and weight of the secondary rock material and the permeability of the core). The complexity of these matters makes it impossible to give a deterministic analysis of the local erosion process. A broader view -i.e. an analysis concerning the overall damage- is necessary to discover causalities between the erosion process of the underlayer and the investigated structural and environmental parameters.

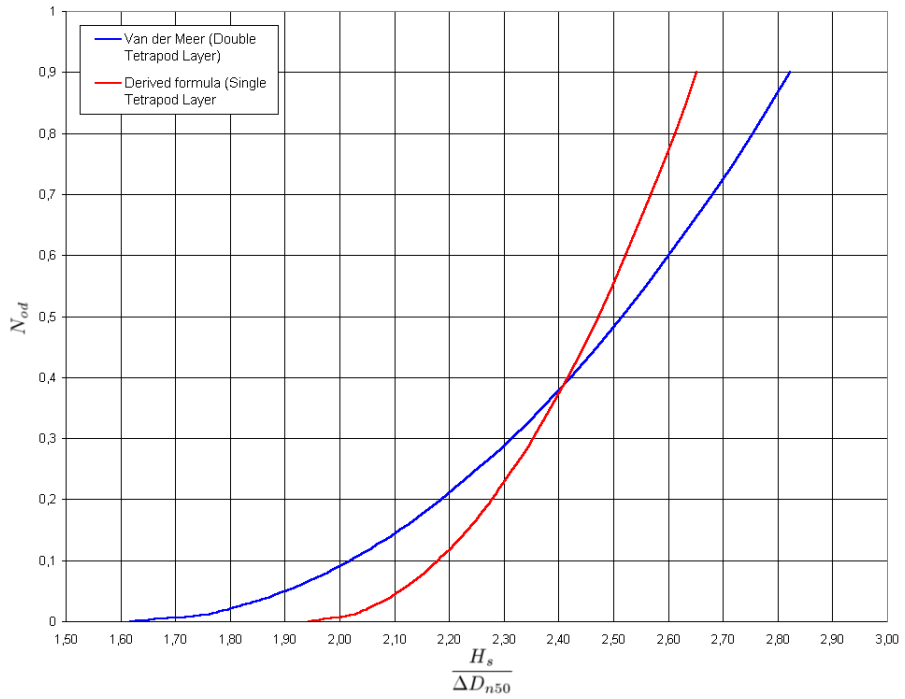

Figure 5.2: Results of the double layer and single layer stability formula for $s_{m0} = 0.04$ and $N = 1000$

5.2.1 Influence of the permeability

The most noticeable result of the experiments was the lack of secondary layer wash-out. Van den Bosch (2001) claimed to observe considerable wash-out of the secondary layer material ($D_{n50} = 14mm$). Tests under nearly similar conditions resulted in a different outcome. No wash-out was perceived in the experiment, only local scoured holes. In order to attribute the deviation in results to the difference in permeability of the core, experiments were carried out with geotextile (see paragraph 4.1). Series A0 and A1 demonstrate the influence of the permeability of the core. With an overall erosion of $S = 6.42$ and $S = 7.46$ for the first series and $S = 9.55$ and $S = 11.79$ for series A0, the decrease in permeability resulted in an increase of damage somewhere between 30% and 80%. Quantifying the influence of the permeability is useless, because of the limited number of tests. However, that its influence is significant, becomes clear.

5.2.2 Influence of the wave steepness and armour packing density

There surely is a relation between underlayer erosion and both the wave steepness and packing density, though it is indirect. In all experiments top layer instability occurred before underlayer instability. The influence of the wave steepness and (the increase of) the packing density on armour layer stability was quite profound. A narrowly packed armour layer made the structure endure higher incoming waves before displacement occurred. Likewise, the structure withstood higher waves if the incoming waves were relatively short. This line of argumentation would also predict less damage to the underlayer with a denser armour packing density. This was not true; all experiments demonstrated the contrary. A dense armour packing and short waves led to more secondary layer erosion then a wide packing and long waves did. Consequently, it is fair to assume that it is predominantly the height of the incoming waves and the size of the underlayer material that determine the amount of erosion to the underlayer.

5.2.3 Influence of the wave height and the diameter of the material

If the incoming wave height -at which failure of the structure occurred- is related to both the nominal diameter and the relative density of the underlayer, the stability number of the secondary layer is acquired. When for every experiment this stability number is plotted against the damage, a surprisingly linear relationship is observed

	$H_s/\Delta D_{n50_S}(-)$	$S(-)$
$H_s/\Delta D_{n50_S}(-)$	1.00	0.97
$S(-)$	0.97	1.00

Table 5.2: Correlation between $H_s/\Delta D_{n50_S}$ and S

But erosion, as became clear from the observations of the experiments, is also influenced by the armour response. Sliding or replacement of units often initiated local erosions. Analysis of the data shows that the total armour response (the sum of all displaced and moved units during the entire experiment, $\sum N_{omov}$) is correlated to the stability number of the secondary layer ($r = 0.75$). A commonly used collinearity diagnostic is the ratio $\kappa = \lambda_1/\lambda_2$ in which λ_1 and λ_2 are the eigenvalues of the correlation matrix $\mathbf{R}$. The eigenvalue ratio for this particular case $\kappa = 2.68/0.03 = 89.3$. The calculation of the *multi-collinearity condition number* must justify the assumption of collinearity and thereby the omittance of this variable in a predictive relation. According to JOBSON (1991) a value κ near and above 100 does so.

The following predictive stability relation for the secondary layer arises (equation 5.8). This relation is of course only a first step, solely based on the small number of executed experiments. Furthermore, it should be noted that this relation is only applicable within a limited parametric range, namely within those tested. Yet within this range, it predicts the overall erosion fairly well ($\alpha < 0.05$).

$$\frac{H_s}{\Delta D_{n50_S}} = 4.68 + 0.32S \tag{5.8}$$

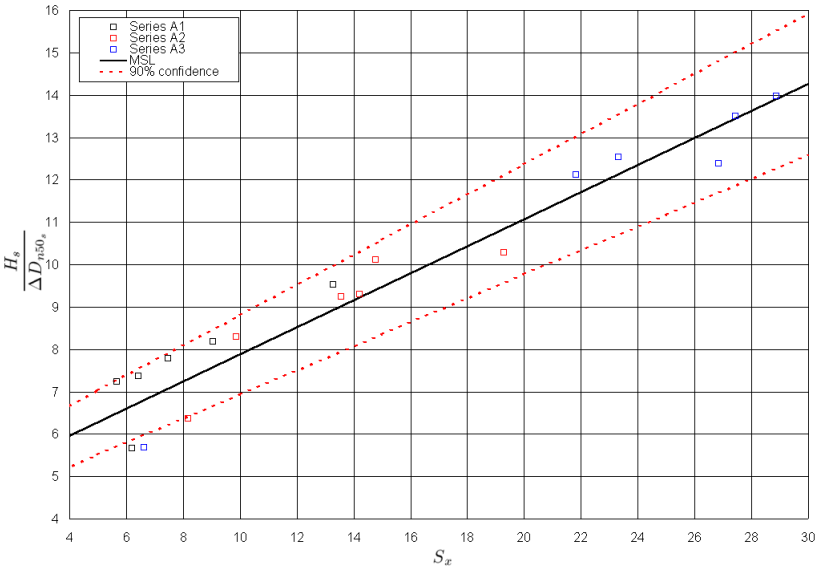

Figure 5.3: Secondary layer stability relation with 90% confidence bands

Chapter 6

Conclusions and Recommendations

In this chapter, conclusions derived from the experimental research, are presented. The conclusions cover the two areas of interest; the single armour layer and the secondary layer. Next, recommendations are given for further research.

6.1 Conclusions

the armour layer

- The experiments demonstrated a positive relation between an increase in the packing density of the armour layer and the overall stability of the structure.
- The experiments demonstrated a positive relation between an increase in wave steepness and the overall stability of the structure.
- The tests showed that there is a distinct influence between armour layer stability and the permeability of the core. A less permeable core leads to more damage to the top layer.
- In all experiments, it was the formation of one or more gaps in the upper part of the armour layer that led to the failure of the structure. In almost all tests, a combination of sliding and displacement caused the formation of these gaps. However, in the experiments with $n_v = 0.4$, the mechanism of sliding was solely responsible.
- Displacement mainly occurred around Still Water Level (SWL), while the gaps were formed around the level of maximum wave run-up.
- At the experiments with $n_v = 0.4$, substantial resettlement occurred very suddenly at relatively low incident waves. This resettlement caused inadmissable gaps in the upper part of the top layer and thus failure of the structure. The experiments demonstrated that a single tetrapod armour layer with a packing density of $n_v \geq 0.4$ is unsuitable.
- There is a distinct interaction between the two failure mechanisms of displacement and sliding. The displacement of units caused units placed higher upon the slope to slide down, while substantial sliding (or resettlement) caused an increase of packing density around and below SWL and hence less units to displace.
- Observations indicated that the resettlement of the armour units was a continuous process, until a 'natural' packing density of $n_v = 0.23 - 0.27$ was reached.
- The rate of increase in armour packing density toward the 'natural' packing density of $n_v = 0.23 - 0.27$ is largely determined by the size of the secondary layer material. Smaller underlayer

material reduced the friction between the armour and underlayer, which consequently led to a rapid increase of the packing density towards $n_v = 0.23 - 0.27$.

- Though with regard to the overall stability of the structure, both displacement and sliding should be taken into account, displacement by itself can serve as a good indication of the stability. An increase in wave steepness caused a decrease in displacement. The experiments further showed that the amount of displacement in the experiments with $n_v = 0.3$ and 0.25 did not really differ. Displacement did decrease, however, if during the tests there was a rapid increase in packing density towards the 'natural' $n_v = 0.23 - 0.27$. Therefore, displacement is also influenced by the size of the secondary layer material.

- A stability formula for a single armour layer of tetrapods was derived from the wave flume data. The formula has the following form:

$$\frac{H_s}{\Delta D_{n_A}} = \left(\frac{D_{n_A}}{D_{n50_S}}\right)^{0.05} \left[3.7 + 8.0\left(\frac{N_{od}}{\sqrt{N}}\right)^{0.5}\right] s_{m0}^{0.2}$$

the secondary layer

- Contrarily to observations of Van den Bosch (2001), no considerable wash-out of secondary layer material was perceived during the experiments. Rather then wash-out, the damage to the secondary layer consisted of local scoured holes that concentrated around SWL.

- Erosion increased with a decrease in secondary layer material. Though, in all experiments the depth of the scoured holes never exceeded $3 \times D_{n50_S}$.

- The influence of the permeability of the core on the erosion of the secondary layer is considerable. A decrease in permeability causes an increase in erosion.

- Sliding or displacement -i.e. an increase in the size of the voids between individual armour units- often initiated the erosion of the underlayer.

- Even during the experiments with the smallest secondary material (with $W_a/W_s \approx 120$ far exceeding the limit of Van der Meer's recommendation) it was the armour instability rather than excessive erosion of the underlayer that caused failure of the structure. The size of the secondary layer material does influence the armour response. Smaller underlayer material causes an increase in armour resettlement. This, however, does not lead to a more rapid failure of the structure per se, especially if the initial packing density of the armour layer is already high.

- The experiments indicated that the amount of eroded material showed no relation with the wave steepness or the packing density of the armour layer. There was, however, a distinct influence between the height of the incoming waves and the overall secondary layer erosion.

- From the wave flume data a relation has been derived that can predict the erosion of the secondary layer. This relation has the following form:

$$\frac{H_s}{\Delta D_{n50_S}} = 4.68 + 0.32S$$

6.2 Recommendations

- The relationship between sliding and displacement of armour units should be studied more closely. Since the influence of sliding on the overall stability of the structure is significant, it should be incorporated in a stability formula.
- The observed influence of the wave steepness regarding the displacement of armour units contradicts the finding of Van der Meer (1988b). More research must be done to determine the effect of the wave steepness.
- The applied core scaling procedure (Burcharth et al., 1999) has a considerable influence on the top and secondary layer stability. Froude-scaling of the characteristic pore velocity from prototype to model dimension led to rather course model core material. This method provides a better representation of the flow regime in the breakwater. Still, scale effects due to the permeability may play a roll. Tests on larger scales to verify the outcome of the model experiments are therefore recommended.
- In all experiments, resettlement occurred to some extent. The structural integrity of the artificial concrete units should therefore also be taken into account in the translation of the experimental results to prototype design.
- To further validate the reliability of both the derived stability formula for a single tetrapod armour layer as the relation predicting the secondary layer damage, more wave flume experiments should be performed.

References

Angremond, K. d', Van Roode, F.C. (2000) *Breakwaters and closure dams. Bed bank and shore protection 2*, Delft University of Technology, Delft, The Netherlands

Battjes, J.A. (1974) *Computation of set-up, longshore currents, run-up and overtopping due to wind-generated waves* , Delft University of Technology, Delft, The Netherlands

Bhageloe, G.S. (1998) *Breakwaters with a single layer*, MSc Thesis, Delft University of Technology, Delft, The Netherlands

Broderick, L.L. (1984) *Riprap stability versus monochromatic and irregular waves*, Conf. on coastal structures

Burcharth, H.F., Andersen, O.H. (1995) *On the one-dimensional steady and unsteady porous flow equations*, Coastal Engineering 24, Elsevier

Burcharth, H.F., Liu, Z., Troch, P. (1999) *Scaling of core material in rubble mound breakwater model tests*, Proceedings of COPEDEC V, Cape Town, South Africa

CUR (1993) *Filters in de waterbouw*, CUR Publication 161, Gouda, The Netherlands

CUR (1995) *Manual on the use of rock in hydraulic engineering*, CUR Publication 169, Gouda, The Netherlands

De Jong, R.J. (1996) *Stability of Tetrapods at front, crest and rear of a low-crested breakwater*, MSc Thesis, Delft University of Technology, Delft, The Netherlands

Hasselman, K. et al. (1973) *Measurement of wind-wave growth and swell during the Joint North Sea Wave Project (JONSWAP)*, Deutches Hydrographisches Institut, Hamburg, Germany

Hudson, R.Y. (1958) *Design of quarry stone cover layer for rubble mound breakwater*, WES, Research Report No 2.2, Vicksburg, USA

Hudson, R.Y. (1959) *Laboratory investigations of rubble mound breakwaters*, WES Report, Vicksburg, USA

Hughes, S.A. (1993) *Physical Models and Laboratory Techniques in Coastal Engineering*, World Scientific Publishing Co. Pte. Ltd., Singapore

Iribarren, R. (1950) *Generalizacion de la formula para el calculo de los diques de escollera y comprobacion de sus coefficientes*, Revista de Obras Publicas, Madrid, Spain

Iribarren, R. (1954) *Other verifications of the formula calculating breakwater embankments*, PIANC, Bull. No 39

Jensen, O.J., Klinting, P. (1983) *Evaluation of scale effects in hydraulic models by analysis of laminar and turbulent flows* , Coastal Engineering 7

Jobson J.D. (1991) *Applied Multivariate Data Analysis*, Volume-I, Springer-Verlag, New York, USA

Langhaar, B. (1951). *Dimensional Analysis and Theory of Models*, New York, USA

Le Méhauté, H.L. (1957) *Perméabilité des digues en enrochement aux ondes de gravité périodique*, Houille Blanche 6

Postma, G.M. (1989) *Wave reflection from rock slopes under random wave attack*, MSc Thesis, Delft University of Technology, Delft, The Netherlands

Price, W.A. (1979) *Static stability of rubble mound breakwaters*, Dock and harbour authority. Vol. LX

Schiereck, G.J. (1998) *Introduction to bed, bank and shore protection*, Delft University of Technology, Delft, The Netherlands

SPM (1984) *Shore Protection Manual* Coastal Engineering Research Center, Washington

Thompson, D.M., Shuttler, R.M. (1975) *Riprap design for wind wave attack. A laboratory study in random waves*, HRS, Report EX 707, Wallingford, UK

Van den Bosch, A.F.M. (2001) *Influence of the density of placement on the stability of armour layers on breakwaters*, MSc Thesis, Delft University of Technology, Delft, The Netherlands

Van Gent, M.R.A. (1995) *Wave interaction with permeable coastal structures*, PhD Thesis, Delft University of Technology, Delft, The Netherlands

Van Gent, M.R.A., Spaan, G.B.H., Plate, S.E., Berendsen, E.,Van der Meer, J.W. and d'Angremond, K. (1999) *Single-layer rubble mound breakwaters*, Proc. International Conference Coastal Structures, Santander, Spain

Van Gent, M.R.A., Kuiper, C. (2000) *Single-layer rubble mound breakwaters with high density concrete cubes*, WL|Delft Hydraulics, Project H3675, Delft, The Netherlands

Van der Meer, J.W. (1988a) *Rock Slopes and Gravel Beaches under Wave attack*, PhD Thesis, Delft University of Technology, Delft, The Netherlands

Van der Meer, J.W. (1988b) *Stability of Cubes, Tetrapods and Accropodes*, Proceedings of the Conference Breakwater '88, Thomas Telford, London, UK

Van der Meer, J.W. (1993) *Conceptual design of rubble mound breakwaters*, WL|Delft Hydraulics, Delft, The Netherlands

Van der Meer, J.W., Tutuarima, W.H., Burger, G. (1996) *Influence of rock shape and grading on stability of low-crested structures*, Proceedings of the International Conference on Coastal Engineering, Orlando, USA

List of Tables

List of Figures

Appendix A: Wave data

$H_{si0}(m)$	$T_{m0}(s)$	$s_{m0}(-)$	$H_{sr0}(m)$	$K_{R0}(-)$	$H_{si}(m)$	$T_m(s)$	$H_{sr}(m)$	$K_R(-)$
0.087	1.15	0.042	0.028	0.32	0.083	1.12	0.030	0.36
0.105	1.25	0.043	0.034	0.33	0.102	1.21	0.039	0.38
0.127	1.33	0.046	0.041	0.32	0.127	1.33	0.048	0.38
0.147	1.42	0.047	0.046	0.31	0.147	1.46	0.053	0.36
0.167	1.50	0.048	0.054	0.32	0.164	1.58	0.057	0.35

Table A.1: Wave data for experiment A0N3S4

$H_{si0}(m)$	$T_{m0}(s)$	$s_{m0}(-)$	$H_{sr0}(m)$	$K_{R0}(-)$	$H_{si}(m)$	$T_m(s)$	$H_{sr}(m)$	$K_R(-)$
0.088	1.15	0.042	0.029	0.33	0.084	1.13	0.030	0.36
0.115	1.32	0.042	0.036	0.32	0.103	1.22	0.039	0.37
0.128	1.35	0.045	0.041	0.32	0.126	1.32	0.048	0.38
0.148	1.45	0.045	0.047	0.32	0.148	1.46	0.053	0.36
0.168	1.55	0.045	0.054	0.32	0.165	1.58	0.058	0.35

Table A.2: Wave data for experimentA0N3S4R

$H_{si0}(m)$	$T_{m0}(s)$	$s_{m0}(-)$	$H_{sr0}(m)$	$K_{R0}(-)$	$H_{si}(m)$	$T_m(s)$	$H_{sr}(m)$	$K_R(-)$
0.088	1.13	0.044	0.024	0.27	0.084	1.12	0.024	0.28
0.107	1.22	0.046	0.030	0.28	0.104	1.24	0.034	0.33
0.125	1.30	0.047	0.035	0.28	0.124	1.35	0.042	0.34
0.146	1.43	0.045	0.039	0.27	0.144	1.48	0.045	0.31
0.168	1.56	0.044	0.044	0.27	0.164	1.58	0.047	0.29

Table A.3: Wave data for experiment A1N3S4

$H_{si0}(m)$	$T_{m0}(s)$	$s_{m0}(-)$	$H_{sr0}(m)$	$K_{R0}(-)$	$H_{si}(m)$	$T_m(s)$	$H_{sr}(m)$	$K_R(-)$
0.087	1.13	0.044	0.024	0.28	0.083	1.10	0.027	0.32
0.108	1.22	0.046	0.031	0.29	0.104	1.21	0.035	0.34
0.129	1.33	0.047	0.036	0.28	0.127	1.35	0.043	0.34
0.146	1.44	0.045	0.040	0.27	0.145	1.49	0.046	0.32
0.167	1.60	0.042	0.046	0.29	0.173	1.63	0.060	0.34

Table A.4: Wave data for experiment A1N3S4R

$H_{si0}(m)$	$T_{m0}(s)$	$s_{m0}(-)$	$H_{sr0}(m)$	$K_{R0}(-)$	$H_{si}(m)$	$T_m(s)$	$H_{sr}(m)$	$K_R(-)$
0.086	1.13	0.043	0.024	0.28	0.082	1.12	0.025	0.30
0.107	1.23	0.045	0.029	0.27	0.104	1.22	0.034	0.33
0.128	1.31	0.047	0.035	0.28	0.126	1.35	0.041	0.33
0.146	1.45	0.045	0.039	0.27	0.146	1.47	0.045	0.31
0.165	1.51	0.046	0.044	0.27	0.161	1.60	0.046	0.29

Table A.5: Wave data for experiment A1N25S4

$H_{si0}(m)$	$T_{m0}(s)$	$s_{m0}(-)$	$H_{sr0}(m)$	$K_{R0}(-)$	$H_{si}(m)$	$T_m(s)$	$H_{sr}(m)$	$K_R(-)$
0.087	1.14	0.043	0.024	0.275	0.083	1.12	0.025	0.30
0.106	1.22	0.046	0.028	0.267	0.103	1.22	0.033	0.32
0.128	1.32	0.047	0.035	0.272	0.126	1.34	0.041	0.32

Table A.6: Wave data for experiment A1N4S4

$H_{si0}(m)$	$T_{m0}(s)$	$s_{m0}(-)$	$H_{sr0}(m)$	$K_{R0}(-)$	$H_{si}(m)$	$T_m(s)$	$H_{sr}(m)$	$K_R(-)$
0.088	1.54	0.024	0.032	0.36	0.089	1.61	0.028	0.31
0.114	1.65	0.027	0.038	0.34	0.117	1.73	0.036	0.31
0.136	1.82	0.026	0.046	0.34	0.142	1.86	0.051	0.36
0.155	1.94	0.026	0.056	0.36	0.162	1.99	0.067	0.41
0.176	2.11	0.025	0.063	0.36	0.182	2.16	0.080	0.44

Table A.7: Wave data for experiment A1N3S2

$H_{si0}(m)$	$T_{m0}(s)$	$s_{m0}(-)$	$H_{sr0}(m)$	$K_{R0}(-)$	$H_{si}(m)$	$T_m(s)$	$H_{sr}(m)$	$K_R(-)$
0.075	0.98	0.050	0.017	0.23	0.089	0.99	0.019	0.21
0.095	1.06	0.054	0.024	0.25	0.117	1.06	0.024	0.20
0.113	1.14	0.056	0.030	0.26	0.142	1.15	0.032	0.23
0.130	1.23	0.055	0.035	0.27	0.162	1.23	0.040	0.24
0.143	1.30	0.055	0.038	0.27	0.182	1.32	0.044	0.24
0.162	1.37	0.056	0.043	0.26	0.193	1.40	0.050	0.26
0.181	1.43	0.057	0.046	0.26	0.212	1.50	0.052	0.25

Table A.8: Wave data for experiment A1N3S6

$H_{si0}(m)$	$T_{m0}(s)$	$s_{m0}(-)$	$H_{sr0}(m)$	$K_{R0}(-)$	$H_{si}(m)$	$T_m(s)$	$H_{sr}(m)$	$K_R(-)$
0.084	1.14	0.041	0.026	0.31	0.082	1.16	0.027	0.33
0.101	1.22	0.044	0.033	0.32	0.103	1.26	0.037	0.36
0.138	1.44	0.043	0.044	0.32	0.144	1.49	0.054	0.37
0.160	1.53	0.044	0.053	0.33	0.161	1.58	0.057	0.36
0.168	1.58	0.043	0.056	0.33	0.168	1.63	0.059	0.35

Table A.9: Wave data for experiment A2N3S4

$H_{si0}(m)$	$T_{m0}(s)$	$s_{m0}(-)$	$H_{sr0}(m)$	$K_{R0}(-)$	$H_{si}(m)$	$T_m(s)$	$H_{sr}(m)$	$K_R(-)$
0.083	1.16	0.040	0.027	0.32	0.082	1.15	0.026	0.32
0.113	1.33	0.041	0.035	0.31	0.112	1.31	0.036	0.32
0.145	1.51	0.041	0.046	0.32	0.143	1.50	0.045	0.31
0.160	1.58	0.041	0.054	0.34	0.158	1.57	0.050	0.32
0.171	1.64	0.041	0.058	0.34	0.167	1.63	0.053	0.32

Table A.10: Wave data for experiment A2N3S4R

$H_{si0}(m)$	$T_{m0}(s)$	$s_{m0}(-)$	$H_{sr0}(m)$	$K_{R0}(-)$	$H_{si}(m)$	$T_m(s)$	$H_{sr}(m)$	$K_R(-)$
0.084	1.14	0.041	0.026	0.30	0.082	1.16	0.027	0.33
0.101	1.22	0.043	0.032	0.32	0.102	1.24	0.037	0.36
0.120	1.33	0.044	0.039	0.32	0.124	1.36	0.046	0.37
0.137	1.42	0.043	0.043	0.31	0.144	1.47	0.052	0.36
0.159	1.51	0.045	0.053	0.33	0.160	1.58	0.056	0.35
0.174	1.60	0.044	0.058	0.33	0.183	1.70	0.072	0.39

Table A.11: Wave data for experiment A2N25S4

$H_{si0}(m)$	$T_{m0}(s)$	$s_{m0}(-)$	$H_{sr0}(m)$	$K_{R0}(-)$	$H_{si}(m)$	$T_m(s)$	$H_{sr}(m)$	$K_R(-)$
0.083	1.14	0.041	0.026	0.32	0.081	1.15	0.027	0.33
0.117	1.22	0.043	0.032	0.32	0.115	1.25	0.032	0.32

Table A.12: Wave data for experiment A2N4S4

$H_{si0}(m)$	$T_{m0}(s)$	$s_{m0}(-)$	$H_{sr0}(m)$	$K_{R0}(-)$	$H_{si}(m)$	$T_m(s)$	$H_{sr}(m)$	$K_R(-)$
0.088	1.54	0.024	0.035	0.39	0.092	1.61	0.037	0.40
0.108	1.69	0.024	0.042	0.39	0.116	1.75	0.046	0.40
0.127	1.84	0.024	0.051	0.40	0.139	1.89	0.060	0.43
0.156	1.95	0.026	0.061	0.39	0.150	2.02	0.061	0.41

Table A.13: Wave data for experiment A2N3S2

$H_{si0}(m)$	$T_{m0}(s)$	$s_{m0}(-)$	$H_{sr0}(m)$	$K_{R0}(-)$	$H_{si}(m)$	$T_m(s)$	$H_{sr}(m)$	$K_R(-)$
0.087	1.03	0.053	0.026	0.30	0.086	1.02	0.027	0.31
0.111	1.08	0.061	0.032	0.29	0.109	1.07	0.033	0.30
0.128	1.17	0.060	0.037	0.29	0.126	1.17	0.038	0.30
0.157	1.26	0.063	0.045	0.29	0.154	1.25	0.044	0.29
0.174	1.36	0.060	0.051	0.29	0.170	1.33	0.051	0.30
0.190	1.42	0.060	0.055	0.29	0.186	1.41	0.060	0.31

Table A.14: Wave data for experiment A2N3S6

$H_{si0}(m)$	$T_{m0}(s)$	$s_{m0}(-)$	$H_{sr0}(m)$	$K_{R0}(-)$	$H_{si}(m)$	$T_m(s)$	$H_{sr}(m)$	$K_R(-)$
0.084	1.15	0.041	0.025	0.30	0.082	1.15	0.026	0.32
0.102	1.22	0.044	0.032	0.32	0.102	1.25	0.037	0.36
0.121	1.32	0.044	0.039	0.32	0.124	1.37	0.047	0.38
0.138	1.43	0.043	0.044	0.32	0.144	1.48	0.053	0.37
0.161	1.52	0.045	0.056	0.35	0.162	1.58	0.058	0.36
0.171	1.59	0.043	0.060	0.35	0.179	1.68	0.073	0.41

Table A.15: Wave data for experiment A3N3S4

$H_{si0}(m)$	$T_{m0}(s)$	$s_{m0}(-)$	$H_{sr0}(m)$	$K_{R0}(-)$	$H_{si}(m)$	$T_m(s)$	$H_{sr}(m)$	$K_R(-)$
0.082	1.13	0.041	0.021	0.26	0.081	1.16	0.022	0.27
0.100	1.22	0.043	0.028	0.28	0.101	1.26	0.032	0.32
0.118	1.31	0.044	0.034	0.29	0.122	1.37	0.041	0.34
0.137	1.44	0.043	0.039	0.29	0.143	1.50	0.049	0.34
0.158	1.51	0.044	0.051	0.33	0.158	1.61	0.053	0.34
0.173	1.62	0.042	0.058	0.34	0.181	1.710	0.073	0.405

Table A.16: Wave data for experiment A3N3S4R

$H_{si0}(m)$	$T_{m0}(s)$	$s_{m0}(-)$	$H_{sr0}(m)$	$K_{R0}(-)$	$H_{si}(m)$	$T_m(s)$	$H_{sr}(m)$	$K_R(-)$
0.082	1.15	0.040	0.024	0.29	0.082	1.16	0.025	0.31
0.102	1.22	0.044	0.032	0.32	0.102	1.25	0.037	0.36
0.119	1.33	0.043	0.036	0.30	0.123	1.39	0.044	0.36
0.136	1.44	0.042	0.041	0.30	0.142	1.49	0.051	0.36
0.158	1.52	0.044	0.052	0.33	0.158	1.60	0.054	0.34
0.172	1.62	0.042	0.059	0.35	0.177	1.72	0.070	0.39
0.186	1.71	0.041	0.067	0.36	0.195	1.83	0.085	0.43

Table A.17: Wave data for experiment A3N25S4

$H_{si0}(m)$	$T_{m0}(s)$	$s_{m0}(-)$	$H_{sr0}(m)$	$K_{R0}(-)$	$H_{si}(m)$	$T_m(s)$	$H_{sr}(m)$	$K_R(-)$
0.084	1.15	0.040	0.022	0.27	0.082	1.16	0.023	0.29

Table A.18: Wave data for experiment A3N4S4

$H_{si0}(m)$	$T_{m0}(s)$	$s_{m0}(-)$	$H_{sr0}(m)$	$K_{R0}(-)$	$H_{si}(m)$	$T_m(s)$	$H_{sr}(m)$	$K_R(-)$
0.086	1.54	0.023	0.028	0.32	0.085	1.62	0.029	0.34
0.109	1.67	0.025	0.040	0.36	0.105	1.78	0.041	0.39
0.123	1.85	0.023	0.048	0.39	0.122	1.91	0.048	0.40
0.149	1.94	0.025	0.062	0.41	0.148	2.04	0.062	0.42
0.175	2.08	0.026	0.074	0.42	0.175	2.17	0.073	0.42

Table A.19: Wave data for experiment A3N3S2

$H_{si0}(m)$	$T_{m0}(s)$	$s_{m0}(-)$	$H_{sr0}(m)$	$K_{R0}(-)$	$H_{si}(m)$	$T_m(s)$	$H_{sr}(m)$	$K_R(-)$
0.113	1.08	0.062	0.023	0.20	0.111	1.07	0.024	0.22
0.126	1.14	0.062	0.026	0.21	0.125	1.15	0.027	0.22
0.155	1.29	0.060	0.032	0.20	0.153	1.28	0.035	0.23
0.173	1.35	0.061	0.037	0.21	0.171	1.34	0.044	0.26
0.190	1.43	0.060	0.042	0.22	0.187	1.42	0.051	0.27
0.210	1.50	0.060	0.045	0.21	0.202	1.47	0.061	0.30

Table A.20: Wave data for experiment A3N3S6

Appendix B: Statistical background

Maximum Likelihood Estimation for the Normal Distribution

Maximum likelihood estimation begins with the mathematical expression known as a likelihood function of the sample data. Loosely speaking, the likelihood of a set of data is the probability of obtaining that particular set of data given the chosen probability model. This expression contains the unknown parameters. Those values of the parameter that maximize the sample likelihood are known as the maximum likelihood estimates.

To investigate wether measured data is normally distributed, it is fitted accordingly. To do so requires a reliable estimation of the parameters μ and σ^2. The normal distribution function is given by:

$$f_X(x;\mu,\sigma^2) = \frac{1}{\sqrt{2\pi\sigma}} e^{-\frac{1}{2}\left(\frac{x-\mu}{\sigma}\right)^2} \tag{B.1}$$

The likelihood function for the normal distribution is a function of μ and σ^2

$$L(x_1, x_2, ..., x_n; \mu, \sigma^2) = \prod_{i=1}^{n} f_X(x;\mu,\sigma^2) = \prod_{i=1}^{n} \frac{1}{\sqrt{2\pi\sigma}} e^{-\frac{1}{2}\left(\frac{x_i-\mu}{\sigma}\right)^2} \tag{B.2}$$

The loglikelihood function is

$$\begin{aligned} logL(x_1, x_2, ..., x_n; \mu, \sigma^2) &= log \prod_{i=1}^{n} f_X(x;\mu,\sigma^2) \\ &= -\frac{n}{2} log(2\pi) - \frac{n}{2} log\sigma^2 - \frac{1}{2\sigma^2} \sum_{i=1}^{n} (x_i - \mu)^2 \end{aligned} \tag{B.3}$$

The estimators μ and σ^2 are found by setting the partially differentiated loglikelihood function equal to zero

$$\frac{\partial[logL(x_1, x_2, ..., x_n; \mu, \sigma^2)]}{\partial\mu} = \left[-\frac{n\mu - \sum_{i=1}^{n} x_i}{\sigma^2} \right] = 0 \tag{B.4}$$

and

$$\frac{\partial[logL(x_1, x_2, ..., x_n; \mu, \sigma^2)]}{\partial\sigma^2} = \frac{\sum_{i=1}^{n} (x_i - \mu)^2 - n\sigma^2}{2\sigma^4} = 0 \tag{B.5}$$

From these equations it follows:

$$\mu = \frac{1}{n}\sum_{i=1}^{n} x_i = \overline{x} \tag{B.6}$$

$$\sigma^2 = \frac{1}{n}\sum_{i=1}^{n}(x_i - \overline{x})^2 \tag{B.7}$$

Kolmogorov-Smirnov test

Establishing the underlying distribution of a data set is is crucial for the correct implementation of some statistical procedures. With Kolmogorov-Smirnov it is possible to test the normality of a data set. This is performed by calculating the test statistic D_{KS}

$$D_{KS} = max\left|\frac{i}{n} - F_X(x_i)\right|, i = 1, 2, ..., n \tag{B.8}$$

Where n is the total number of observations. The data set can be considered normal if the KS statistic D_{KS} is less than a pre-defined critical value of $\alpha/\sqrt{n}$. For an error of $P = 0.05$, CUR (1997) denotes $\alpha = 1.36$ (see table (B.1)). This value was used in the current measurements.

P	α
0.10	1.23
0.05	1.36
0.01	1.63

Table B.1: α-values

Appendix C: Properties of the materials

Tetrapod units

A total of 100 tetrapod units were weighed both dry and under water to determine the overall nominal diameter and mass density. The Maximum-Likelihood estimators were used to fit the normal distribution curve. The derived data is assumed to follow this distribution. The Kolmogorov-Smirnov test demonstrated that this assumption was correct.

n	$W_{50}(g)$	$\sigma_{W_{50}}(g)$	$\rho_a(kg/m^3)$	$D_n(mm)$	D_{KS}	$\alpha/\sqrt{n}$	KS-test
100	206	12.23	2367	44.3	0.133	0.136	*passed*

Table C.1: Summary of properties

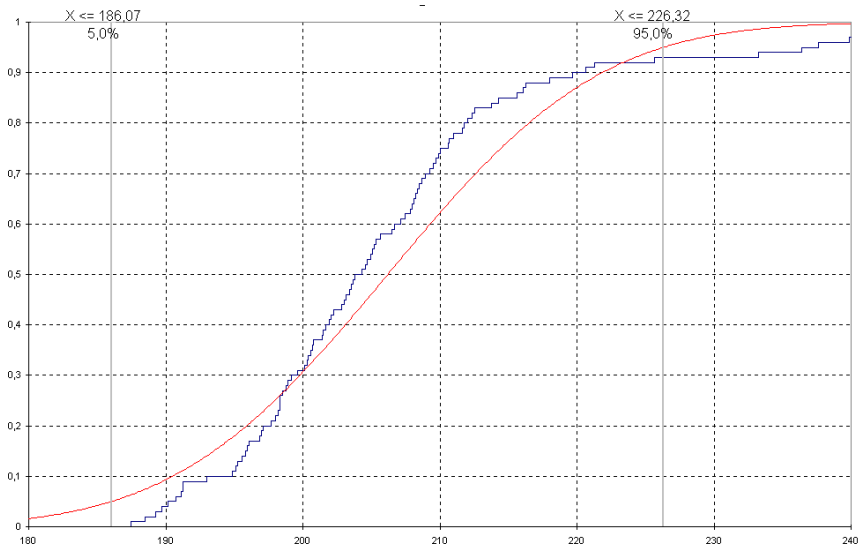

Figure C.1: Distribution of the weight ($W[g]$) of the tetrapod units

nr	$W_{dry}(g)$	$W_{wet}(g)$	$\rho_a(kg/m^3)$	$D_n(mm)$	nr	$W_{dry}(g)$	$W_{wet}(g)$	$\rho_a(kg/m^3)$	$D_n(mm)$
1	210.64	123.88	2428	44.27	51	211.02	122.13	2374	44.63
2	207.86	110.92	2144	45.94	52	200.33	114.79	2342	44.06
3	189.26	120.66	2759	40.94	53	208.50	119.39	2340	44.67
4	209.26	120.13	2348	44.67	54	250.00	158.22	2724	45.11
5	198.19	111.09	2275	44.33	55	205.68	119.01	2373	44.25
6	239.85	152.74	2753	44.33	56	225.68	129.42	2344	45.83
7	198.89	112.32	2297	44.24	57	199.19	110.33	2242	44.62
8	195.83	112.38	2347	43.70	58	201.39	115.29	2339	44.16
9	202.23	116.21	2351	44.14	59	196.84	109.62	2257	44.35
10	209.74	120.98	2363	44.61	60	195.54	112.48	2354	43.63
11	221.26	134.12	2539	44.33	61	190.14	107.87	2311	43.49
12	205.24	118.99	2380	44.18	62	219.69	126.54	2358	45.33
13	198.20	114.12	2357	43.81	63	203.01	116.78	2354	44.18
14	241.75	153.79	2748	44.47	64	208.71	121.33	2389	44.37
15	206.68	120.59	2401	44.16	65	200.56	115.85	2368	43.92
16	189.73	103.24	2194	44.22	66	195.81	112.94	2363	43.60
17	208.03	119.64	2354	44.55	67	220.64	125.82	2327	45.60
18	198.21	113.22	2332	43.97	68	208.25	118.92	2331	44.70
19	233.26	149.08	2771	43.83	69	204.58	117.51	2350	44.32
20	203.41	119.56	2426	43.77	70	205.10	115.39	2286	44.77
21	195.26	122.71	2691	41.71	71	188.49	105.88	2282	43.55
22	236.37	135.42	2341	46.56	72	196.93	112.94	2345	43.79
23	206.51	117.22	2313	44.70	73	198.02	108.91	2222	44.67
24	204.97	116.18	2308	44.61	74	190.71	104.74	2218	44.13
25	197.71	115.34	2400	43.51	75	199.60	114.02	2332	44.07
26	204.33	116.60	2329	44.43	76	218.02	126.07	2371	45.14
27	201.69	115.12	2330	44.24	77	211.63	122.80	2382	44.62
28	213.77	122.96	2354	44.95	78	208.94	120.82	2371	44.50
29	205.29	117.94	2350	44.37	79	191.20	107.92	2296	43.67
30	207.49	119.30	2353	44.51	80	209.88	121.34	2370	44.57
31	201.91	115.53	2337	44.20	81	242.50	154.68	2761	44.45
32	198.25	113.90	2350	43.86	82	200.29	111.73	2262	44.57
33	208.13	120.00	2362	44.50	83	210.58	121.05	2352	44.74
34	192.97	109.26	2305	43.74	84	237.59	151.98	2775	44.07
35	212.32	119.37	2284	45.30	85	210.04	119.71	2325	44.87
36	197.12	113.35	2353	43.76	86	212.52	123.06	2376	44.72
37	204.70	118.31	2369	44.21	87	187.48	102.63	2210	43.94
38	200.58	115.04	2345	44.06	88	194.84	112.38	2363	43.53
39	200.11	114.29	2332	44.11	89	207.17	118.95	2348	44.52
40	198.80	109.94	2237	44.62	90	200.80	114.76	2334	44.15
41	207.98	120.98	2391	44.31	91	202.07	113.50	2281	44.58
42	191.18	104.84	2214	44.20	92	215.62	124.08	2355	45.07
43	203.06	115.98	2332	44.32	93	203.71	114.60	2286	44.67
44	203.45	116.08	2329	44.37	94	209.54	120.90	2364	44.59
45	191.15	108.60	2316	43.54	95	211.76	121.82	2354	44.80
46	216.26	124.70	2362	45.07	96	195.10	112.70	2368	43.52
47	196.09	112.42	2344	43.74	97	201.40	113.61	2294	44.44
48	214.28	124.41	2384	44.79	98	203.57	117.53	2366	44.15
49	216.08	123.98	2346	45.16	99	202.86	114.50	2296	44.54
50	212.01	122.87	2378	44.67	100	198.51	113.96	2348	43.89

Table C.2: Properties of the tetrapod units

Secondary layer material of series A1

Approximately $150kg$ of rock material was sieved using different sieves. To accurately determine the properties of this secondary layer material a sample size of 108 rocks were weighed. To establish the mass density, 49 of the 108 rocks were also weighed under water . The same statistical procedure was followed as with the tetrapod units. Only the rocks that were weighed both dry and under water are listed in table (C.4).

n	$W_{50}(g)$	$\sigma_{W_{50}}(g)$	$\rho_r(kg/m^3)$	$D_{n50}(mm)$	$D_{85}/D_{15}(-)$	D_{KS}	$\alpha/\sqrt{n}$	KS-test
108	6.50	3.07	2600	13.6	1.43	0.129	0.131	*passed*

Table C.3: Summary of properties

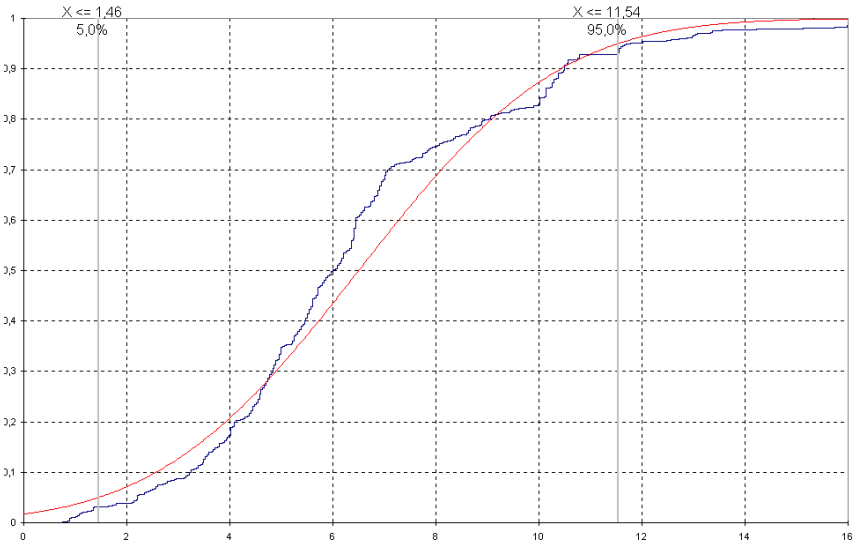

Figure C.2: Distribution of the weight ($W[g]$) of the secondary layer rocks of series A1

nr	$W_{dry}(g)$	$W_{wet}(g)$	$\rho_r(kg/m^3)$	$D_n(mm)$	nr	$W_{dry}(g)$	$W_{wet}(g)$	$\rho_r(kg/m^3)$	$D_n(mm)$
1	7.61	4.69	2606	14.29	11	10.51	6.36	2533	16.07
2	9.67	5.94	2592	15.51	12	10.28	6.4	2649	15.71
3	10.88	6.69	2597	16.12	13	8.77	5.44	2634	14.93
4	6.09	3.75	2603	13.28	14	6.92	4.21	2554	13.94
5	6.55	4.02	2589	13.63	15	11.14	6.73	2526	16.40
6	6.97	4.32	2630	13.84	16	6.38	3.85	2522	13.63
7	8.18	4.96	2540	14.77	17	9.77	6.01	2598	15.55
8	8.79	5.38	2578	15.05	18	10.54	6.45	2577	15.99
9	5.15	3.12	2537	12.66	19	13.34	8.19	2590	17.27
10	5.22	3.23	2623	12.58	20	13.88	8.53	2594	17.49

nr	$W_{dry}(g)$	$W_{wet}(g)$	$\rho_r(kg/m^3)$	$D_n(mm)$	nr	$W_{dry}(g)$	$W_{wet}(g)$	$\rho_r(kg/m^3)$	$D_n(mm)$
21	14.84	9.12	2594	17.88	36	12.12	7.52	2635	16.63
22	16.78	10.28	2582	18.66	37	11.48	7.03	2580	16.45
23	8.41	5.17	2596	14.80	38	8.76	5.43	2631	14.93
24	15.13	9.26	2578	18.04	39	8.00	4.94	2614	14.52
25	15.37	9.58	2655	17.96	40	9.11	5.6	2595	15.20
26	8.28	5.14	2637	14.64	41	9.43	5.77	2577	15.41
27	8.69	5.35	2602	14.95	42	14.27	8.83	2623	17.59
28	6.97	4.26	2572	13.94	43	15.58	9.60	2605	18.15
29	8.51	5.27	2627	14.80	44	12.33	7.58	2596	16.81
30	5.51	3.42	2636	12.79	45	9.02	5.55	2599	15.14
31	6.20	3.83	2616	13.33	46	13.35	8.26	2623	17.20
32	10.72	6.64	2627	15.98	47	6.90	4.23	2584	13.87
33	7.75	4.83	2654	14.29	48	7.94	4.87	2586	14.53
34	12.08	7.51	2643	16.59	49	7.90	4.84	2582	14.52
35	9.11	5.62	2610	15.17					

Table C.4: Properties of the secondary layer rock material of series A1

Secondary layer material of series A2

Approximately $150kg$ of rock material was sieved using different sieves. A sample of 69 rocks was weighed both dry and under water. Their properties are listed in table (C.6).

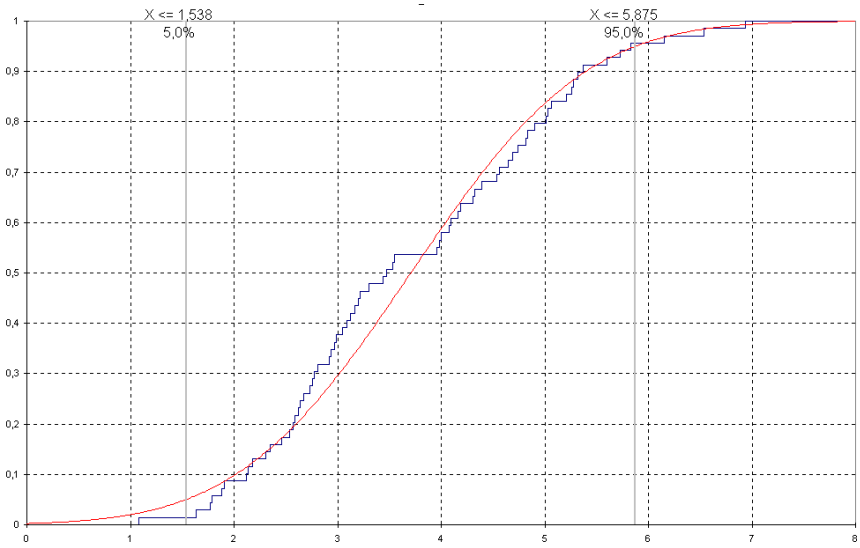

Figure C.3: Distribution of the weight ($W[g]$) of the secondary layer rocks of series A2

n	$W_{50}(g)$	$\sigma_{W_{50}}(g)$	$\rho_r(kg/m^3)$	$D_{n50}(mm)$	$D_{85}/D_{15}(-)$	D_{KS}	$\alpha/\sqrt{n}$	KS-test
69	3.71	1.32	2600	11.3	1.29	0.108	0.164	*passed*

Table C.5: Summary of properties

nr	$W_{dry}(g)$	$W_{wet}(g)$	$\rho_r(kg/m^3)$	$D_n(mm)$	nr	$W_{dry}(g)$	$W_{wet}(g)$	$\rho_r(kg/m^3)$	$D_n(mm)$
1	4.54	2.88	2740	11.83	36	1.91	1.08	2291	9.42
2	4.09	2.57	2700	11.48	37	3.30	2.07	2686	10.71
3	5.06	3.20	2720	12.30	38	2.58	1.46	2312	10.37
4	3.53	2.20	2639	11.02	39	2.18	1.26	2367	9.73
5	4.39	2.79	2740	11.70	40	4.08	2.57	2703	11.48
6	3.09	1.88	2565	10.64	41	4.56	2.91	2771	11.80
7	3.22	1.98	2598	10.74	42	4.16	2.63	2710	11.54
8	3.05	1.88	2601	10.54	43	2.99	1.82	2557	10.53
9	6.54	4.17	2762	13.33	44	3.12	1.93	2623	10.60
10	1.88	1.07	2329	9.31	45	2.76	1.70	2616	10.18
11	4.65	2.96	2744	11.92	46	6.15	3.91	2747	13.08
12	5.60	3.52	2688	12.77	47	4.69	2.91	2630	12.13
13	5.01	3.12	2651	12.36	48	4.31	2.68	2651	11.76
14	3.55	2.19	2620	11.06	49	5.32	3.28	2601	12.70
15	2.35	1.40	2478	9.83	50	2.67	1.63	2571	10.12
16	3.47	2.15	2614	10.99	51	2.46	1.46	2457	10.01
17	2.62	1.56	2474	10.19	52	2.73	1.66	2540	10.24
18	3.98	2.48	2650	11.45	53	5.37	3.41	2740	12.52
19	6.94	4.47	2807	13.52	54	5.83	3.67	2700	12.93
20	4.82	3.06	2734	12.08	55	2.31	1.32	2333	9.97
21	3.44	2.12	2610	10.97	56	1.77	1.02	2364	9.08
22	3.20	1.97	2600	10.72	57	2.12	1.37	2812	9.11
23	2.54	1.36	2156	10.56	58	2.76	1.70	2598	10.21
24	2.92	1.78	2573	10.43	59	2.64	1.52	2352	10.39
25	4.90	3.08	2694	12.21	60	4.32	2.72	2697	11.70
26	3.96	2.47	2661	11.42	61	5.03	3.17	2701	12.30
27	5.26	3.30	2686	12.51	62	2.57	1.54	2485	10.12
28	1.79	1.04	2370	9.11	63	1.08	0.64	2453	7.60
29	2.93	1.76	2510	10.53	64	4.82	3.03	2694	12.14
30	5.21	3.28	2701	12.45	65	2.12	1.33	2667	9.27
31	5.28	3.32	2700	12.50	66	1.63	0.92	2299	8.91
32	4.74	2.98	2691	12.07	67	3.17	1.93	2569	10.72
33	4.19	2.64	2702	11.57	68	2.97	1.83	2609	10.44
34	5.73	3.64	2742	12.78	69	2.81	1.77	2695	10.14
35	4.00	2.45	2581	11.57					

Table C.6: Properties of the secondary layer rock material of series A2

Secondary layer material of series A3

After the sieving of approximately $125kg$ of rock, a sample of 97 rocks was weighed to determine the distribution of the weight. 20 rocks were also weighed under water in order to determine the density of the material. As with the previous material, only the properties of the rocks that were weighed both dry and under water are listed in table (C.8).

n	$W_{50}(g)$	$\sigma_{W_{50}}(g)$	$\rho_r(kg/m^3)$	$D_{n50}(mm)$	$D_{85}/D_{15}(-)$	D_{KS}	$\alpha/\sqrt{n}$	KS-test
97	1.69	0.63	2680	8.6	1.31	0.061	0.138	*passed*

Table C.7: Summary of properties

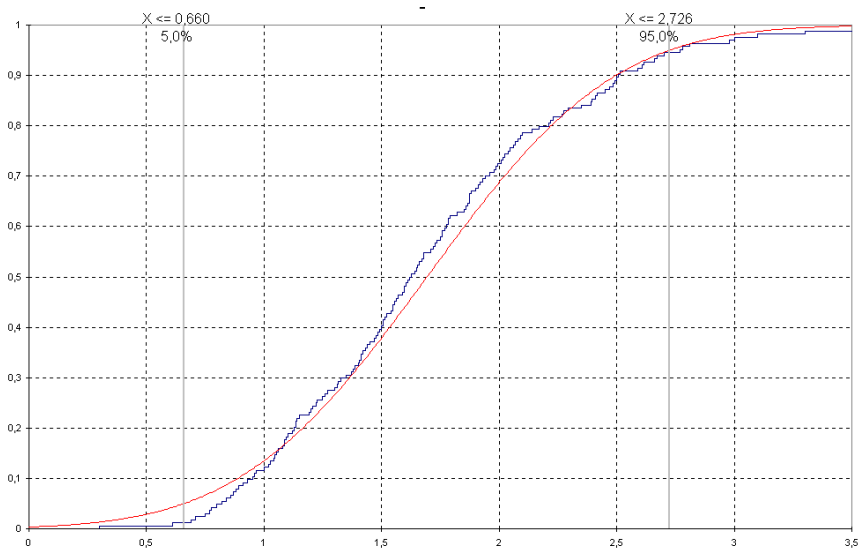

Figure C.4: Distribution of the weight ($W[g]$) of the secondary layer rocks of series A3

nr	$W_{dry}(g)$	$W_{wet}(g)$	$\rho_r(kg/m^3)$	$D_n(mm)$	nr	$W_{dry}(g)$	$W_{wet}(g)$	$\rho_r(kg/m^3)$	$D_n(mm)$
1	1.71	1.0	2485	8.82	11	2.49	1.6	2689	9.74
2	1.56	1.0	2676	8.36	12	1.62	1.0	2699	8.43
3	2.01	1.3	2671	9.10	13	1.67	1.1	2690	8.54
4	2.47	1.5	2666	9.75	14	1.33	0.8	2673	7.92
5	1.50	1.0	2751	8.17	15	1.51	0.9	2684	8.26
6	1.41	0.9	2713	8.04	16	2.27	1.4	2690	9.45
7	1.22	0.8	2690	7.69	17	1.56	1.0	2678	8.36
8	1.19	0.8	2725	7.59	18	2.39	1.5	2678	9.63
9	1.38	0.9	2708	7.99	19	1.68	1.1	2692	8.55
10	1.25	0.8	2650	7.78	20	2.29	1.4	2696	9.47

Table C.8: Properties of the secondary layer rock material of series A3

Intermediate layer material

The intermediate layer was positioned between the core and the secondary layer. After the sieving process, 89 rocks were weighed dry. 40 rocks out of the total sample were also weighed under water. The properties of these rocks are presented in table (C.10).

n	$W_{50}(g)$	$\sigma_{W_{50}}(g)$	$\rho_r(kg/m^3)$	$D_{n50}(mm)$	$D_{85}/D_{15}(-)$	D_{KS}	$\alpha/\sqrt{n}$	KS-test
89	9.21	3.89	2600	15.2	1.37	0.123	0.144	*passed*

Table C.9: Summary of properties

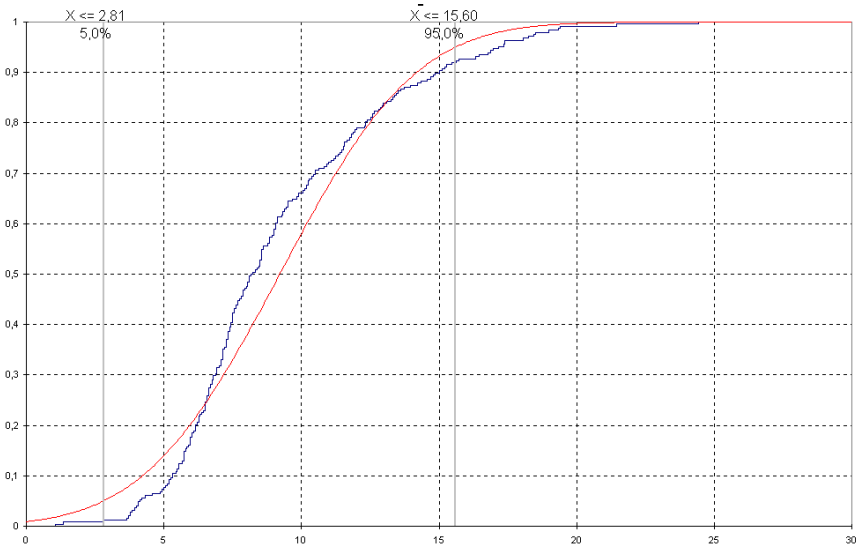

Figure C.5: Distribution of the weight ($W[g]$) of the intermediate material

nr	$W_{dry}(g)$	$W_{wet}(g)$	$\rho_r(kg/m^3)$	$D_n(mm)$	nr	$W_{dry}(g)$	$W_{wet}(g)$	$\rho_r(kg/m^3)$	$D_n(mm)$
1	9.67	5.94	2592	15.51	11	9.77	6.01	2598	15.55
2	8.18	4.96	2540	14.77	12	10.88	6.69	2597	16.12
3	7.61	4.69	2606	14.29	13	10.51	6.36	2533	16.07
4	6.97	4.32	2630	13.84	14	10.28	6.40	2649	15.71
5	13.34	8.19	2590	17.27	15	8.79	5.38	2578	15.05
6	5.51	3.42	2636	12.79	16	6.55	4.02	2589	13.63
7	6.20	3.83	2616	13.33	17	6.09	3.75	2603	13.28
8	6.97	4.26	2572	13.94	18	5.22	3.23	2623	12.58
9	16.78	10.28	2582	18.66	19	5.15	3.12	2537	12.66
10	7.75	4.83	2654	14.29	20	8.77	5.44	2634	14.93

nr	$W_{dry}(g)$	$W_{wet}(g)$	$\rho_r(kg/m^3)$	$D_n(mm)$	nr	$W_{dry}(g)$	$W_{wet}(g)$	$\rho_r(kg/m^3)$	$D_n(mm)$
21	6.92	4.21	2554	13.94	31	15.37	9.58	2655	17.96
22	10.54	6.45	2577	15.99	32	11.14	6.73	2526	16.40
23	8.28	5.14	2637	14.64	33	6.38	3.85	2522	13.63
24	8.41	5.17	2596	14.80	34	12.08	7.51	2643	16.59
25	8.51	5.27	2627	14.80	35	9.11	5.62	2610	15.17
26	8.69	5.35	2602	14.95	36	12.12	7.52	2635	16.63
27	10.72	6.64	2627	15.98	37	11.48	7.03	2580	16.45
28	13.88	8.53	2594	17.49	38	8.76	5.43	2631	14.93
29	14.84	9.12	2594	17.88	39	8.00	4.94	2614	14.52
30	15.13	9.26	2578	18.04	40	9.11	5.60	2595	15.20

Table C.10: Properties of the intermediate layer rock material

Core material

Roughly $1750kg$ of core material was obtained after the sieving process. A sample of 112 rocks was weighed to fit a distribution curve of the core rock weight. 40 rocks were also weighed under water.

n	$W_{50}(g)$	$\sigma_{W_{50}}(g)$	$\rho_r(kg/m^3)$	$D_{n50}(mm)$	$D_{85}/D_{15}(-)$	D_{KS}	$\alpha/\sqrt{n}$	KS-test
112	15.74	5.39	2700	18.00	1.32	0.083	0.129	*passed*

Table C.11: Summary of properties

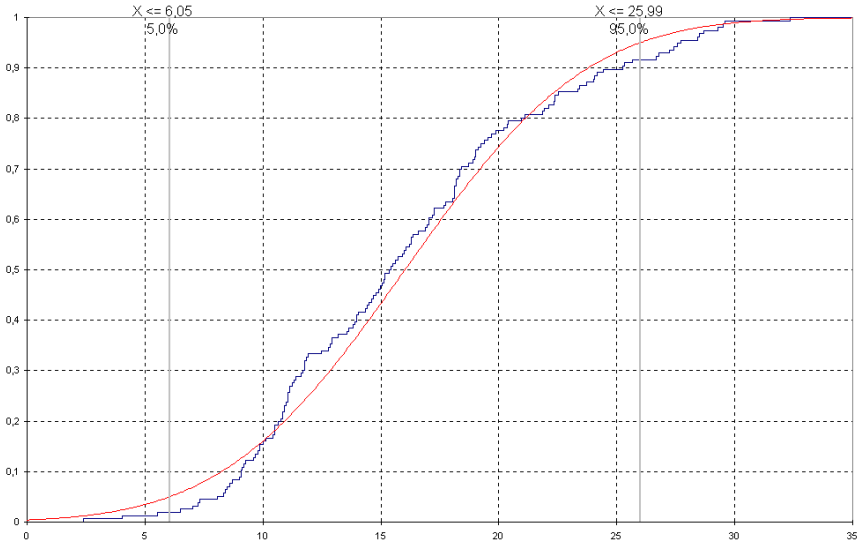

Figure C.6: Distribution of the weight ($W[g]$) of the core material

Appendix D: Contents of the wave flume data DVD

This thesis includes a DVD with various data regarding the wave flume experiments. The data includes:

- displacement plots
- digital images taken during the preparation phase of the experiments
- digital images taken during the experiments
- video files of the wave flume experiments
- a digital version of this thesis

The digital images of the experiments can be found in the directory:

\Images\Experiments

In this directory, the images of all four series can be found. The same terminology is used on the DVD as in this thesis. For example, the images of the experiment with the smallest secondary layer material, a wave steepness of $s_{m0} = 0.04$ and an armour packing density of $n_v = 0.25$, can be found in the directory:

\Images\Experiments\seriesA3\s4\n25\

If, for instance, during this experiment, at a certain sea-state (e.g $H_{m0} = 0.16m$), sliding took place, a displacement plot was generated. The plot indicates which units have moved between $0.5D_n$ and $2.0D_n$. Also -possible- displaced units are indicated by means of a circle. The plot for this particular sea-state, for example, can be found in:

\Images\Experiments\seriesA3\s4\n25\h16\Start-End\plot.dwg

The plot is an *Autodesk Autocad* file (.DWG). The Start-End directory also includes the first an last photo of that particular run.

The digital images taken during the preparation phase of the experiments can be found in the directory:

\Images\Preparations\

Video files of the wave flume experiments are found in the directory:

\Video\Experiments\

The video files are .AVI files (supported by *Microsoft Media Player*). The recordings only have a demonstrative character; they do not show entire experiments.

The digital version of this thesis can be found in the directory:

\Thesis\

The thesis comes in two file formats, namely as a .PDF file (supported by *Adobe Acrobat Reader*) and as a .DVI file.